

SYNTHESIS AND APPLICATIONS OF NOVEL RESORCIN[4]ARENE CAVITANDS

by

XIAOXUAN LEAYM

B.S., Nankai University of China, 2002

AN ABSTRACT OF A DISSERTATION

submitted in partial fulfillment of the requirements for the degree

DOCTOR OF PHILOSOPHY

Department of Chemistry
College of Arts and Sciences

KANSAS STATE UNIVERSITY
Manhattan, Kansas

2008

Abstract

A series of methylene-bridged resorcin[4]arenes featuring electrochemically active and hydrophilic viologene-units chemically attached to their “rim”-regions have been synthesized. Depending on the choices of pendent groups (feet) and the numbers of positive charges on the “rim” (four or eight), moderate to very good solubilities in water were obtained. A fluorescent coumarin tag designed for the purpose of photophysical studies was chemically linked to the feet of some of the synthesized resorcin[4]arenes.

These compounds were designed to act as guests in mycobacterial channel proteins (channel blockers). The proven host-guest interaction between resorcin[4]arenes and the mycobacterial porin MspA suggests potential application of my research in TB treatment. Both, hydrophilic nutrients and metabolites have to diffuse through the porin channels of mycobacteria because of the lack of an active transport mechanism. If these channels are successfully blocked, the mycobacteria have either to synthesize new channels, which make their outer membrane more susceptible to conventional antibiotics, or they become dormant.

(3,3'-dimethyl)-4,4'-bipyridinium units are very suitable electron relays. They can be reduced stepwise to viologen monoradical cations and then to uncharged viologen diradicals which possess highly negative redox potentials, allowing them to reduce C-Cl bonds. Therefore, the deep cavitand viologen resorcin[4]arenes, are expected to bind and detoxify chlorinated hydrocarbons by reductive dechlorination. In this work, the step wise reduction process of viologen- resorcin[4]arenes and the formation of negative redox potentials of double-reduced viologen resorcin[4]arenes are demonstrated by electrochemistry studies. These results encourage future studies toward an efficient electrocatalytic system for the reductive dehalogenation of organic compounds.

Besides highly charged resorcin[4]arene cavitands, the synthesis of a thiol-footed resorcin[4]arene was also attempted. The product was used for gold nanoparticle binding studies. The results of the photochemistry measurements provided a proof-of-concept for using the emission of gold nanoparticles in chemical sensors after covering their surfaces with thiol-footed resorcin[4]arenes.

Two heterocyclic resorcin[4]arene cavitands were synthesized for DNA-intercalation studies. The results of the photochemical measurements suggested binding between DNA and the heterocyclic resorcin[4]arenes and provided proof-of-principle for potential drug applications of this type of macrocycle.

SYNTHESIS AND APPLICATIONS OF NOVEL RESORCIN[4]ARENE CAVITANDS

by

XIAOXUAN LEAYM

B.S., Nankai University of China, 2002

A DISSERTATION

submitted in partial fulfillment of the requirements for the degree

DOCTOR OF PHILOSOPHY

Department of Chemistry
College of Arts and Sciences

KANSAS STATE UNIVERSITY
Manhattan, Kansas

2008

Approved by:

Major Professor
Dr. Stefan H. Bossmann

Abstract

A series of methylene-bridged resorcin[4]arenes featuring electrochemically active and hydrophilic viologene-units chemically attached to their “rim”-regions have been synthesized. Depending on the choices of pendent groups (feet) and the numbers of positive charges on the “rim” (four or eight), moderate to very good solubilities in water were obtained. A fluorescent coumarin tag designed for the purpose of photophysical studies was chemically linked to the feet of some of the synthesized resorcin[4]arenes.

These compounds were designed to act as guests in mycobacterial channel proteins (channel blockers). The proven host-guest interaction between resorcin[4]arenes and the mycobacterial porin MspA suggests potential application of my research in TB treatment. Both, hydrophilic nutrients and metabolites have to diffuse through the porin channels of mycobacteria because of the lack of an active transport mechanism. If these channels are successfully blocked, the mycobacteria have either to synthesize new channels, which make their outer membrane more susceptible to conventional antibiotics, or they become dormant.

(3,3'-dimethyl)-4,4'-bipyridinium units are very suitable electron relays. They can be reduced stepwise to viologen monoradical cations and then to uncharged viologen diradicals which possess highly negative redox potentials, allowing them to reduce C-Cl bonds. Therefore, the deep cavitand viologen resorcin[4]arenes, are expected to bind and detoxify chlorinated hydrocarbons by reductive dechlorination. In this work, the step wise reduction process of viologen- resorcin[4]arenes and the formation of negative redox potentials of double-reduced viologen resorcin[4]arenes are demonstrated by electrochemistry studies. These results encourage future studies toward an efficient electrocatalytic system for the reductive dehalogenation of organic compounds.

Besides highly charged resorcin[4]arene cavitands, the synthesis of a thiol-footed resorcin[4]arene was also attempted. The product was used for gold nanoparticle binding studies. The results of the photochemistry measurements provided a proof-of-concept for using the emission of gold nanoparticles in chemical sensors after covering their surfaces with thiol-footed resorcin[4]arenes.

Two heterocyclic resorcin[4]arene cavitands were synthesized for DNA-intercalation studies. The results of the photochemical measurements suggested binding between DNA and the heterocyclic resorcin[4]arenes and provided proof-of-principle for potential drug applications of this type of macrocycle.

Table of Contents

List of Figures.....	vi
List of Schemes.....	viii
List of Tables.....	x
Synthesized Structure-Number Correlation Chart.....	xi
Acknowledgements.....	xiv
CHAPTER 1 - Introduction.....	1
CHAPTER 2 - Resorcin[4]arenes as Mycobacterial Channel Blockers.....	13
· Introduction.....	13
· Synthetic Work.....	17
· Binding Investigation	26
· Experimental Session	41
CHAPTER 3 - Gold Nanoparticle-binding Resorcin[4]arene Cavitand.....	53
· Introduction.....	53
· Synthesis of Resorcin[4]arene Designed for the Binding on Gold.....	60
· Binding the tetra-thiol-substituted Resorcin[4]arene to the surface of gold nanoparticles.....	60
· Experimental Session	66
CHAPTER 4 - Towards an Organic Reduction Catalyst Based on a Resorcin[4]arene Featuring Four Viologene Units.....	69
· Introduction.....	68
· Results and Discussion	68
CHAPTER 5 - DNA-intercalating Heterocyclic Resorcin[4]arene Cavitands	77
· Introduction.....	77
· Results and Discussion	78
· Synthesis.....	81
· Experimental Session	92
Appendix A - References	96
Appendix B - ¹ H-NMR Spectra, ¹³ C-NMR Spectra and Elemental Analysis Data.....	101

List of Figures

Figure 2.1 Schematic representation of the mycobacterial cell envelope.....	15
Figure 2.2 Crystal Structure of MspA of <i>M. smegmatis</i>	16
Figure 2.3 Proposed binding Geometry of a 4-charged Fluorescent-tagged Cavitand.....	20
Figure 2.4A MspA on Mica	27
Figure 2.4B Resorcin[4]arene 20 on Mica	27
Figure 2.4C Resorcin[4]arene, bound to MspA on Mica.....	27
Figure 2.5 UV/Vis-Absorption spectrum of resorcin[4]arene 20.....	28
Figure 2.6 UV/Vis-Absorption spectrum of 17.....	32
Figure 2.7 Emission spectrum of methylcoumarinamide.....	34
Figure 2.8 Emission spectrum of the resorcin[4]arene	35
Figure 2.9 Integrated luminescence intensity of the resorcin[4]arene	36
Figure 2.10 Normalized luminescence intensity of the resorcin[4]arene.....	36
Figure 2.11 Integrated luminescence intensity of methylcoumarinamide	37
Figure 2.12 Normalized luminescence intensity of methylcoumarinamide.....	36
Figure 2.13 Luminescence spectra of coumarin-resorcin[4]arene and MspA.....	38
Figure 2.14 Luminescence spectra of coumarin-resorcin[4]arene in 0.05M phosphate	39
Figure 2.15 Monomer/excimer-ratios of the fluorescence from coumarin-resorcin[4]arene.....	40
Figure 2.16 Quotient of the monomer/excimer-ratios.....	41
Figure 3.1 Expression of MspA mutants in the mutant <i>M. smegmatis</i> ML10	53
Figure 3.2 Dimensions of the MspA-homopore	55
Figure 3.3 Adsorption of MspA (wt) on gold.....	57
Figure 3.4 Simulated absorption spectra of 50nm spherical gold nanoparticles in aqueous.....	59
Figure 3.5 Absorption spectra of gold nanoparticles	62
Figure 3.6 Emission spectra of gold nanoparticles	63
Figure 3.7 Emission spectra of gold nanoparticles	64
Figure 3.8 Supramolecular complex between the thio-footed resorcin[4]arene.....	65
Figure 3.9 Plasmon-emission occurring from thiol-feet-resorcin[4]arene.....	66

Figure 3.10 Enlargement of Figure 3.5	67
Figure 4.1 Redox-active viologen-resorcin[4]arene and dimethylviologen-resorcin[4]arene	71
Figure 4.2 DPV of viologen-resorcin[4]arene	72
Figure 4.3 DPV of dimethyl-viologen-resorcin[4]arene	74
Figure 4.4 PM3-calculations of the most stable conformations	76
Figure 5.1 Occurrence of Major and Minor Grooves in the structure of B-DNA	80
Figure 5.2 Major and Minor Groove in B-DNA.....	80
Figure 5.3 Absorption spectra of 25 and 26 in MeOH/buffer	83
Figure 5.4 Concentration-dependence of the phosphorescence	85
Figure 5.5 Stern-Volmer plot of the self-quenching of 25 in MeOH/buffer	85
Figure 5.6 Concentration-dependence of the phosphorescence of 26 in MeOH/buffer	86
Figure 5.7 Phosphorescence intensity of 26 in MeOH/buffer	86
Figure 5.8 Phosphorescence increase of 25 in the presence of DNA	87
Figure 5.9 Intensity in the phosphorescence maxima taken from Figure 5.8.....	87
Figure 5.10 PM3 of the asymmetric pyrene-bridged resorcin[4]arene	88
Figure 5.11 PM3 of the asymmetric quinoxaline-bridged resorcin[4]arene	88
Figure 5.12 Scatchard-plot generated from data shown in Figure 5.8.....	89
Figure 5.13 Phosphorescence increase of 26 in the presence of DNA	90
Figure 5.14 Intensity in the phosphorescence maxima taken from Figure 5.13.....	90
Figure 5.15 Scatchard-plot generated from data shown in Figure 5.13.....	91

List of Schemes

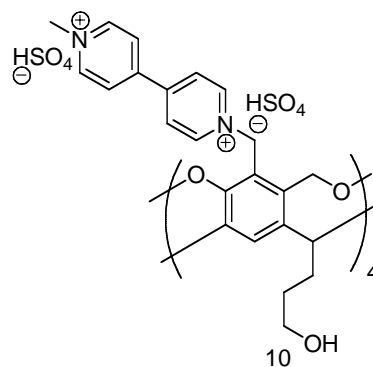
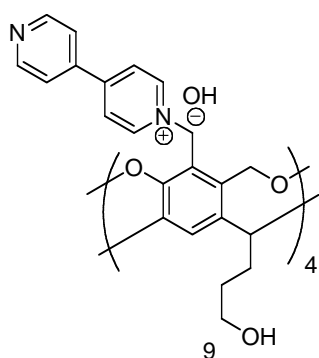
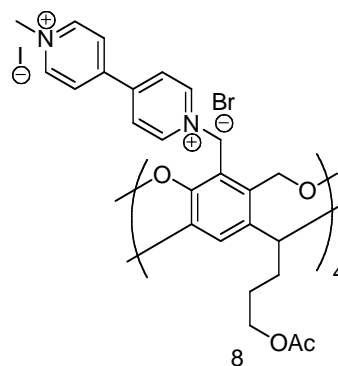
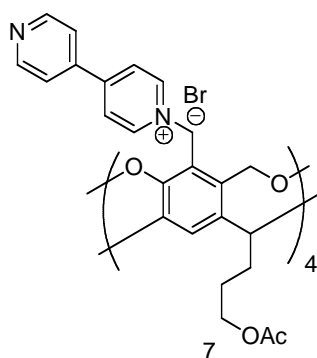
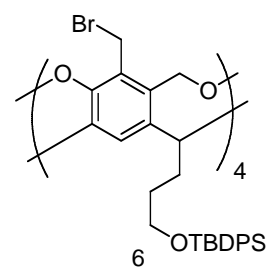
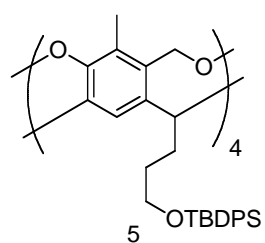
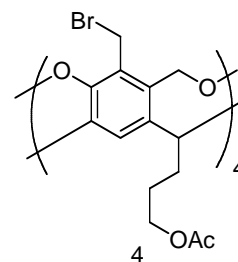
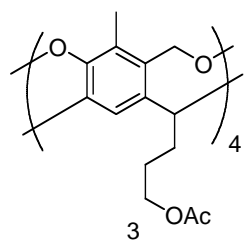
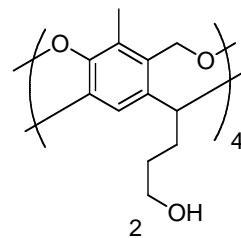
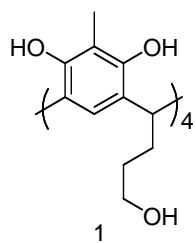
Scheme 1.1 Resorcinarenes Produced from Aliphatic Aldehydes and Resorcinol or 2-Substituted Resocinols.....	1
Scheme 1.2 Synthesis of Sherman's Water Soluble Phosphate Feet Cavitands.....	2
Scheme 1.3 Rebek's a) Assembly of Capsule and b) Encapsulated Rigioselective Cycloaddition.....	3
Scheme 1.4 A Resorcin[4]arene Cavitand Bridged by Naphthal Bromide.....	4
Scheme 1.5 Rebek's Tall Bridge Cavitand with Top Hydrogen Bonding Cyclic Seam.....	4
Scheme 1.6 Self-assembly Cavitand and a Cartoon Representation of Non-covalent Polymer Formation.....	5
Scheme 1.7 Rebek's Kite and Vase Conformation Change of Cavitands.....	5
Scheme 1.8 A Carcerplex.....	6
Scheme 1.9 Examples of Hemicarcerands.....	7
Scheme 1.10 A Hemicarcerand Bottling a Singlet Carbenen.....	7
Scheme 1.11 Warmuth's Hemicarcerand that Stabilizes 1-azacyclohepta-1,2,4,6 tetraene.....	8
Scheme 1.12 First Water-soluble Hemicarcerand.....	9
Scheme 1.13 MacGillivray's Spherical Molecular Assembly of six Cavitands Held Together by Hydrogen Bonds.....	9
Scheme 1.14 Representation of a D and A Labeled Resorcinarene Brought within FRET Distance in a Hexameric Assembly.....	10
Scheme 2.1.....	17
Scheme 2.2.....	18
Scheme 2.3.....	18
Scheme 2.4.....	19
Scheme 2.5.....	19
Scheme 2.6.....	21
Scheme 2.7.....	21

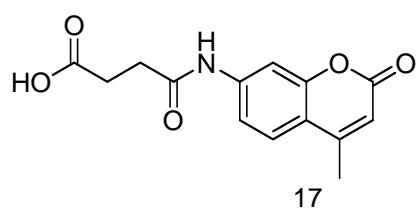
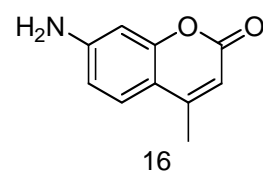
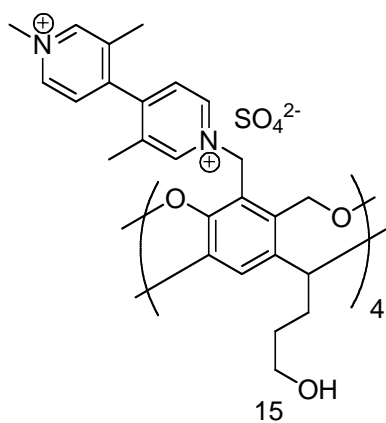
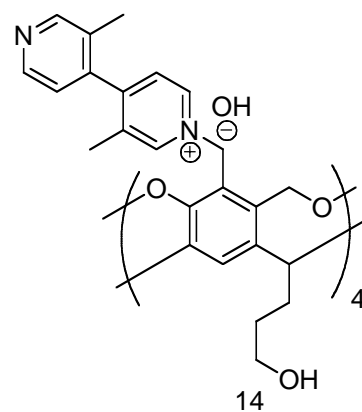
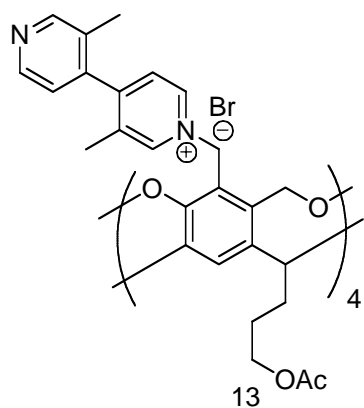
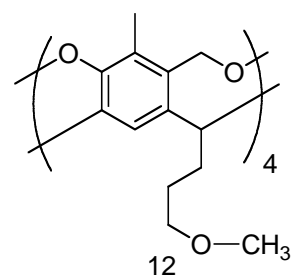
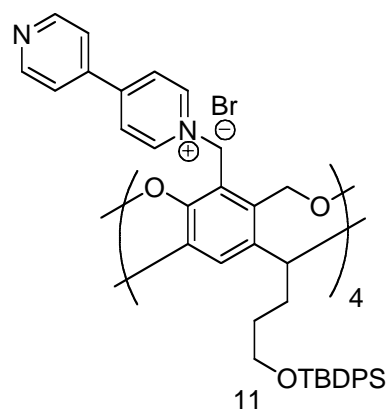
Scheme 2.8.....	22
Scheme 2.9.....	22
Scheme 2.10.....	22
Scheme 2.11.....	23
Scheme 2.12.....	24
Scheme 2.13.....	25
Scheme 2.14.....	25
Scheme 2.15 Formation of asymmetric and symmetric coumarin-excimer.....	29
Scheme 2.16 Singlet Excimer formation explained by simple MO-theory.....	30
Scheme 2.17 Jablonski-Diagram.....	33
Scheme 2.18 Singlet Excimer formation explained by simple MO-theory.....	35
Scheme 3.1.....	60
Scheme 5.1.....	82

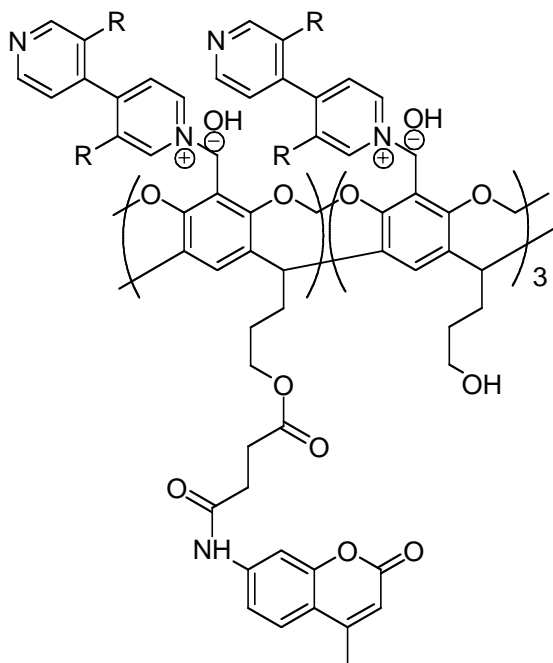
List of Tables

Table 2.1 Absorption Maxima and Absorption Coefficients of Resorcin[4]arene.....	28
Table 5.1 Structural Features of A-, B-, and Z-DNA102.....	79
Table 5.2 Absorption coefficients of 25 and 26	83

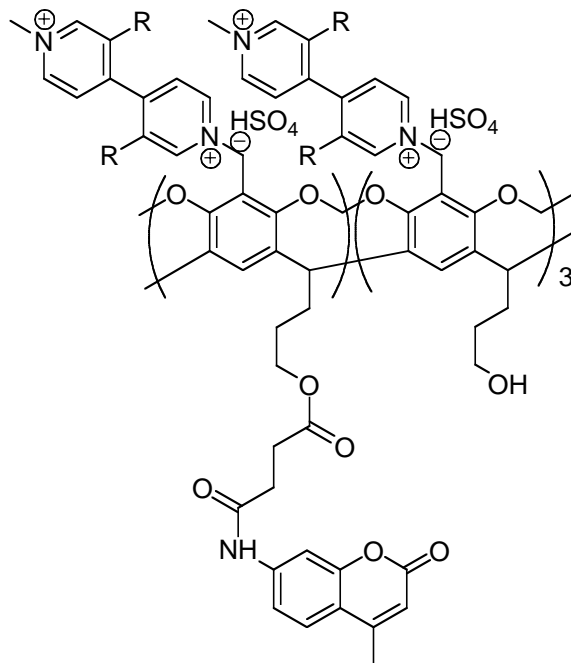
Synthesized Structure-Number Correlation Chart



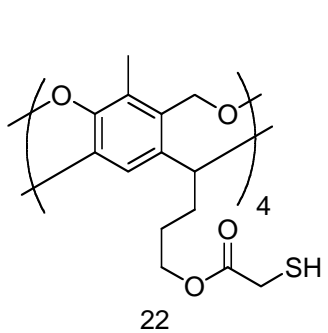




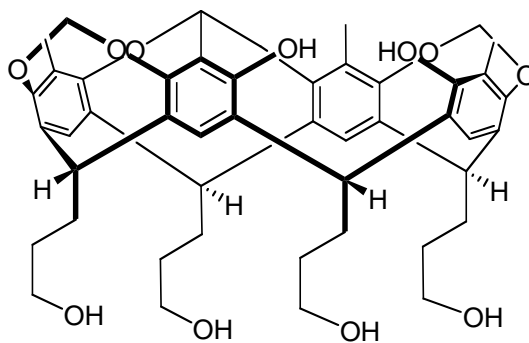
R=H : 18
R=CH₃ : 19



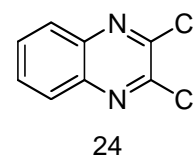
R=H : 20
R=CH₃ : 21



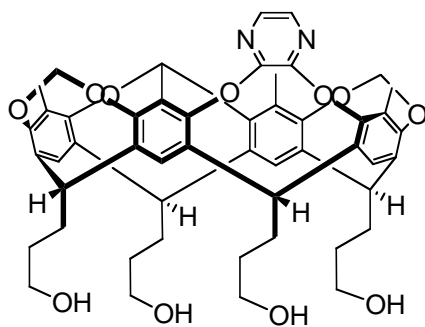
22



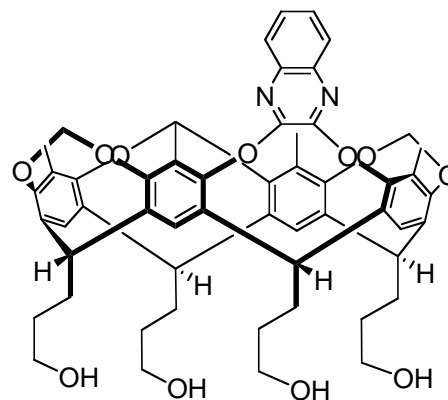
23



24



25



26

Acknowledgements

I would like to give my special thanks to my advisor, Dr. Stefan Bossmann for his warm-hearted guidance and his expert advice. Thanks also go to all my committee members Dr. Christer Aakeröy, Dr. Kenneth Klabunde, Dr. Mark Hollingsworth and Dr. Om Prakash.

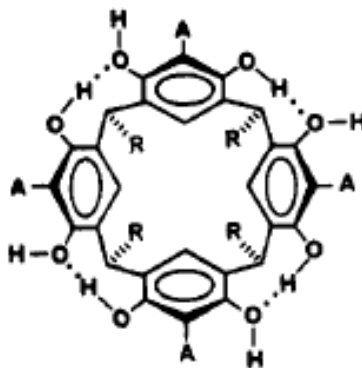
I would also like to thank my labmates. It has been my pleasure to work with you these years and I appreciate your help and support: Thilani Nishanthika Samarakoon, Pubudu Siyambalagoda Gamage, Matthew Thomas Basel, Mausam Kalita, and Tej Shrestha.

Thanks also go to the support staff at Chemistry Department of Kansas State University. Thanks for all the help during my time here.

CHAPTER 1 - Introduction

Introduction

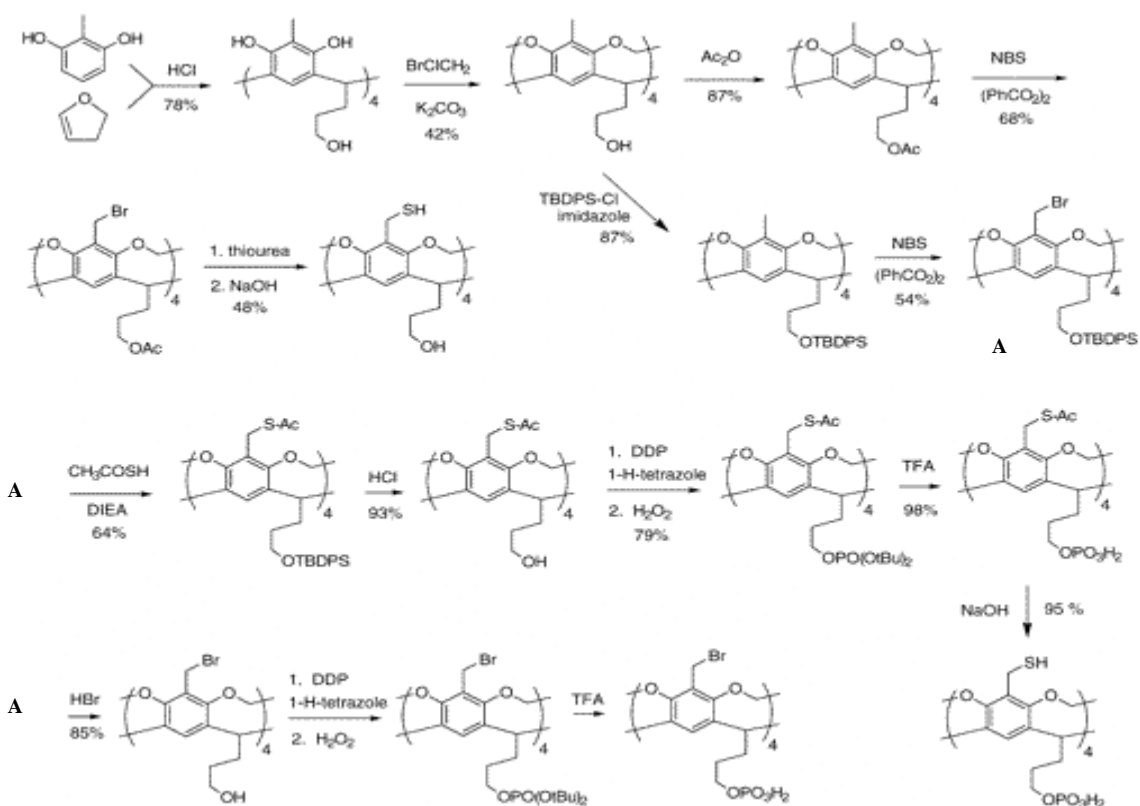
In 1980, the first resorcin[4]arene was synthesized by Sherman and coworkers by means of a condensation reaction between resorcinol and an aldehyde. The introduction of resorcin[4]arenes into the chemistry world spawned a whole new field of host-guest chemistry. Resorcin[4]arenes are “bowl shaped molecules” and have been used as molecular containers to bind small molecules via van-der-waals forces. Linking the phenol groups on neighboring aromatic rings with carbon bridges provides a more rigid cavitaⁿd. Subsequent bromination of the benzene ring between the phenol groups gives tetrabromo- cavitands that can have more possibilities of upper rim functioning. Besides upper rims, cavitands can also be modified at the feet. In Linda M. Tunstad’s early work in 1988ⁱ, resorcinarenes were condensed with 13 different feet functional groups (R) and 4 different rim functional groups (A) (Scheme 1.1).



No.	1	2	3	4	5	6	7	8	9
R	CH ₃	CH ₃ CH ₂	CH ₃ (CH ₂) ₂	CH ₃ (CH ₂) ₃	CH ₃ (CH ₂) ₄	CH ₃ (CH ₂) ₁₀	(CH ₃) ₂ CH -CH ₂	HO(CH ₂) ₄	Cl(CH ₂) ₅
A	H	H	H	H	H	H	H	H	H
No.	10	11	12	13	14	15	16	17	18
R	C ₆ H ₅ CH ₂	C ₆ H ₅ CH ₂ .CH ₂	4-O ₂ N- C ₆ H ₄ (CH ₂) ₂	4-Br- C ₆ H ₄ (CH ₂) ₂	CH ₃	CH ₃ (CH ₂) ₄	CH ₃	CH ₃	CH ₃
A	H	H	H	H	CH ₃	CH ₃	COOH	Br	NO ₂

Scheme 1.1 Resorcinarenes Produced from Aliphatic Aldehydes and Resorcinol or 2-Substituted Resorcinols¹

In 1998, Sherman published various modification of the upper rim and feet of 2-methyl resorcin[4]areneⁱⁱ. The purpose of this research was to work toward water-soluble cavitands. This aim was achieved by introducing phosphate feet (Scheme 1.2).

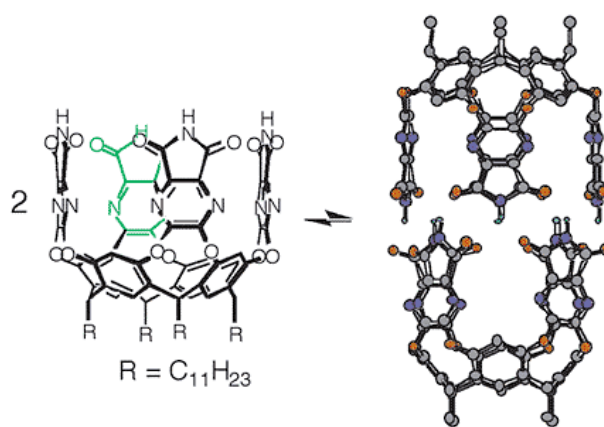


Scheme 1.2: Synthesis of Sherman's Water Soluble Phosphate Feet Cavitands²

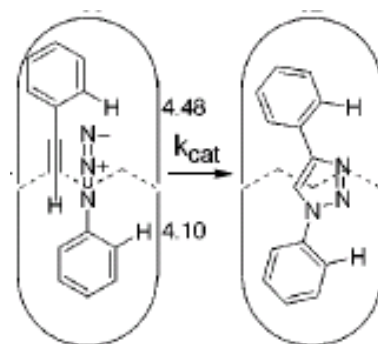
In a later publication, Sherman and coworkers achieved enhanced solubility of cavitands in water and used them for thermodynamic studies of the binding of simple guest molecules, such as ethyl acetateⁱⁱⁱ. Making cavitands water soluble remains a very important aim. It is anticipated that water soluble resorcin[4]arenes and hemicarcerands and carcerands that are based on these systems, will permit the targeted delivery of encapsulated drugs (e.g. to cancer cells or *M. tuberculosis* cells) and many other applications in areas of medicinal chemistry, bioengineering and for future bio-mimetic physical organic chemistry^{iv}.

Besides rims and feet, the bridge of cavitands can also be modified. In 1998, Rebek and coworkers synthesized a resorcin[4]arene with pyrazine-2,3, dicarboxylic acid imide bridge instead of the conventional carbon bridge^v. This cavitand is known to be deeper and capable of forming dimers via hydrogen bonds. The dimer is a capsule that is large enough to contain more

than one guest molecules. This kind of encapsulation allows synthetic reactions of two molecules that are both bound to the inner cavity (“bowl”) of the resorcin[4]arene. Interestingly, when an aromatic alkyne and an aromatic azide are encapsulated together, the constrictions of the container promotes their 1,3 dipolar addition with complete regiochemistry control^{vi} (Scheme 1.3).



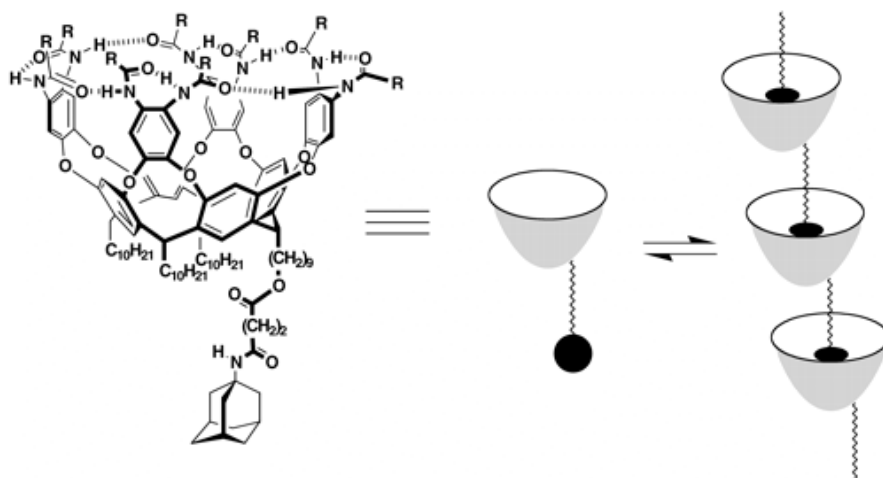
a



b

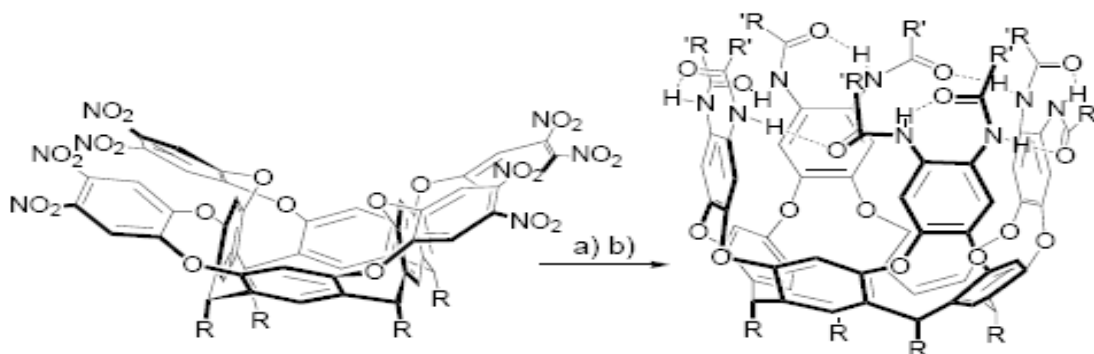
Scheme 1.3: Rebek's a) Assembly of Capsule and b) Encapsulated Regioselective Cycloaddition

There are numerous examples for synthesis within cavitands/capsules where the transition state energies of desired products are lowered while these of undesired products are raised^{vii}. Another type of deep cavitant resorcin[4]arenes is bridged by dihalides^{viii} (Scheme 1.4).



Scheme 1.6: Self-assembly Cavitaand and a Cartoon Representation of Non-covalent Polymer Formation⁹

Rebek and coworkers published a series of cavitaands with carboxymethylphosphonate-group functioned rims. The cyclic seam of hydrogen bonds between the rims helps to stabilize the vase conformation of this particular cavitaand. Interestingly, Ln^{2+} titration alters the “vase” conformation into the “kite” conformation, since the lanthanide-cations’ coordination with the C=O and P=O group disrupts the cyclic array of hydrogen bonds^x. An example of the opposite direction change of a cavitaand from the “kite” to the “vase”-conformation was also reported by Rebek^{xi} (Scheme 1.7). In the starting material (left), the repulsion among the nitro groups on the top of the cavitaand keeps it in a “kite” conformation while in the product (right), the hydrogen bonding around the seam of the upper rim holds the cavitaand in the “vase” conformation.

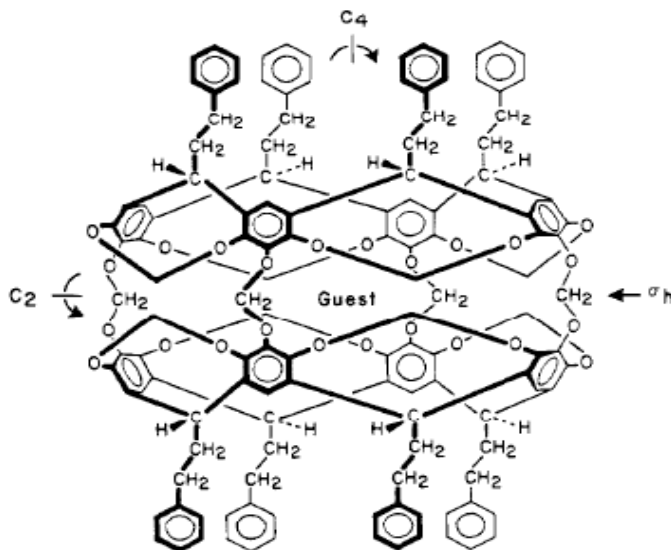


Scheme 1.7: Rebek's Kite and Vase Conformation Change of Cavitaands¹¹
 a) Raney-Ni, H_2 , toluene, 12h b) $\text{R}'\text{C}(\text{O})\text{Cl}$, K_2CO_3 , $\text{AcOEt}/\text{H}_2\text{O}$ 1:1, r.t. 2h



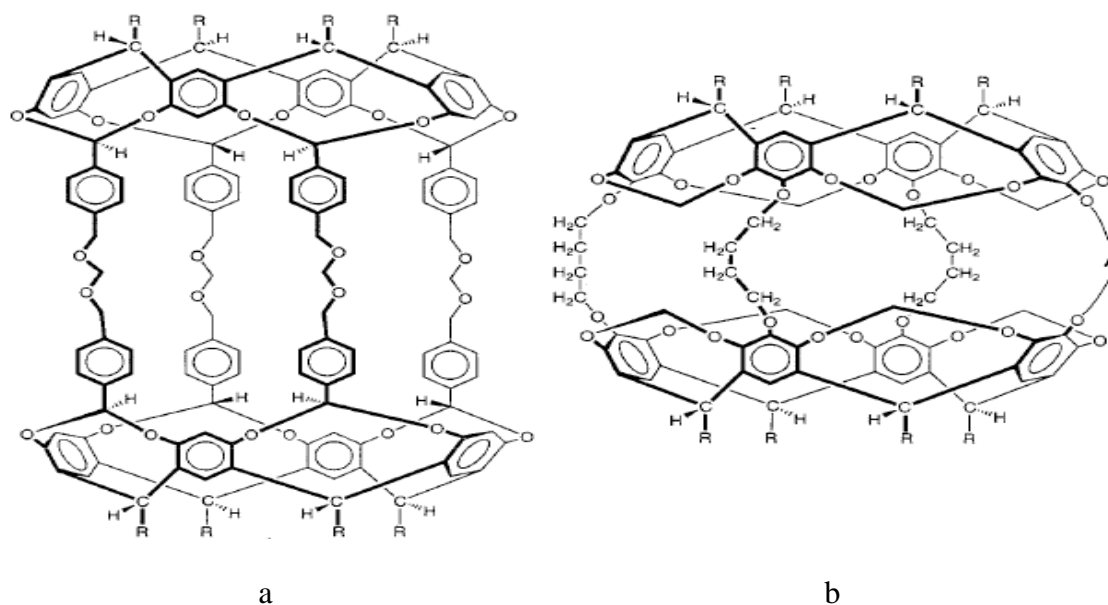
An up to date summary of deep cavitands and water soluble cavitands was published by Shannon, Biro and Rebek in 2007^{xii}.

In 1985, Cram for the first time created a closed surface with two cavitands. The resulting organic structure is called a carcerand^{xiii}. As already stated, the carcerand is able to encapsulate small organic molecules to form a carceplex, whose interior is a new phase of matter^{xiv} (Scheme 1.8).



Scheme 1.8: A Carcerplex¹⁴

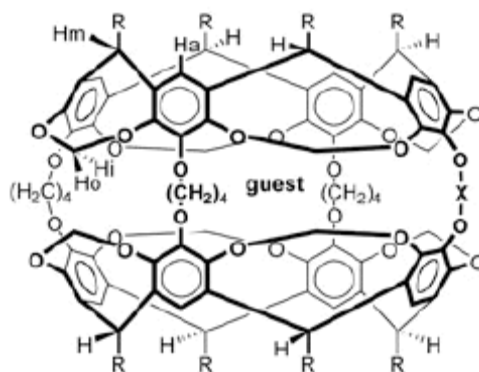
Carceplexes are often extremely stable and, therefore, they don't release their cargo that easily. However, the release of guest molecules from a carcerand will be required for any successful application of drug-delivery. In 1991, Cram published the synthesis of a similar molecular container, which is called hemicarcerand, that allows guest exchange and/or the release of bound organic molecules^{xv}. To date, various derivatives of hemicarcerands that consist of two linked resorcin[4]arene cavitands have been synthesized. Linking of two resorcin[4]arenes can be achieved by covalent or non-covalent linking, either by suitably derivatized feet or bowl structures^{xvi} (Scheme 1.9)

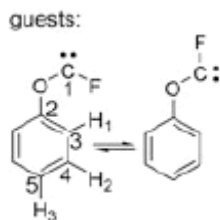


Scheme 1.9: Examples of Hemicarcerands¹⁶ a) $R=CH_2CH_2Ph$ b) $R=CH_2CH_2C_6H_5$ $A=H$

Different sizes of hemicarcerplexes have been synthesized and numerous host-guest studies have been successfully carried out, such as hemicarcerplex self-assembly studies, reactive intermediates studies^{xvii} and studies of reaction kinetics occurring within the hemicarcerands^{xviii}.

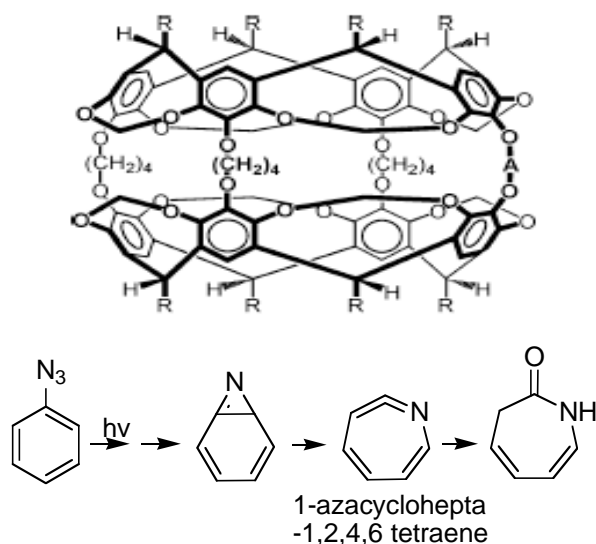
A noteworthy example of a study of an otherwise very reactive intermediate is the incarceration of fluorophenoxy carbene in a hemicarcerand^{xix} (Scheme 1.10). The incarceration prevents the carbenes' dimerization reaction and its reaction with water molecules that belong to the bulk phase and, therefore, cannot enter the hemicarcerand. Therefore, incarcerated fluorophenoxy carbenes can persist at room temperature for days. A suitable hemicarcerand for "bottling" a singlet carbene has to provide a good fit for the guest carbene and it needs to be unlikely to promote C=C addition between itself and the guest carbene.





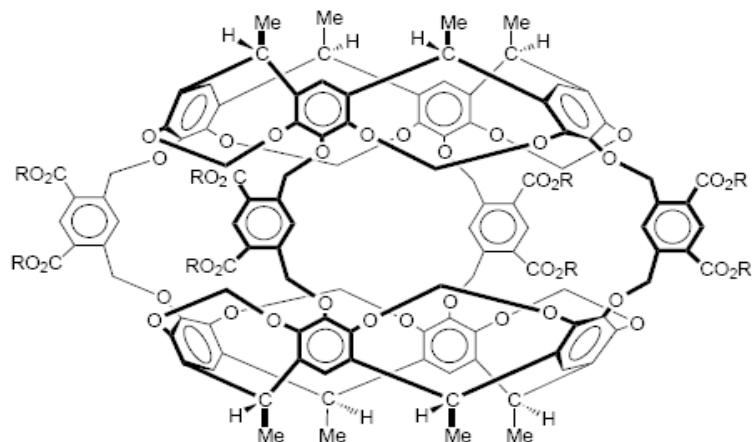
Scheme 1.10: A Hemicarcerand Bottling a Singlet Carbenen¹⁹ $R=(CH_2)_4CH_3$ $X=(CH_2)_4$

Besides the binding and stabilization of carbene, other reactive intermediates can be bonded and stabilized inside a hemicarcerand as well. Warmuth and coworkers published the NMR characterization of the strained intermediate 1-azacyclohepta-1,2,4,6 tetraene, which was formed by the photolysis of benzyl azide, in the inner phase of a hemicarcerand^{xx} (Scheme 11).



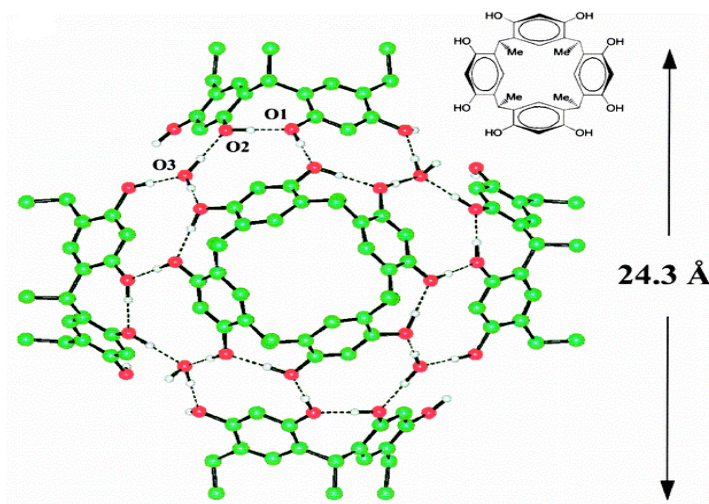
Scheme 1.11: Warmuth's Hemicarcerand that Stabilizes 1-azacyclohepta-1,2,4,6 tetraene²⁰
 $R=(CH_2)_4CH_3$ $A=(CH_2)_4$

The first water-soluble hemicarcerand was reported by Cram and Yoon in 1997^{xxi} (Scheme 1.12). However, it is only soluble in basic aqueous media. Since the major parts of cavitands and hemicarcerands are hydrophobic, the limited water solubility of these molecules is still impeding many bio-mimic and (micro) biological applications and studies of complete structure-solvent relationship between these molecules and water.



Scheme 1.12: First Water-soluble Hemicarcerand²¹

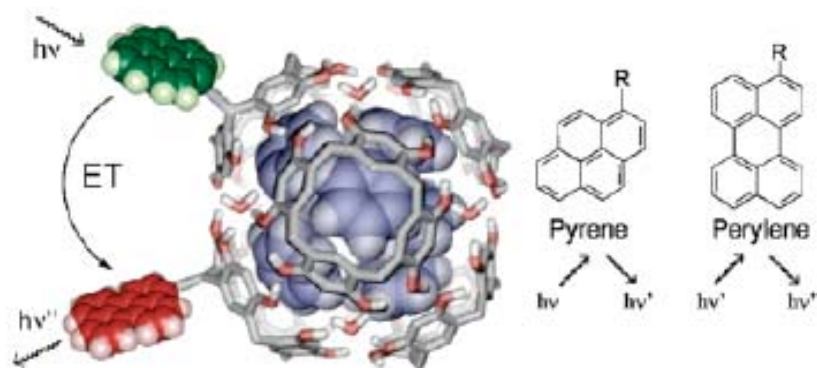
It is noteworthy that resorcin[4]arene capsules can also be formed by more than two cavitands. In 1997, MacGillivray and Atwood reported the self-assembly of six bowls via hydrogen bonding^{xxii} (Scheme 1.13), capable of enclosing 8 water molecules.



Scheme 1.13: MacGillivray's Spherical Molecular Assembly of six Cavitands Held Together by Hydrogen Bonds²²

This study was followed by a thorough kinetic and thermodynamic study of similar hexameric capsules with different alkyl feet encapsulating one tetraalkylammonium salt in solution by Rebek and coworkers^{xxiii}.

To study the encapsulation process and dynamic behavior of the resorcin[4]arene, Rebek and coworkers linked fluorescent tags to the feet of resorcin[4]arene monomers. Pyrene donor tags and perylene acceptor tags were separately linked to the feet of different cavitands. When two cavitands with different tags are in the same hexameric capsule, fluorescence resonance energy transfer (FRET) is observed (Scheme 1.14). This team of authors also studied the FRET between a guest donor inside the hexameric capsule and a receptor tag linked to the surface of the capsule^{xxiv}.



Scheme 1.14: Representation of a D and A Labeled Resorcinarene Brought within FRET Distance in a Hexameric Assembly. Pyrene and Perylene are the Donor and Acceptor Fluorophores, Respectively²⁴.

Motivation for my thesis work and synthetic aims

1) As I have pointed out above, the synthesis of water-soluble resorcin[4]arenes, which can be easily derivatized to bind a suitable guest, is one of the major challenges in the field. Hydroxy-footed resorcin[4]arenes, which contain several charges, should have superior solubility properties in water, compared to these resorcin[4]arenes, which only feature hydroxyl pendant groups. Therefore, I have explored new synthetic routes to prepare water-soluble resorcin[4]arenes.

2) Another major synthetic challenge is the introduction of a suitable chemical function for the binding of gold and other inorganic nanoparticles. Numerous strategies for the synthesis of water-soluble nanoparticles by using hydrophilic ligands that bind to the surface of the nanoparticles during synthesis (e.g. reduction in microheterogeneous media, Solvated Metal Atom Dispersion (SMAD) or digestive ripening, are known. In many of these procedures, the

size of the resulting inorganic nanoparticles is usually not independent of the chemical nature of the stabilizing ligand. Therefore, the exchange of a stabilizing mono-dentate ligand by a tetra-dentate resorcin[4]arene at room temperature (or slightly above) may preserve the size of the nanoparticles after their synthesis had been tailored according to the needs of future applications. Furthermore, the pendant group (“feet”) and the rim-regions of resorcin[4]arenes can be derivatized independently of each other, resulting in bifunctional octa-dentate molecules. One region of the resorcin[4]arene (feet or rim) can be bound to the inorganic nanoparticle, whereas the other can achieve the chemical linkage of the nanoparticle@resorcine[4]arene-assembly to a protein or another biological structure of interest.

3) There are numerous examples known from the literature (see above), where resorcine[4]arenes, hemicarcerands and carcerands act as hosts for reactive organic molecules. In the course of my thesis, I wanted to explore possible reactions between a suitable resorcine[4]arene and guest. Since my synthetic efforts to enhance the water-solubility of resorcin[4]arenes led to 4,4'-bipyridinium-derivatized macrocycles, it was straightforward to use the electron-relay capability of these “viologen-units” for electron-transfer reactions. This work has been guided by the mechanistic paradigm that the binding of chlorinated hydrocarbons within the resorcin[4]arene cavity will lead to their enhanced reactivity in thermal reduction reactions. The electrons will be taken up by the viologen-units, which are a part of the resorcin[4]arenes' rim. From there, outer-sphere electron transfer reactions to the guests will occur, depending on the electrochemical reduction potentials of the bound guests and the viologene-units.

4) The use of resorcin[4]arenes as drug-containers has been studied extensively. However, their use as drugs had not been attempted at the beginning of our studies. It was my strategy to modify water-soluble resorcine[4]arenes with DNA-intercalating heterocyclic units. Binding of these macrocycles at DNA will impede the activity of DNA-binding enzymes, such as DNA-polymerase, DNA-ligase and the topoisomerases I and II.

5) Although the use of resorcin[4]arenes as host systems was reported numerous times (indeed this system had be designed as a host!), their use as guest has not been reported to date to the best of our knowledge! One interesting application of cationic resorcin[4]arenes is their use

as mycobacterial channel blockers. I have used viologen-derivatized resorcin[4]arenes possessing propanol feet for binding studies within the mycobacterial model porin MspA from *Mycobacterium smegmatis*. The concept of channel blocking can be regarded as a novel strategy for treating mycobacterial infections. For studying the binding characteristics within the mycobacterial protein channel, a coumarin-fluorophore was chemically attached to one of the resorcin[4]arene's feet.

CHAPTER 2 - Resorcin[4]arenes as Mycobacterial Channel Blockers

Introduction

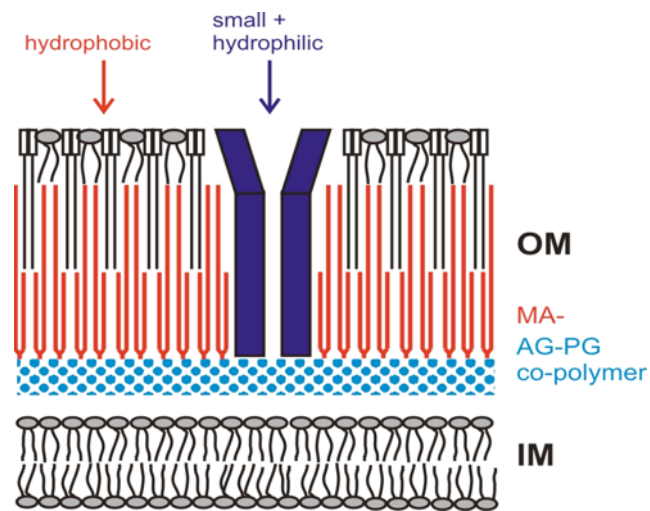
In resorcin[4]arene cavitands host-guest chemistry, the cavitands have always been used as the host, but never as the guest. The tunable vase-kite conformations can actually make it possible to use these cavitands as flexible guests in bigger cavities, and the charged upper rim of resorcin[4]arene cavitands can bring potential selectivity toward hosts that bears opposite charges.

Tuberculosis and the Mycobacterial Cell Envelope

Mycobacterium tuberculosis, which lives in humans since at least 5,000 B.C., causes more deaths than any other single bacterial infection^{xxv}. Approximately one third of the world's population is already infected. More than 2,000,000 deaths have to be accounted for each year.²⁵ During the last two decades, multi-resistant strains have appeared due to the discontinuing treatment of tuberculosis in many countries, threatening all countries which experience immigration.²⁵ A successful treatment of a multi-resistant case of tuberculosis (MDR-TB) requires up to 6 different antibiotics and 18-24 months of continuing care. In the United States, the typical costs per patient with MDR-TB are approximately \$200,000. Since no new TB drug has been developed in the past 40 years using classical methods, it is believed that new strategies are required for TB drug discovery.^{xxvi} Our approach aims to understand the fundamental basis of drug transport which often limits the efficiency of existing drugs against *M. tuberculosis*. To this end, we describe here the biophysical characterization of the cell surface of *M. tuberculosis*. It is envisioned that current and new TB treatment strategies will profit from these results. Mycobacteria are known to possess an extremely stable and unique outer membrane that has an extremely low permeability and plays a crucial role in the intrinsic drug resistance and in survival of mycobacteria under harsh conditions.²⁹ Therefore, the aim of this study was to analyze the outer membrane of *M. tuberculosis* by AFM.

Biological background: Mycobacteria form a Unique Outer Membrane

Mycobacteria produce mycolic acids that are α -branched β -hydroxy fatty acids consisting of up to 90 carbon atoms and are the longest fatty acids known in nature.^{xxvii} Minnikin originally proposed that the mycolic acids, which are covalently bound to the arabinogalactan-peptidoglycan co-polymer, form the inner layer of a unique outer membrane (OM) (Figure 2.1A).^{xxviii} In addition, the mycobacterial cell envelope contains a fascinating diversity of other lipids, many of which are unique to mycobacteria.^{xxix} Some of these extractable lipids were shown to be an important part of the OM and are assumed to form the outer leaflet of this unique OM (e.g. TDM, Figure 2.1B).²⁶ Thus the mycobacterial OM resembles a supported asymmetric lipid bilayer and provides an extraordinarily efficient permeability barrier, which is 100 to 1000-fold less permeable than that of *E. coli*.^{xxx} The existence of an additional lipid bilayer requires a set of dedicated OM proteins. *E. coli* uses more than 60 proteins to functionalize its OM^{xxxi}, many of which are channel proteins to permeabilize the membrane for nutrient transport. The observation³¹, discovery^{xxxii} and structural analysis of mycobacterial porins^{xxxiii} provided the first conclusive example that functionally similar, but structurally completely different OM proteins also exist in mycobacteria. Whereas the porins determine the permeability of the mycobacterial OM for hydrophilic substances, the extremely hydrophobic and covalently bound mycolic acids form the so-called cell-wall-skeleton. Mycobacteria are able to synthesize a fascinating variety of mycolic acids, more than 500 different structures are known to date.²⁷ Together they form an almost impenetrable cell wall.



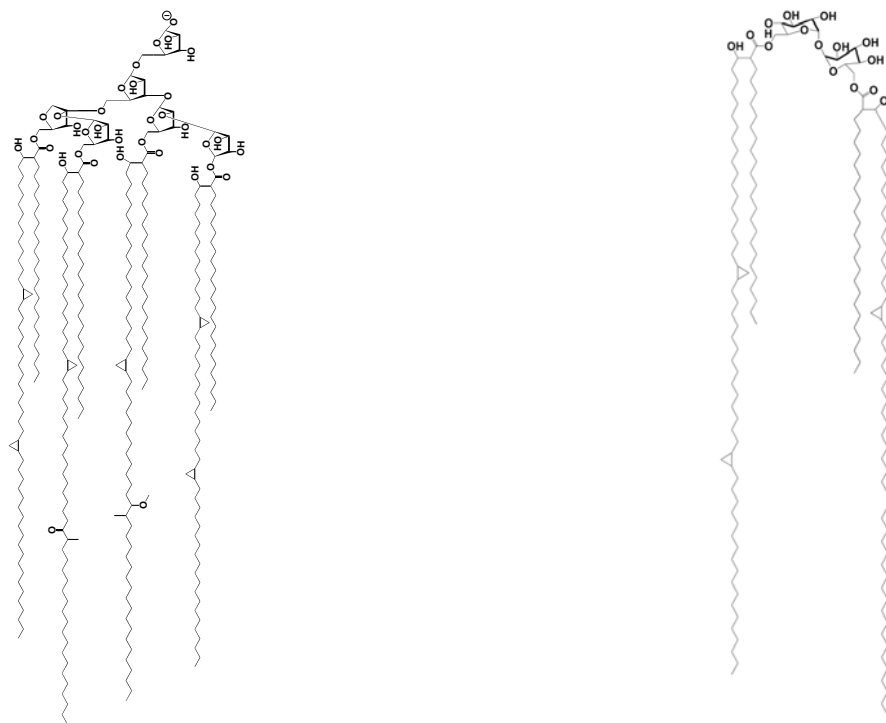


Figure 2.1: A (top): Schematic representation of the mycobacterial cell envelope, based on the model proposed by Minnikin.²⁷ The inner leaflet of the outer membrane (OM) is composed of mycolic acids (MA), which are covalently linked to the arabinogalactan (AG) – peptidoglycan (PG) copolymer. B (bottom): A variety of extractable lipids presumably form the outer leaflet of the OM exists. Left is general structure of AG, right is trehalose dimycolate (TDM), a typical extractable lipid from the OM of mycobacteria.^{xxxiv}

As shown in Figure 2.1A, the outer layer of the mycobacterial cell envelope is approximately 10nm in diameter. It consists of mycolic acids (see Figure 2.1A), which are covalently attached to an arabinogalactan-peptidoglycan copolymer (AG-PG). A fraction of these mycolic acids, as well as a variety of other lipids, is extractable as well (see Figure 2.1B). Mycobacterial channel porins permit the exchange of hydrophilic molecules between the exterior of the mycobacterium and the periplasm. MspA from *M. smegmatis* was the first channel protein, which was isolated by the group of Dr. Michael Niederweis in 1999.³² MspA has a goblet shaped inner channel and consists of 8 protein monomers with 184 amino acid residues each. It is extremely stable and approximately 10nm in length and 9 nm in diameter. Its inner diameter is approximately 1nm at the constriction zone and 4.8nm at the broadest region. The MspA porin can be regarded as a prototype for all mycobacterial channels. It is very important for the understanding of the slow metabolism of mycobacteria in general that the mycobacterial porins

allow the exchange of small molecules and hydrophilic solutes between the exterior of the periplasm by diffusion controlled processes only! There is no active transport mechanism discernible and the porins are water-filled at all times! MspA is the only mycobacterial porin that can be purified in milligram quantities and using microscopic buffer droplets, it can easily deposit on surfaces.^{xxxv}

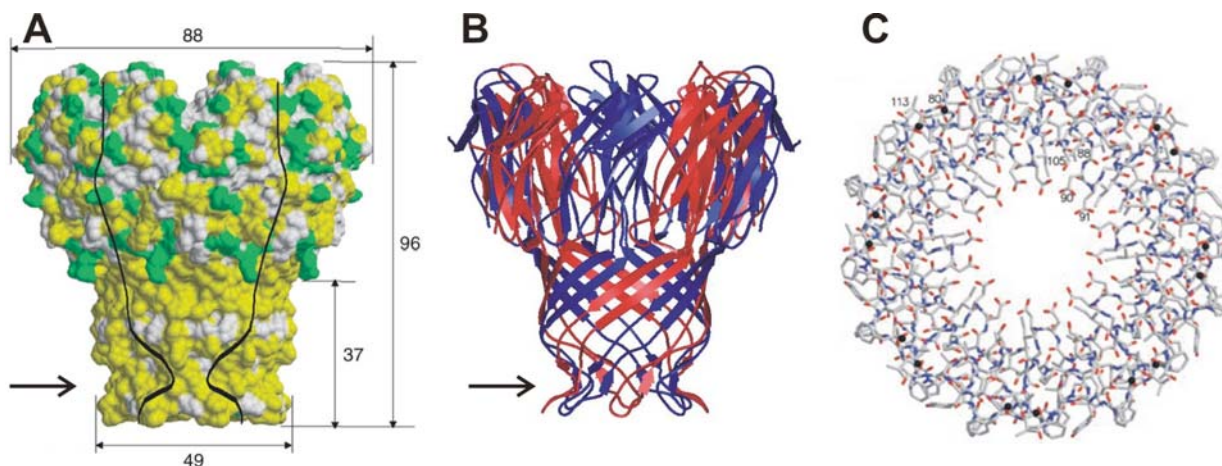


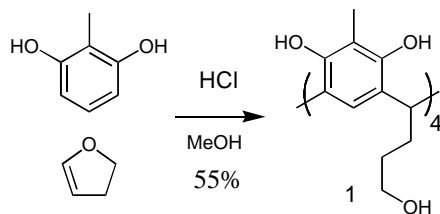
Figure 2.2: Crystal Structure of MspA of *M. smegmatis*. A. Surface representation (side view). green: hydrophilic amino acids; yellow: hydrophobic amino acids; dimensions given in Å. B. Secondary structure (side view). Arrows depict the constriction zone. C. Constriction zone formed by aspartates 90 and 91 (top view)^{33b}

I have developed a series of partially and fully water soluble resorcin[4]arene cavitands. These cavitands are soluble in neutral water and their solubility is caused by 4 or 8 positive charges of the bipyridinium units that are connected to the upper rim of the cavitand. Among these charged cavitands, two possessing hydroxyl feet are completely water-soluble (solubilities $> 50\text{g L}^{-1}$). The charge repulsion between the bipyridine units locks the cavitand in a kite conformation. This kind of charged kite cavitands can potentially be used as channel blocker for porins by fitting into their hydrophilic and negatively charged inside walls. This appears to be a viable strategy to kill mycobacteria, especially *M. tuberculosis*, by starvation or metabolic poisoning. Also, after all the existing porins in the cell membrane are blocked, the bacteria might open up more pores to compensate the blockage, which might make the cell wall structure fragile and more liable to the attack of antibiotics.^{xxxvi} In order to investigate the binding of the charged cavitand within the porin, I have attached a fluorescent coumarin tag to one of the hydroxyl feet of the cavitand.

Synthetic Work:

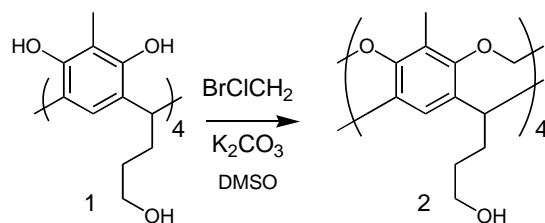
Part of the synthetic work described in this chapter is based on an article by J. C. Sherman published in 1998 in the Journal of Organic Chemistry.²

The goal of this project was to synthesis a series of water soluble new resorcin[4]arene cavitands that bear positive charges on the rim and hydroxyl groups on the feet for fluorescent tags addition. For this purpose, a feet protected cavitand was synthesized and the 2-methyl rim was brominated for future SN₂ functionalization. The unbridged cavitand **1** condensed, according to Sherman's procedure², except that, the 2,3-dihydrofuran was added over 3 minutes period into the methanol-HCl solution of 2-methyl resorcinol while the solution was cooled in ice bath and vigorously stirred at the same time. When the reaction was ran under air, the yield was not different from when it was ran under nitrogen, so this step is not air sensitive. The driving force for the equilibrium to shift right is the precipitation of the product. Since non-water soluble byproducts are dissolved in the methanol solution after the reaction is done, it is essential to filter out precipitate in a dry state before water and THF wash.



Scheme 2.1

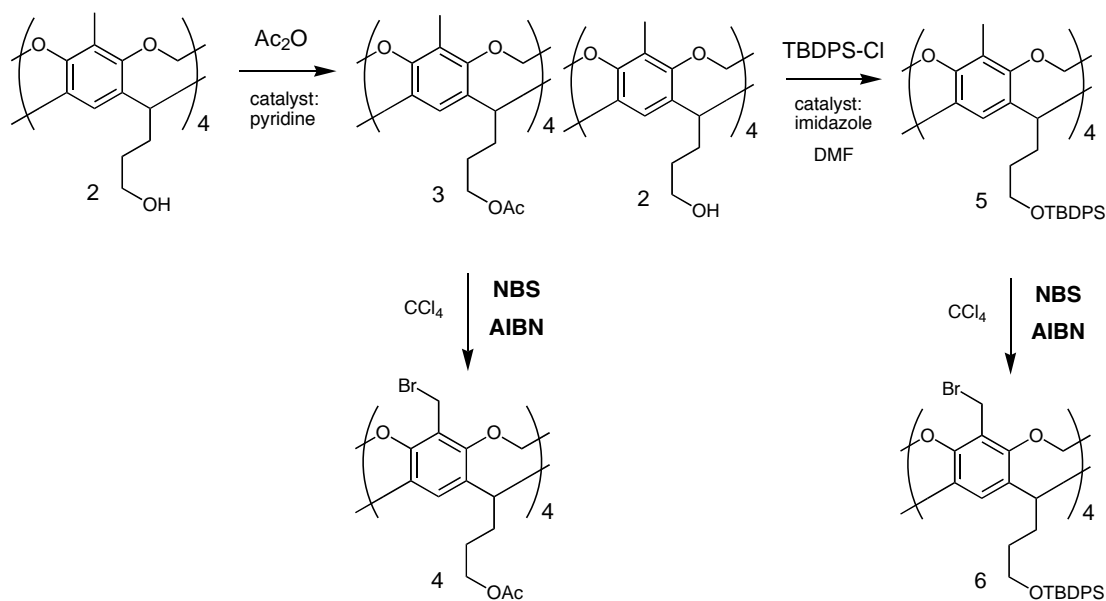
The next step is to connect the upper part of the cavitand **1** with methylene bridges via SN₂ reaction to give cavitand **2**. Bromochloromethane was chosen as bridging reagent and potassium carbonate as the base to deprotonate the phenols. In this reaction, bridging reagent need to be added gradually to avoid formation of “over functionalized open top product”. Also it is preferred to add bridge reagent when the reaction mixture is cooled to room temperature. The reaction is air sensitive because the phenol can be easily oxidized under basic conditions. Although water molecules would destroy some bridging reagents, it wouldn't result in any supramolecular byproducts, so ACS grade solvent can be used instead of anhydrous solvent.



Scheme 2.2

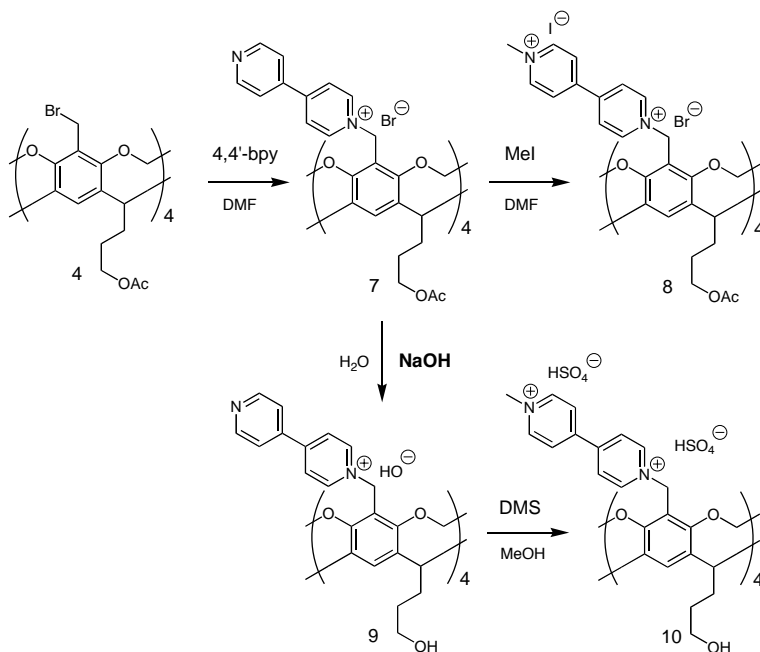
After adding methylene bridges, acetyl or TBDPS protection groups were installed onto the hydroxyl feet of cavitand **2** to give cavitand **3** and **5**. TBDPS group is very non polar and can greatly drop the polarity of the cavitand and increase its solubility in not so polar solvents.

The bromination of cavitand **3** and **5**, which give cavitand **4** and **6** were carried out via free radical reaction with benzoyl peroxide or AIBN as initiator. Bromination of cavitand **5** is harder than bromination of cavitand **3** possibly due to steric hindrance of TBDPS group. To succeed in bromination of cavitand **5**, solvent carbon tetrachloride needs to be distilled before using to exclude radical scavenger species, the reaction mixture need to be strictly water and air free and it is preferred to bring the reaction mixture to reflux as quickly as possible.

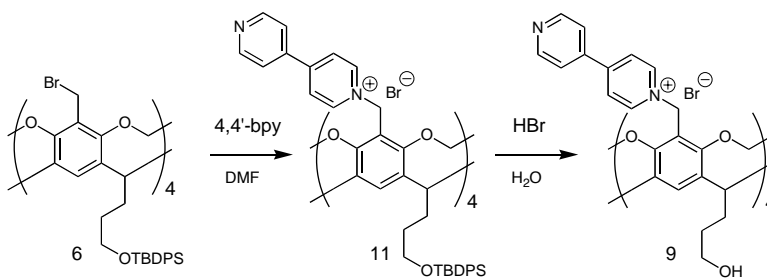


Scheme 2.3

After finishing synthesis of literature reported compounds, I started installing positive charges on the rim of the cavitands by S_N2 reaction between bipyridine molecules and the brominated rims. Four charged cavitands **7** and **11** can be obtained by heating cavitand **4** and **6** with 8-10 fold of 4-4' bipyridine in DMF for 3-5 days. The charged cavitands with increased depth are more likely to bind with small solvent molecules like water, acetone and DMF. And due to their high polarity it is impossible to purify the product by column chromatography.



Scheme 2.4



Scheme 2.5

Because of the charge repulsion among the four bipyridine units, the rim of the charged cavitands adopts the kite conformation which has a biggest diameter of 2.5nm. The diameter is suitable for binding in MspA channel right above its constriction zone with the

hydrophilic bipyridine units pointing down at the hydrophilic inside wall of the bottom part of MspA and the hydrophobic cavitand skeleton upward at the hydrophobic inside wall of the upper part of MspA. The hydrophilic inside wall of MspA also contains negative charges from Asp under neutral pH conditions, which is another reason for the affinity between MspA channel and the positively charged cavitands. After addition of a coumarin tag on one foot, a 4-charged cavitand is proposed to bind inside MspA as Figure 2.3 indicates.

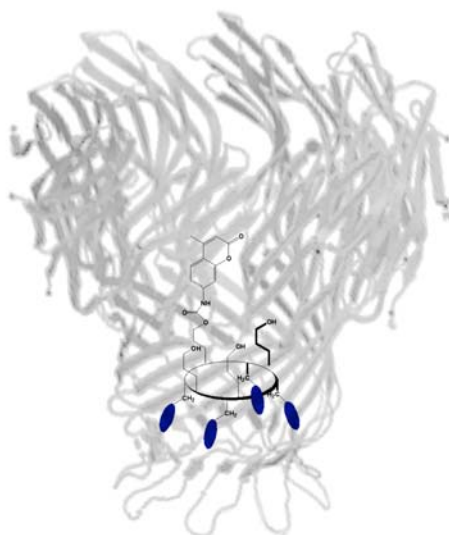
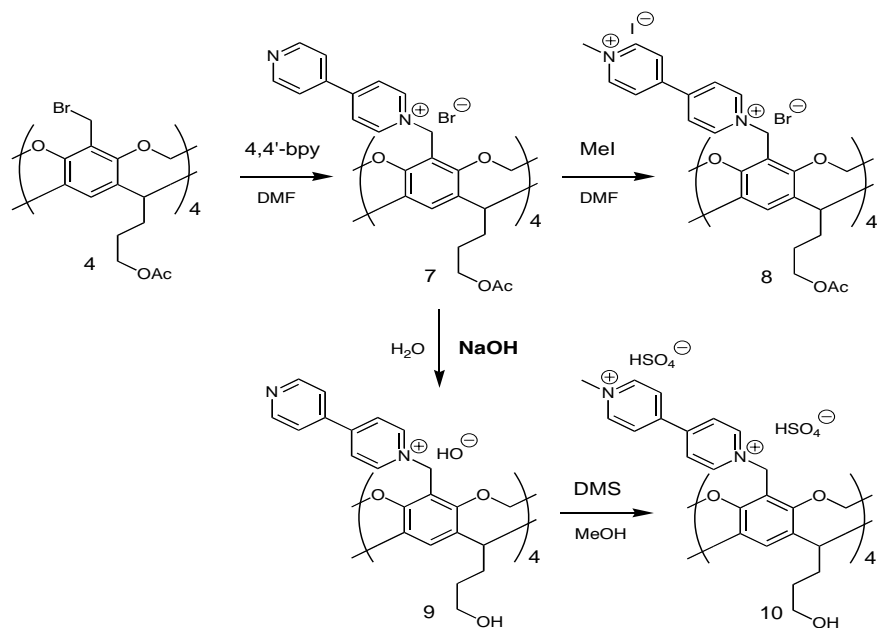


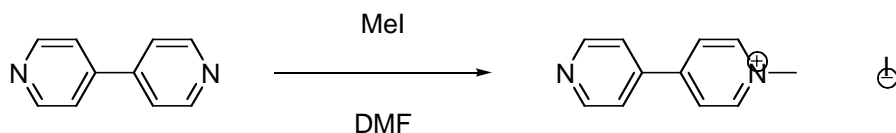
Figure 2.3: Proposed binding Geometry of a 4-charged Fluorescent-tagged Cavitand in MspA Channel

In order to get higher cavitand-MspA affinity, eight charged cavitands **8** and **10** were also synthesized.



Scheme 2.6

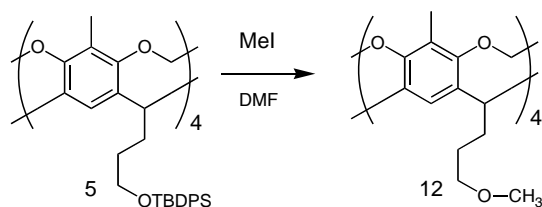
For acetyl protected cavitands, eight-charged derivative can be obtained by either reacting four-charged cavitant **7** with excess amount of methyl iodide, or reacting cavitant **4** with four folds of (N-methyl 4, 4' bipyridine) for longer time or in pressure reactor. N-methyl 4, 4' bipyridine was made from 4,4'-bipyridine and methyl iodide and purified by ethanol extraction.



Scheme 2.7

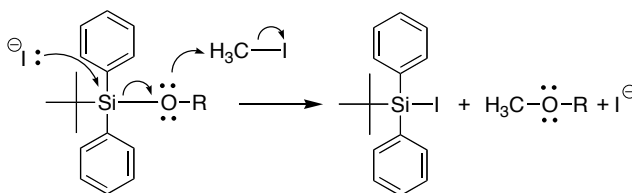
Cavitant **7** can be easily deprotected by sodium hydroxide water solution pH=10. Cavitant **11** can be deprotonated by 10% HBr water solution. In this reaction, if methanol is added to the solution to increase the solubility of the cavitant **11**, polymer is recovered as product. Eight charged hydroxyl feet cavitant **10** was synthesized by treating cavitant **9** with dimethyl sulfate. Synthesis for eight charged TBDPS protected cavitant has been attempted by reacting cavitant **11** with methyl iodide and resulted in (N,N dimethyl 4, 4'-bipyridine) as the only charged organic compound after acetone wash. The cavitant moiety was not isolated. In

order to shine some light on what might have happened to the TBDPS protection group after methyl iodide treatment, a test reaction was conducted.



Scheme 2.8

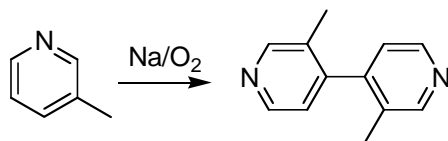
Cavitand **5** was mixed with excess of methyl iodide in DMF and gently heated. Methylated cavitand **12** was isolated as one of the products. The proposed mechanism is as follows.



Scheme 2.9

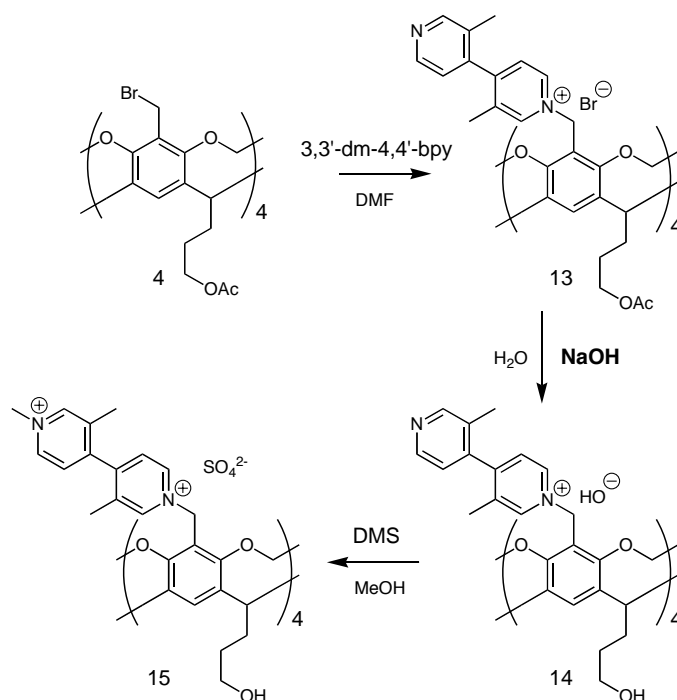
Since this reaction results in a mixture of multiple compounds that are difficult to separate even after proceeding for a long time, it is not recommended to use this reaction for methylation synthesis.

Besides 4,4'-bipyridine, (3,3'-dimethyl)-4,4-bipyridine was also used to introduce charges onto cavitand rims. The charged (3,3'-dimethyl)-4,4-bipyridinium cavitands are a little less polar and more hydrophobic. (3,3'-dimethyl)-4,4-bipyridine was synthesized through slow air oxidation of 3-picoline and sodium mixture. Sodium metal was first put into distilled neat 3-picoline, the mixture was heated gently till all sodium dissolved, and slow air oxidation was conducted for a week.



Scheme 2.10

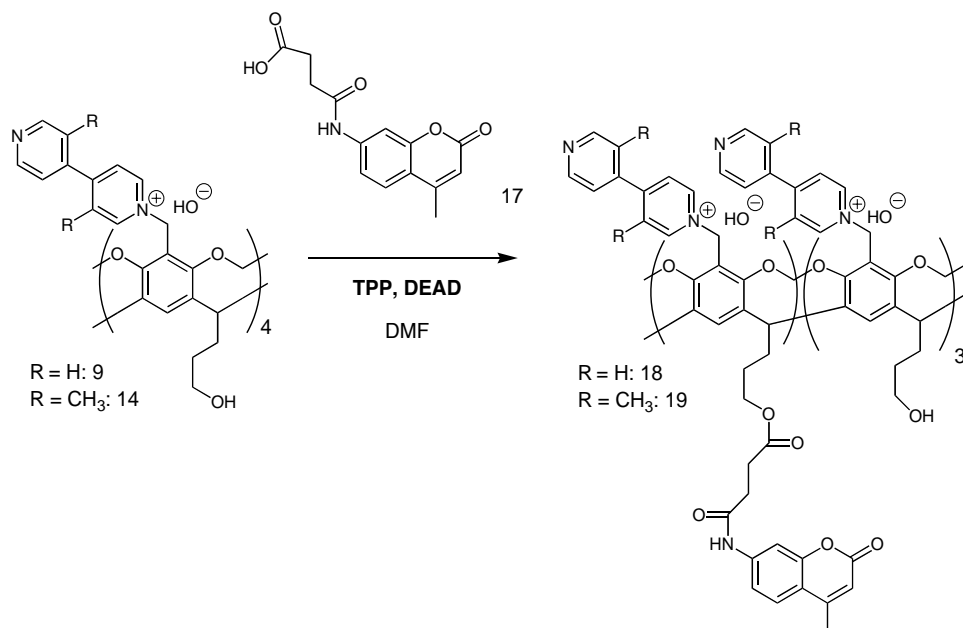
Synthesis of (3,3'-dimethyl)-4,4-bipyridinium cavitands is similar to 4,4-bipyridinium cavitands, but to synthesize 8-charged cavitand **15**, only dimethyl sulfate method was used. Methyl iodide is not suitable because the I resulted from SN₂ reaction could serve as an electron source to reduce the bipyridine unit.



Scheme 2.11

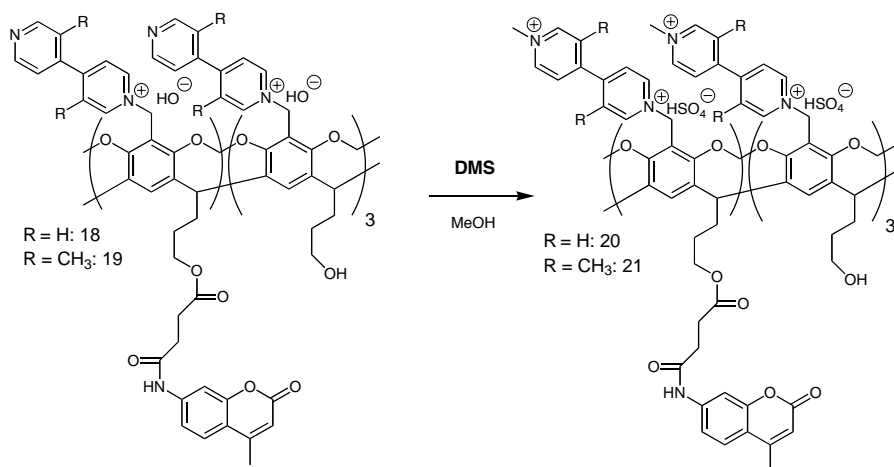
The hydroxyl feet charged cavitands are fully water soluble (solubility >50g/L) in neutral pH pure water. And this is an important property for future biology or biomimic applications.

In order to study the binding of charged cavitands and MspA, a fluorescent coumarin tag was attached to one of the four hydroxyl feet of either cavitand **9** and cavitand **10**. The attachment was made through Mitsunobu reaction between one hydroxyl foot and one coumarin molecule **17**.



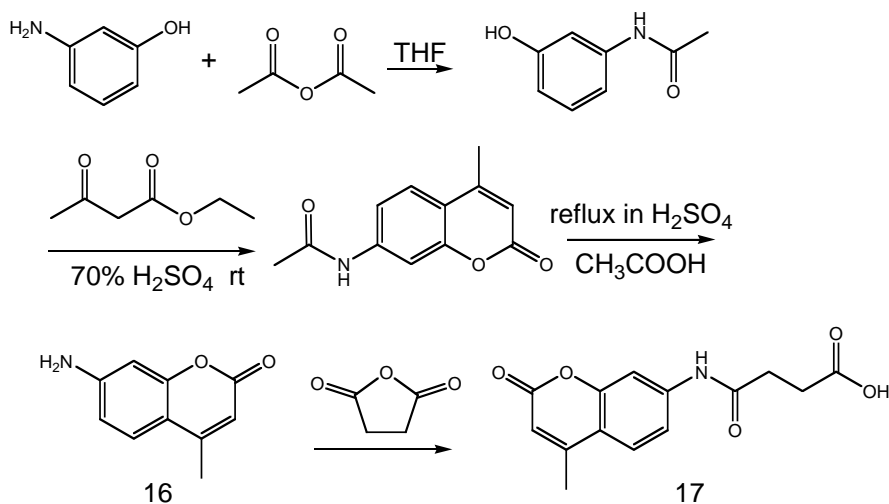
Scheme 2.12

Due to poor solubility of eight charged cavitands in non-aqueous solvent, four charged cavitands were first selected for the attachment of coumarin. During the synthesis of four charged hydroxyl feet cavitands, the work up includes neutralization of NaOH or HBr, which results in a mixture of product and inorganic salts. The salts can't be completely removed by recrystallization due to the solubility similarity and the product can't be purified by column chromatography. So, for the Mitsunobu reaction, when intend to weigh out 1:1 molar ratio of four charged hydroxyl feet cavitands and coumarin **17**, the coumarin would be in a little excess in reality. After 4-charged coumarin tagged cavitands were obtained, another four charges can be added to the bipyridinium unit using dimethyl sulfate. This step could be completed under room temperature and product would precipitate out from solvent DMF.



Scheme 2.13

The coumarin compound **17** used in the Mitsunobu reaction was synthesized from 3-aminophenol. First, the amine is protected by (methyl carbonyl) group, followed by ring closure with ethyl acetoacetate, deprotection of amine group and addition of acid chain with succinic anhydride.



Scheme 2.14

During the design of this procedure, it is important to make sure that final step is not done in concentrated sulfuric acid, because there is difficulty precipitating compound **17** out from strongly acidic water and neutralizing the sulfuric acid would result in a lot of salt.

Binding Investigation

Investigation of the Binding Behavior of Eight -times Charged Resorcin[4]arenes within the MspA Channel by Atomic-Force-Studies of MspA and Resorcin[4]arene@MspA Assemblies on MICA Surfaces

A direct proof for the binding of resorcin[4]arene **20** inside MspA was obtained by using AFM by my fellow graduate student Matthew T. Basel. MspA was deposited on Mica from (H₂O/MeOH)-phosphate buffer solutions (pH=6.8), dried in high vacuum and then imaged. Our AFM (Pico SPM 2000) has been operating in the Magnetic A/C mode (MACMode™), which uses a magnetically driven oscillating probe with an oscillation amplitude significantly smaller than that of the so-called tapping mode.^{xxxvii} The result is a superior resolution and less distortion of the sample by AFM-imaging. Typical results are shown in Figure 2.4. From Figure 2.4A it becomes apparent that single MspA pores can be successfully imaged on Mica if their deposition took place from a methanol-containing buffer (MeOH > 40 percent by weight). Apparently, methanol serves as a blocker for the formation of hydrogen bonds and hydrophobic interactions between individual MspA-octamers. However, the strength of the interaction between the MspA-monomers is sufficient (at MeOH < 60 percent) for MspA to remain (mostly) an octamer. This is true for the octamer possessing the characteristic homopore. Furthermore, it must be noted that approximately 98 percent of the MspA-“goblets” are standing upright on Mica. Their large pore openings are directed outwards, whereas the loop-region and also the constriction zone are directed towards the Mica support. MspA has been found to be stable on Mica. When in the MACMode (oscillation frequency: 75kHz (air), the oscillating AFM-probe conveys a force of approximately 20-100 pN. MspA is able to withstand that force for up to five consecutive imaging procedures.

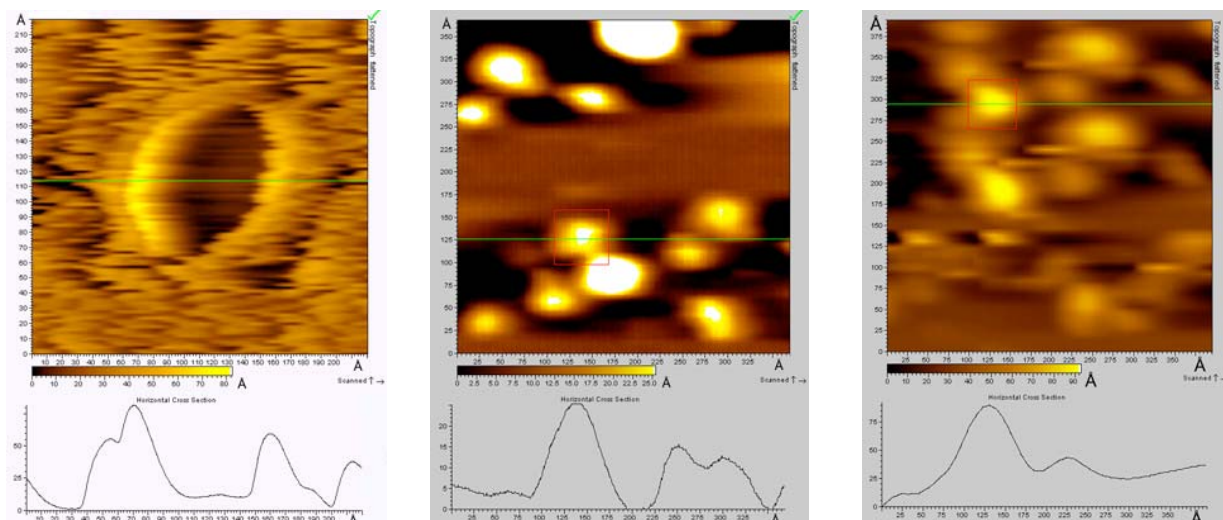


Figure 2.4 A: MspA on Mica

2.4 B: Resorcin[4]arene 20 on Mica

2.4 C: Resorcin[4]arene 20, bound to MspA on Mica

As it becomes apparent from the comparison of the three AFM-images shown in Figure 2.4, the resorcinarene **20** is able to block the inner pore of MspA. In Figure 2.4A, the pore opening of the MspA-homopore on Mica is clearly discernible. This opening cannot be detected anymore in the presence of the resorcin[4]arene, shown in Figure 2.4B, which acts as a channel blocker. The molar ratio of resorcin[4]arene to MspA is 10:1. Note that according to Equation 2.1^{xxxviii}, the apparent diameter of objects that were imaged by using AFM varies in dependence on the tip diameter. This is the main reason for the deviations of the MspA-diameters in Figure 2.4A and 2.4C. The second reason is that different parameter files were used for the imaging process due to an update in the AFM firmware and software.

$$W = d + 2\sqrt{[h(2R - h)]} \quad (2.1)$$

d: lateral size

h: height

R: radius of curvature of the tip apex

W: observed width of the feature

Photophysical Studies: UV/Vis-Measurements

The first step of the photophysical measurements of the resorcin[4]arene macrocycle **20** featuring four chemically attached 4,4'-bipyridinium units consisted in the recording of its UV/Vis-absorption spectra in dependence on its concentration. These studies were performed in

methanol in order to permit a direct comparison between the coumarin-luminophore and the macrocycle featuring one chemically attached coumarin-luminophore. Without chemical attachment to the eight-fold charged macrocycle, the coumarin-derivative is not sufficiently water-soluble.

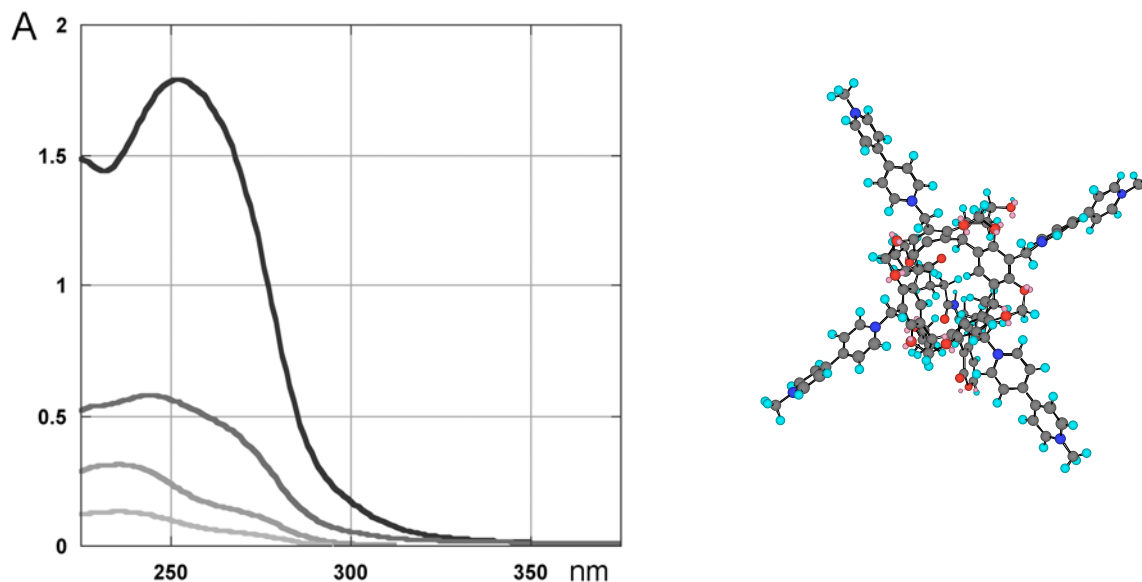


Figure 2.5: UV/Vis-Absorption spectrum of *resorcin[4]arene 20* as a function of its concentration in MeOH, $c=1 \times 10^{-6}$ M, 2×10^{-6} M, 5×10^{-6} M, 2×10^{-5} M.

Table 2.1: Absorption Maxima and Absorption Coefficients of *Resorcin[4]arene* as a Function of Concentration.

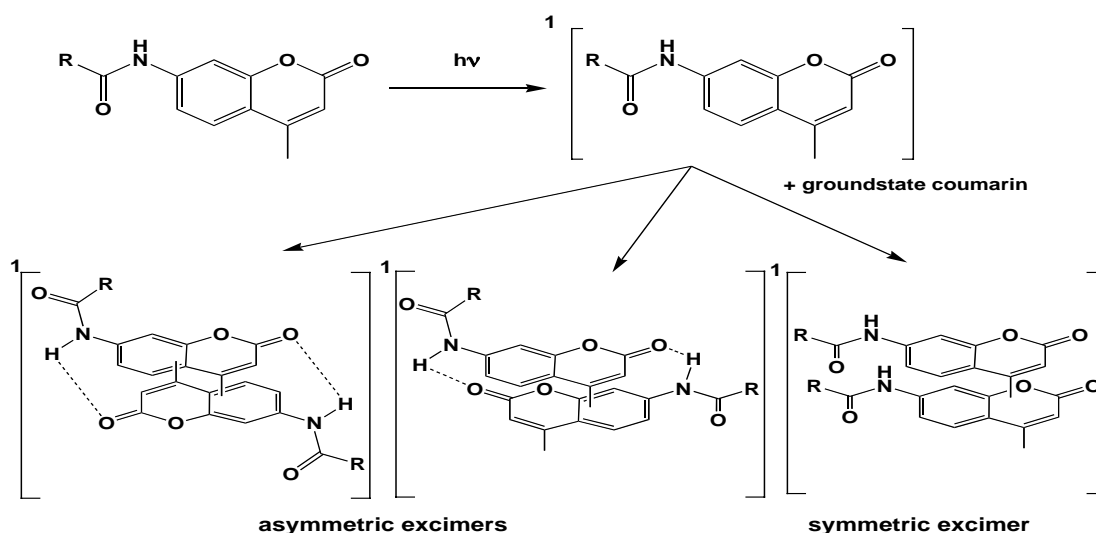
C [M]	$\lambda_{\max 1}$ (nm)	ϵ [$M^{-1} \text{ cm}^{-1}$]	$\lambda_{\max 2}$	ϵ [$M^{-1} \text{ cm}^{-1}$]
1×10^{-6}	241	124,000	274 (sh)	82,000
2×10^{-6}	243	126,000	275 (sh)	85,000
5×10^{-6}	247	118,000	275 (sh)	84,000
2×10^{-5}	253	88,000	285 (sh)	86,000
5×10^{-5}			309	94,000

For reasons of comparison, the same concentration-sequence has been measured using the coumarin-luminophore without the chemically attached macrocycle. In agreement with literature^{39,40}, methylaminocoumarin has a strong tendency towards the following photophysical processes:

1) Excimer and Excited Multiplex Formation^{xxxix} and 2) Fluorescence Resonance Energy Transfer (FRET)^{xi}. Whereas the second process strongly influences the fluorescence spectra and intensity of the strongly fluorescent coumarins, the first process has a strong effect on the absorption spectra as a function of concentration as well, as Figure 2.5 and Figure 2.6 indicate.

Excimer Formation^{xli}

The formation of exciplexes proceed according to Scheme 2.15: The first step consists of the absorption of a photon of suitable energy by an isolated coumarin chromophore. The energy of the absorbed photon causes the transition of an electron from the HOMO (highest occupied molecular orbital) into the LUMO (lowest unoccupied molecular orbital) generating the excited singlet state (S^1) of the organic molecule. This excited molecule can, depending on the concentration of ground state coumarins, react with a second (ground state) coumarin to form an “excited dimer” excimer. For methylcoumarinamide, there are, principally, three excimers possible, depending on the relative orientation of the two coumarin-molecules with respect to each other in the excimers as it is shown in Scheme 2.15.

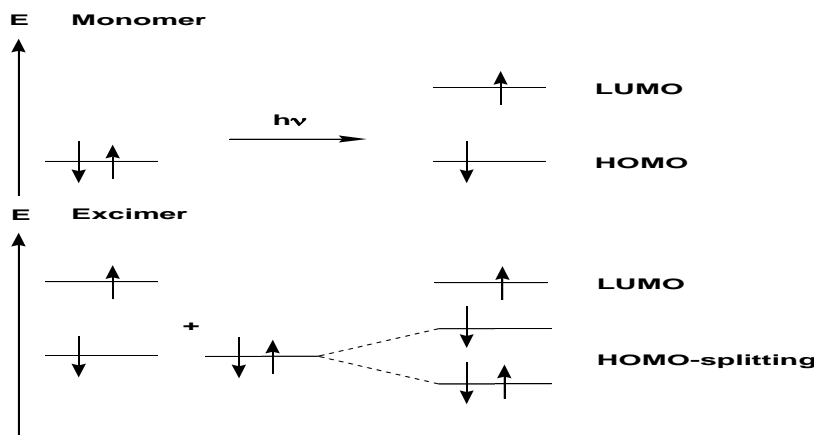


Scheme 2.15: Formation of asymmetric and symmetric coumarin-excimer.

Scheme 2.16 explains the energetic driving force that leads to the formation of excimers.

Note that two coumarins in the ground state are repulsive and do not form any aggregate with each other. The first step consists of the absorption of a photon and the formation of the electronically excited singlet state (S^1). In the presence of a second, fully occupied HOMO, the two HOMO's undergo splitting. In this process, one HOMO becomes lower in energy and the other increases by the same energy, respectively. The energy gain is the driving force for the formation of the excimer occurs. When two singlet electrons occupy the lowest orbital, only one electron can be found in the higher orbital of the two former HOMO's. Note that during the lifetime of an excimer, the LUMO stays occupied. Once the electron returns from the LUMO to the homo (deactivation), there is no electronic advantage for the splitting anymore and the two ground-state coumarins are no longer bound to each other.

It is of great importance for the observed changes in the UV/Vis-absorption spectra of the coumarins that excimers can be created via photoexcitation of two neighboring coumarins by one photon, if the two coumarins are close enough. This phenomenon is called “preformed excimers”. Therefore, the spectra of many coumarins and coumarin-derivatives change remarkably with increasing concentration. Furthermore, at even higher concentration, two or several ground-state coumarins can form a complex with one excited coumarin. This causes an even bigger redshift of the UV/Vis-absorption spectrum.



Scheme 2.16: Singlet Excimer formation explained by simple MO-theory (MO: molecular orbital)

2) **Fluorescence resonance energy transfer** (FRET)⁴¹ describes a nonradiative energy transfer mechanism between two chromophores. The mechanism of transfer is usually a long-range dipole-dipole coupling between a chromophore and an acceptor chromophore in close proximity (typically <10nm). When both molecules are fluorescent, the term "fluorescence resonance energy transfer" is often used. This can be misleading, because the energy is not actually transferred by fluorescence.

The FRET efficiency E depends on many parameters. The most important parameters are:

- The distance between the donor and the acceptor chromophores
- The spectral overlap of the donor's emission spectrum and the acceptor's absorption spectrum.
- The orientation of the donor emission dipole moment and the acceptor absorption dipole moment with respect to each other.

According to Theodor Förster⁴¹, E depends on the donor-to-acceptor separation distance with an inverse 6th power law (dipole-dipole coupling mechanism)

$$E = \frac{1}{1 + (r/R_0)^6} \quad (2.2)$$

R_0 , the *Förster distance*, is defined as the distance between fluorescence donor and acceptor, where the FRET efficiency is exactly 50%. The Förster distance is usually calculated by means of the Equation 2.3:

$$R_0^6 = 8.8 \times 10^{-23} \kappa^2 n^{-4} \Phi_0 J \quad (2.3)$$

where κ^2 is the dipole orientation factor, n is the refractive index of the medium, Φ_0 is the fluorescence quantum yield of the donor in the absence of the acceptor, and J is the spectral overlap integral calculated as

$$J = \int f_D(\lambda)\epsilon_A(\lambda)\lambda^4 d\lambda \quad (2.4)$$

where f_D is the normalized donor emission spectrum, and ϵ_A is the acceptor molar extinction coefficient.

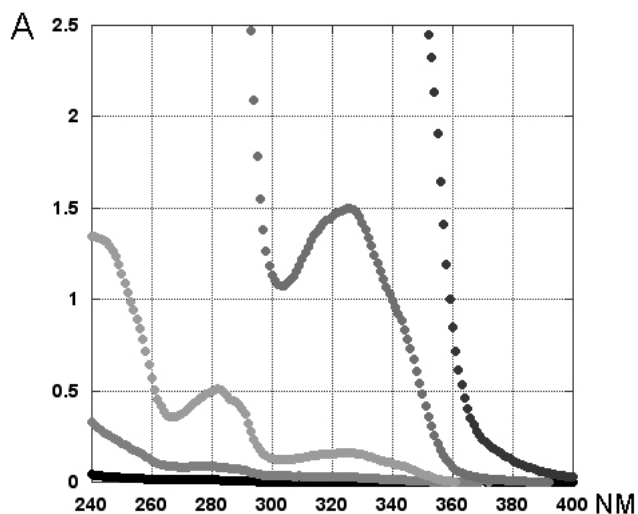
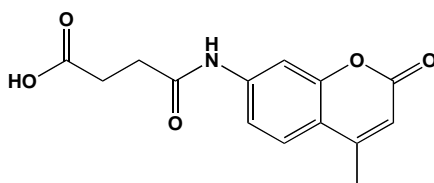
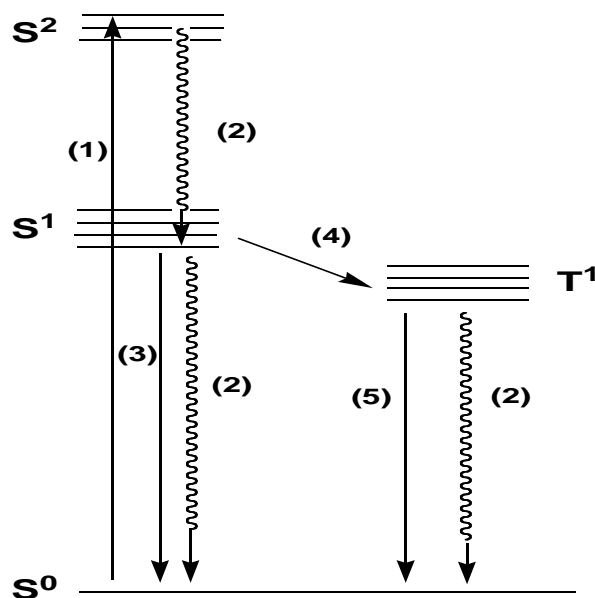


Figure 2.6: UV/Vis-Absorption spectrum of 3-(4-methyl-2-oxo-2H-chromen-7-ylcarbamoyl)propanoic acid (methylcoumarinamide) 17 as a function of its concentration in MeOH, $c=1 \times 10^{-6}$ M, 2×10^{-6} M, 1×10^{-5} M, 1×10^{-4} M and 1×10^{-3} M (intensities from low to high).



Fluorescence Spectra of Resorcin[4]arene Bound Coumarin in Comparison to the free Coumarin Dye.

It is known that the literature that most coumarin-dyes show very strong luminescence. For methylcoumarinamide the quantum yield of luminescence, which comprises the short-lived fluorescence and the much longer-lived phosphorescence, is approximately 0.5. This means that for every two photons absorbed at the excitation wavelength $\lambda=284\text{nm}$, one photon is emitted. Fluorescence is found at shorter wavelengths, whereas phosphorescence occurs at longer wavelengths (in the absence of oxygen). The principal photophysical processes of an organic molecule are summarized in the Jablonski-diagram shown in Scheme 2.17.



Scheme 2.17: Jablonski-Diagram

(1) electronic excitation by absorption of a photon ($\tau \sim 10^{-16} - 10^{-15} \text{ s}$)

(2) internal conversion ($\tau \sim 10^{-12} \text{ s}$)

(3) fluorescence ($\tau \sim 10^{-10} - 10^{-8} \text{ s}$)

(4) intersystem crossing ($\tau \sim 10^{-12} - 10^{-10} \text{ s}$)

(5) phosphorescence ($\tau \sim 10^{-7} - 10^{-3} \text{ s}$)

S^n : singlet states

T^n : triplet states

According to the literature^{xlii}, methylcoumarinamide possesses a fluorescence lifetime of 200 to 500 picoseconds (2×10^{-10} s - 5×10^{-10} s) in protic media. In the absence of oxygen (degassed by three consecutive freeze-pump and thaw cycles), its phosphorescence has a lifetime of approximately 500 nanoseconds (5×10^{-7} s). A typical emission spectrum of methylcoumarinamide (in MeOH) is shown in Figure 2.7. It indicates that monomers and excimers exist not only in the singlet state, but in the triplet state as well. Scheme 2.4 illustrates the energy advantage for a triplet excimer. Furthermore, the low viscosity of MeOH^{xliii} enhanced the probability for diffusional encounters between excited (triplet) coumarins and ground-state coumarins.

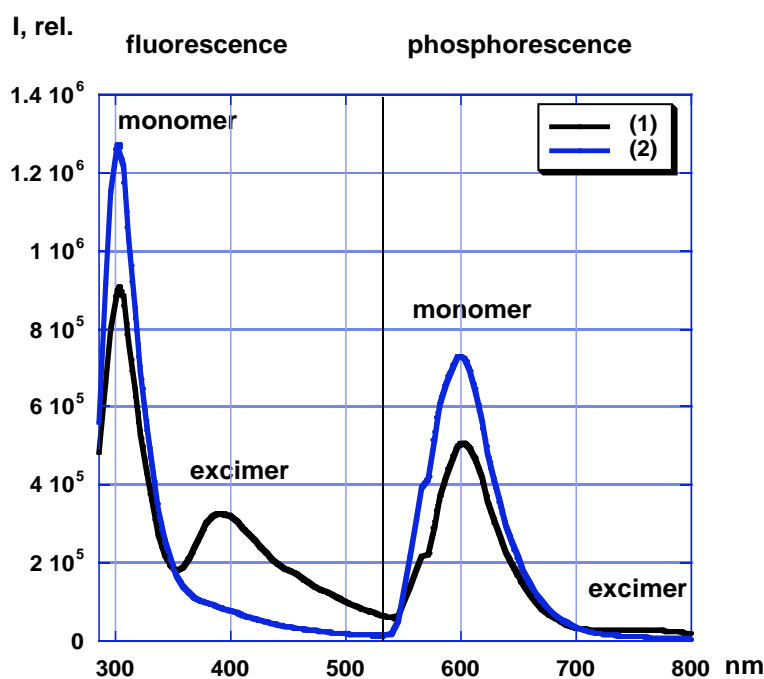
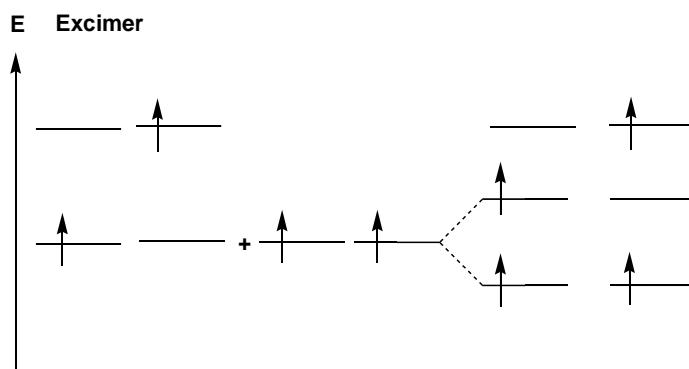


Figure 2.7: Emission spectrum of methylcoumarinamide 17

($\lambda_{exc} = 284$ nm) in MeOH. Note that both, fluorescence and phosphorescence form monomers and excimers.

(1): $c = 1.0 \times 10^{-5}$ M

(2): $c = 1.0 \times 10^{-6}$ M



Scheme 2.18: Singlet Excimer formation explained by simple MO-theory.

As it becomes apparent from the comparison of Figure 2.7 and Figure 2.8, the luminescence spectra of methylcoumarinamide and of the resorcin[4]arene featuring one chemically linked methylcoumarinamide unit in methanol are nearly identical. Both show monomer and excimer formation.

Before the binding of the resorcin[4]arene featuring the chemically linked coumarin fluorophore to the mycobacterial porin MspA has been investigated, the photophysical properties of the macrocycle itself, in comparison to methylcoumarinamide, were studied. Of special interest were the observed fluorescence and phosphorescence intensities as a function of concentration.

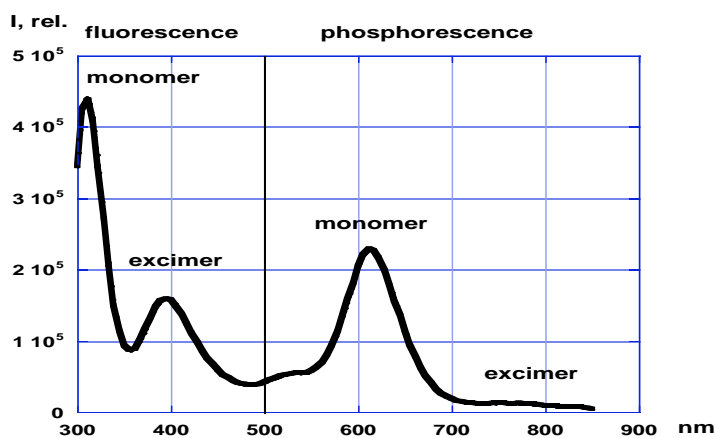


Figure 2.8: Emission spectrum of the resorcin[4]arene possessing a chemically linked coumarin 20 ($\lambda_{exc} = 284 \text{ nm}$) in MeOH ($c = 1.0 \times 10^{-6} \text{ M}$).

Note that both, fluorescence and phosphorescence form monomers and excimers.

It was our intention to distinguish FRET between two electronically excited and ground-state coumarin luminophors and the luminescence quenching of the coumarin luminophore by the four viologen units that are chemically attached to the rim of the resorcin[4]arene. Therefore, we have measured the concentration dependence of the coumarin-resorcin[4]arene and methylcoumarinamide.

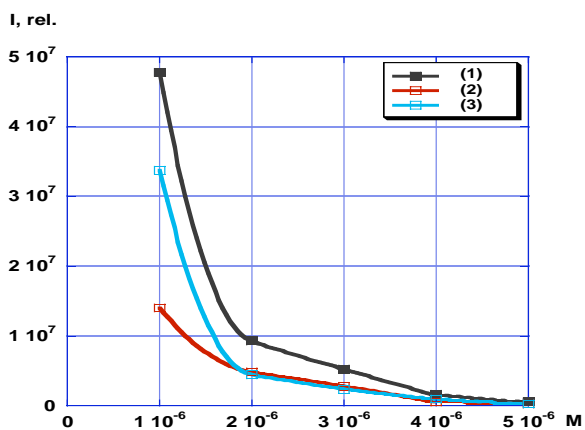


Figure 2.9: Integrated luminescence intensity of the resorcin[4]arene featuring one chemically attached methylcoumarinamide 20 as a function of concentration in MeOH

- (1) integrated luminescence from 300-700 nm
- (2) integrated luminescence from 300-500 nm
- (3) integrated luminescence from 500-700 nm

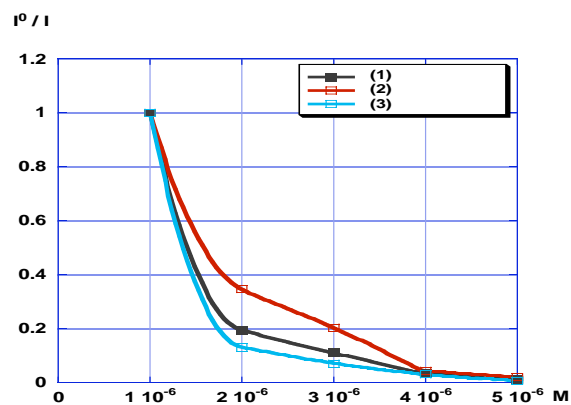


Figure 2.10: Normalized luminescence intensity of the resorcin[4]arene featuring one chemically attached methylcoumarin-amide 20 as a function of concentration in MeOH

- (1) integrated luminescence from 300-700 nm
- (2) integrated luminescence from 300-500 nm
- (3) integrated luminescence from 500-700 nm

Coumarin-resorcin[4]arene shows a strong decrease of its luminescence intensity ($\lambda_{exc}=284\text{nm}$) with increasing concentration (Figure 2.9). It is noteworthy that the four chemically attached viologen units quench the coumarin luminescence with a very low efficiency, otherwise strong luminescence would not occur when the concentration of the coumarin-linked macrocycle is increased. Since the charge of coumarin-resorcin[4]arene **20** is plus eight and at least a partial dissociation of the chloride salts that have been used can be expected in methanol, we can assume a certain degree of charge repulsion. Therefore, we can assume that the luminescence quenching occurs via a diffusional pathway and NOT within the macrocycle itself. Furthermore, it is of interest that the fluorescence part of the luminescence spectrum (300-500 nm) decreases faster than the phosphorescence part (Figure 2.10). This

behavior is surprising, because viologen is known to quench both singlet and triplet states and the much longer lifetime of the electronically excited triplet state of the attached coumarin should increase the probability of diffusional quenching by the viologen. A comparison of the phosphorescence behavior of methylcoumarinamide and coumarin-resorcin[4]arene **20** indicates that the former shows an increase of phosphorescence with increasing concentration, whereas the overall decrease of luminescence is certainly decreased. This finding can be regarded as mechanistic proof for a) the diffusional quenching of the coumarin-luminescence by the viologen units and b) the remarkably increased efficiency of intersystem crossing of resorcin[4]arene-linked and free methylcoumarinamide at higher concentrations. In the absence of a quencher, we attribute the observed decrease in luminescence to the occurrence of FRET between the coumarin-chromophors.

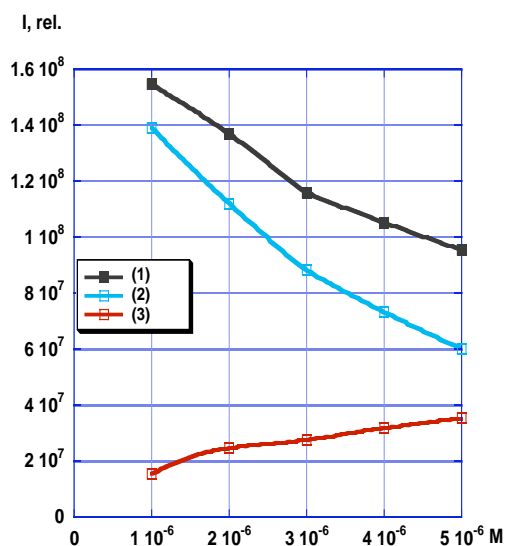


Figure 2.11: Integrated luminescence intensity of methylcoumarinamide as a function of concentration in MeOH

- (1) integrated luminescence from 300-700 nm
- (2) integrated luminescence from 300-500 nm
- (3) integrated luminescence from 500-700 nm

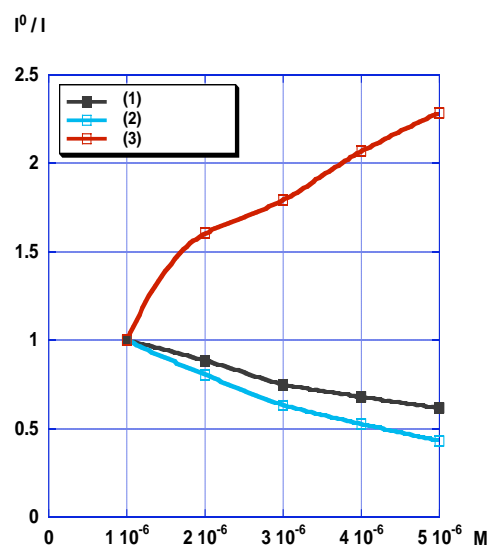
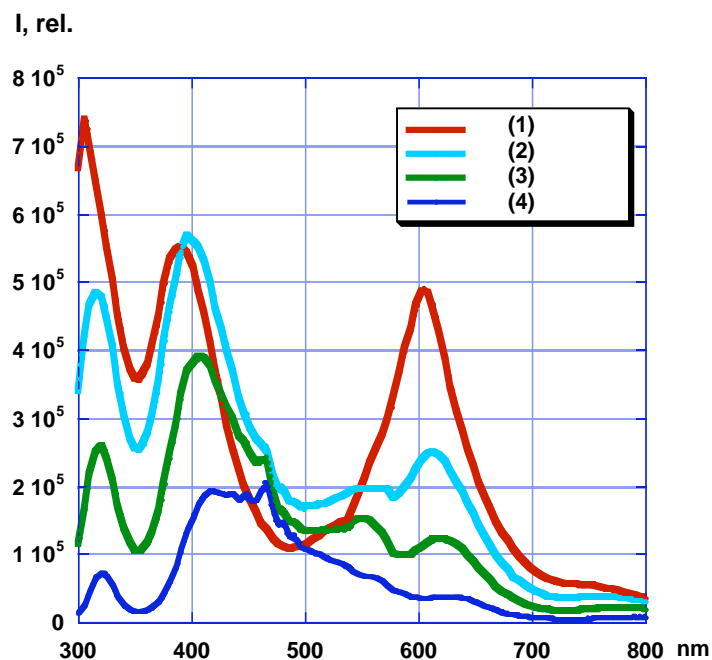


Figure 2.12: Normalized luminescence intensity of methylcoumarinamide as a function of concentration in MeOH

- (1) integrated luminescence from 300-700 nm
- (2) integrated luminescence from 300-500 nm
- (3) integrated luminescence from 500-700 nm

Channel Blocking of MspA: Coumarin-resorcin[4]arene as Guest

In Figure 2.13 and 2.14, the luminescence spectra of coumarin-resorcin[4]arene **20** in the presence of MspA in aqueous phosphate buffer and the reference spectra of coumarin-resorcin[4]arene **20** in the absence of MspA are shown. It is noteworthy that the intensity of both, fluorescence and phosphorescence, is enhanced in the presence of MspA. However, the mechanistic reason for this finding remains to be determined.



*Figure 2.13: Luminescence spectra of coumarin-resorcin[4]arene **20** (variable concentrations) and MspA ($2.2 \times 10^{-8} M$) in 0.05M phosphate buffer (pH=6.8)*

(1) $1.0 \times 10^{-6} M$

(2) $2.0 \times 10^{-6} M$

(3) $3.0 \times 10^{-6} M$

(4) $5.0 \times 10^{-6} M$

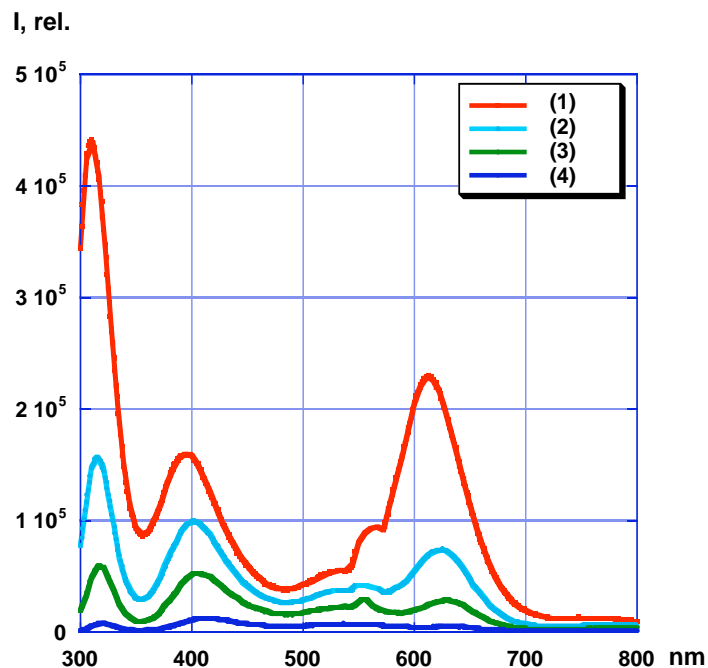


Figure 2.14: Luminescence spectra of coumarin-resorcin[4]arene 20 (variable concentrations) in 0.05M phosphate buffer (pH=6.8)

(1) $1.0 \times 10^{-6} M$

(2) $2.0 \times 10^{-6} M$

(3) $3.0 \times 10^{-6} M$

(4) $5.0 \times 10^{-6} M$

In order to show that coumarin-resorcin[4]arene **20** is indeed bound within MspA, as AFM-results have indicated (see above), the (singlet) monomer/excimer ratios in the presence and absence of MspA have been determined and then compared to each other. The results are shown in Figures 2.15 to 2.16.

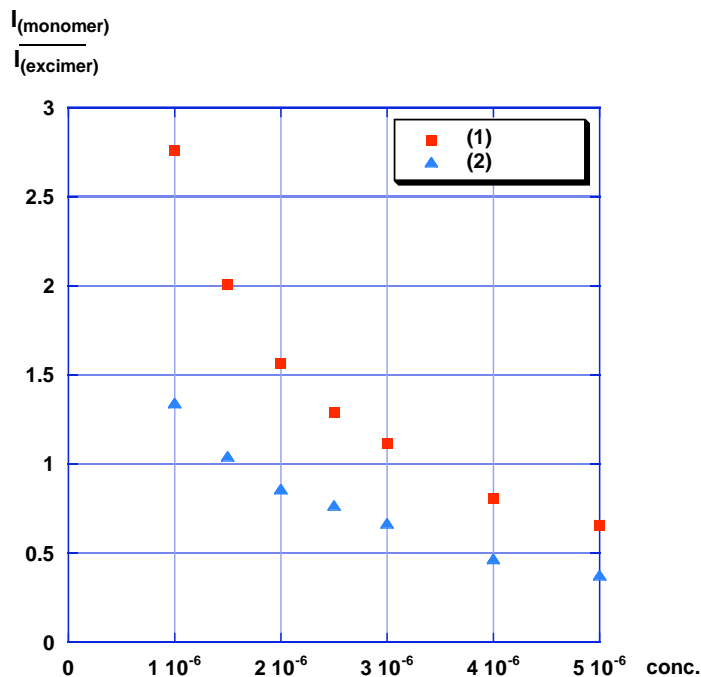


Figure 2.15: Monomer/excimer-ratios of the fluorescence from coumarin-resorcin[4]arene20 in variable concentrations in 0.05M aqueous phosphate buffer (pH=6.8), $I_{exc}=284nm$.

(1) coumarin-resorcin[4]arene in the absence of MspA

(2) coumarin-resorcin[4]arene in the presence of MspA ($2.2 \times 10^{-8} M$).

It is apparent that the amount of excimer increases in both systems with increasing concentration, as this is to be expected. However, the increase proceeds differently in the presence and absence of MspA. This can be used to determine the concentration when the binding inside and at the outside of MspA is saturated. We are aware that we cannot determine a binding constant by using this method, because we are unable to determine the amount of free MspA as a function of concentration. Another “unknown” is the stoichiometry of binding. It can be expected that coumarin-resorcin[4]arene will be bound in the inside of MspA, because MspA features up to 72 negative charges in its interior channel, whereas the channel blocker is eight-fold positive. However, more than one channel blocker can fit into the MspA-funnel. Furthermore, coumarin-resorcin[4]arene may also be bound to the outside of MspA. This might be a reason for the observed increase of excimer formation in the presence of MspA. The

determination of the saturation concentration for the binding of coumarin-resorcin[4]arene to MspA provides a first indication, whether this organic channel blocker could be used. 2.75×10^{-6} M, about 100 times higher than the protein concentration can be considered relatively low. Therefore, we regard this finding as a proof of principle that organic channel blockers for mycobacterial porins can indeed be developed!

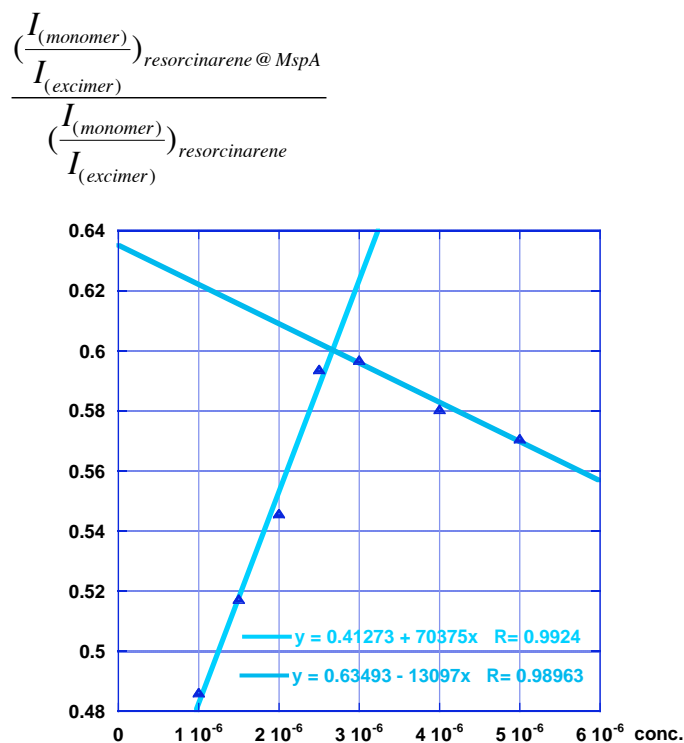


Figure 2.16: Quotient of the monomer/excimer-ratios as shown in Figure 2.15.

Experimental Section

General methods:

Solvents (ACS-grade) and inorganic chemicals were purchased from Aldrich and Acros Organics. DMF was further purified by azeotropic distillation of DMF/toluene/H₂O (85:10:5 v/v/v), anhydrous and amine-free DMF has been collected when reaching 152°C at the top of a 20 cm Vigreux-column. All other chemicals and chromatography materials were either purchased from Aldrich or Acros Organics and used without further purification. H₂O was of bidistilled quality.

All distillations in vacuum were performed using a Büchi-rotavap equipped with a solvent recovery system and pressure control.

All high-pressure reactions were performed in a PARR-reactor (V=50mL).

Further instrumentation: 200 and 400 MHz NMR (Varian Gemini 2000 and Unit INOVA 400), FT-IR (Nicolet 870), MS: Bruker Esquire 3000, Melting point apparatus ((Fisher) All melting points are uncorrected), Carlo Erba Strumentatione (CHN).

2-Methyl-dodecol **1** was prepared by following a published procedure². The maximal yield was 80% (published 78%).

TBDPS-protected 2-methyl cavitand **5** was prepared by following a published procedure as well.² My maximal yield was 85% (published 87%).

Compounds **8-12** melted partially under decomposition in the temperature interval between 140-150°C

Compounds **1,14-20** underwent decomposition when heated above 300°C without melting.

2-Methyl-dodecol **1**

FT-IR (KBr) (cm⁻¹): 3237, 2950, 2873, 1475, 1347, 1306, 1214, 1107, 1066

¹H NMR (200 MHz, DMSO-d₆): 8.62 (8H, s), 7.27 (4H, s), 4.19 (4H, t, J=7.8Hz), 4.1 (4H, s), 3.44 (8H, t, J=6.7Hz), 2.24 (8H, m), 1.94 (12H, s), 1.35 (8H, m)

¹³C NMR (200 MHz, DMSO-d₆): 149.11, 124.82, 121.31, 111.61, 60.71, 34.02, 31.31, 30.69, 29.34, 10.05

Yield: 55%

2-Methyl Cavitand **2**

46.0g (0.333 mol) of anhydrous potassium carbonate (pre-dried for 24 h at 100°C) was added under a nitrogen atmosphere to a solution of 2-methyl-dodecol **1** (20.0 g, 0.0258 mol) in 800ml of anhydrous DMSO. Bromochloromethane (7.5 ml, 0.0113 mol) was added dropwise under a nitrogen atmosphere. It is of great importance to stir the mixture rigorously during addition. The reaction mixture was stirred over night and then heated to 50°C in 1h and then kept at that temperature for additional 8 h. Then the mixture was removed from the heating bath. Another 1.0 mL (0.0015 mol) of bromochloromethane was added after the mixture had cooled to room temperature. After stirring for additional 5 h at room temperature, the mixture was poured into

2.4 L of saturated aqueous ammonium chloride and the precipitation was collected by filtration. The whitish solid obtained was washed three times with 200 mL of water and then dried under normal pressure. The product was further purified by descending column chromatography using silica as stationary phase. After the impurities have been eluted with chloroform/methanol 12:1 (v/v), the product was obtained employing CHCl₃/MeOH 10:1 (v/v). After removal of the solvent mixture at reduced pressure the product was obtained as a white powder, yield 17.0 g (80%) mp 227°C (dec.).

FT-IR (KBr) (cm⁻¹): 3406, 2940, 1470, 1306, 1245, 973

¹H NMR (200 MHz, DMSO-d₆): 7.43 (4H, s), 5.86 (4H, d, J=7.4Hz), 4.59 (4H, t, J=6.1Hz), 4.43 (4H, t, J=5.1Hz), 4.19 (4H, d, J=7.4Hz), 3.48 (8H, m), 2.35 (8H, m), 1.88 (12H, s), 1.42 (8H, m)

¹³C NMR (200 MHz, DMSO-d₆): 152.50, 137.72, 123.65, 119.30, 98.08, 60.51, 40.41, 36.63, 30.98, 25.57, 10.01

Acetylated 2-methyl cavitand **3**

2-Methyl cavitand **2** (0.72 g, 0.00087 mol) was slowly dissolved in a mixture of 1.0 ml anhydrous pyridine and 16 ml acetic anhydride. The reaction mixture was stirred for 5 h and then heated to 60°C for additional 12 h. The solvent mixture was removed in high vacuum and the crude product purified by descending column chromatography using silica as stationary phase and CHCl₃/MeOH 96:4 (v/v) as eluent, yield 0.82 g (95%) mp 211°C.

FT-IR (KBr) (cm⁻¹): 2942, 1726, 1480, 1240, 973

¹H NMR (200 MHz, CDCl₃): 6.93 (4H, s), 5.86 (4H, d, J=6.9Hz), 4.82 (4H, t, J=9.1Hz), 4.23 (4H, d, J= 6.9Hz), 4.15 (8H, t, J=6.5Hz), 2.26 (8H, m), 2.03 (12H, s), 1.95 (12H, s), 1.69 (8H, m)

¹³C NMR (200 MHz, CDCl₃): 171.29, 153.62, 137.63, 124.42, 117.14, 98.60, 64.32, 36.60, 27.12, 26.65, 21.01, 10.48

Acetylated 2-bromomethyl cavitand **4**

Acetylated 2-methyl cavitand **3** (0.74 g, 0.00075 mol), NBS (0.58 g, 0.0033 mol) and AIBN (20mg) were dissolved in CCl₄ and then refluxed under argon for 24h. The reaction mixture was stirred for another 12h at room temperature, cooled to 10°C and filtered. The solvent was removed in vacuum and the reddish-brown residue was subjected to descending column chromatography using silica as stationary phase and EtOAc/n-hexane 1:1 (v/v) as eluent. After

removing the solvent in vacuum, the product was obtained as a slightly yellow powder, yield 1.0g (88%) mp 186°C (dec.).

FT-IR (KBr) (cm⁻¹): 2942, 1726, 1480, 1240, 973

¹H NMR (200 MHz, CDCl₃): 7.09 (4H, s), 6.01 (4H, d, J=6.1Hz), 4.82 (8H, t, J=8.1Hz), 4.55 (4H, d, J=6.7Hz), 4.39 (8H, s), 4.15 (8H, t, J=6.5Hz), 2.28 (8H, m), 2.05 (12H, s), 1.67 (8H, m)

¹³C NMR (200 MHz, CDCl₃): 185.25, 153.38, 138.10, 123.67, 118.81, 98.75, 63.03, 41.19, 37.20, 26.76, 21.79, 10.52

TBDPS-protected 2-methyl cavitand **5**

FT-IR (KBr) (cm⁻¹): 2937, 2863, 1475, 1112, 973, 702, 513

¹H NMR (200 MHz, CDCl₃): 7.60 (16H, m), 7.28 (24H, m), 6.91 (4H, s), 5.85 (4H, d, J=6.9Hz), 4.77 (4H, t, J=8.2Hz), 4.23 (4H, d, J=6.9Hz), 3.66 (8H, t, J=6.4Hz), 2.22 (8H, m), 1.95 (12H, s), 1.59 (8H, m), 0.99 (36H, s)

¹³C NMR (200 MHz, CDCl₃): 153.50, 137.94, 135.72, 134.10, 129.72, 127.82, 123.95, 117.61, 98.65, 63.63, 36.58, 30.80, 27.11, 26.23, 19.43, 10.56

TBDPS-protected 2-bromomethyl cavitand **6**

TBDPS-protected 2-methyl cavitand **5** (6.83 g, 0.00374 mol), NBS (2.93 g, 0.0041 mol) and AIBN (20 mg) were dissolved in CCl₄ (20 mL) and then refluxed under argon for 24 h. The reaction mixture was stirred for another 12h at room temperature, cooled to 10°C and filtered. The solvent was removed in vacuum and the reddish-brown residue was purified by descending column chromatography using silica as stationary phase and n-hexane/EtOAc 96:4 (v/v) as eluent. After removing the solvent in vacuum, the product was obtained as a slightly yellow powder, yield 3.30 g (74%) mp 134°C (dec.).

FT-IR (KBr) (cm⁻¹): 2935, 2858, 1475, 1434, 1265, 1117, 979, 707, 507

¹H NMR (200 MHz, CDCl₃): 7.59 (16H, m), 7.30 (24H, m), 7.06 (4H, s), 6.00 (4H, d, J=6.2Hz), 4.78 (4H, t, J=7.9Hz), 4.54 (4H, d, J=6.2Hz), 4.39 (8H, s), 3.65 (8H, t, J=6.3Hz), 2.22 (8H, m), 1.56 (8H, m), 0.99 (36H, s)

¹³C NMR (200 MHz, CDCl₃): 153.78, 138.00, 135.65, 133.88, 129.76, 127.82, 124.84, 120.96, 99.22, 63.38, 36.37, 30.53, 27.08, 26.73, 26.19, 23.14, 19.38

Acetylated 2-(4-(pyridin-4-yl)-4-pyridinium)-methyl cavitand **7**

Acetylated 2-bromomethyl cavitand **4** (0.40 g, 0.00040 mol) and 4,4'-bipyridine (0.376 g, 0.0024 mol) was dissolved in DMF (6 mL) and kept at 60°C for 3 d. The solvent was removed at normal pressure by purging with N₂ and collection in a liquid N₂ cooled trap. The residue was washed 3 times with 5 ml of acetone each, then recrystallized from acetone and dried at reduced pressure. The product was obtained as a yellow brown powder, yield 0.50 g (85.3%).

FT-IR (KBr) (cm⁻¹): 3053, 2945, 1736, 1644, 1465, 1250, 958, 978, 815

¹H NMR (200 MHz, DMSO-d₆): 9.16 (8H, d, J=6.4Hz), 8.93 (8H, d, J=6.4Hz), 8.62 (8H, d, J=6.4Hz), 8.03 (8H, d, J=6.4Hz), 8.00(4H, s), 6.64 (4H, d, J=5Hz), 5.85 (8H, d, J=4Hz), 4.52 (12H, m), 4.05 (12H, m), 1.93 (12H, s), 1.54 (8H, m)

Concentration in DMSO-d₆ too low to record a ¹³C- NMR within 1d.

Acetylated 2-(4-(4-methylpyridinium)-4-pyridinium)-methyl cavitand **8**

Acetylated 2-(4-(pyridin-4-yl)-4-pyridinium)-methyl cavitand **7** (0.50 g, 0.00026 mol) was dissolved in DMF (6 mL), then iodomethane (0.13 ml, 0.00208 mol) was added to the solution. The mixture was heated to 40°C under nitrogen for 3 d. 0.10 mL of water was added to the mixture before the solvent was removed at normal pressure by purging with N₂ and then collected in a liquid N₂ cooled trap. The residue was washed 3 times with 5 ml of water each and recrystallized from 3ml of acetone. It was then dried in vacuum. The product was obtained as a dark brown powder, yield 0.61 g (95%).

FT-IR (KBr) (cm⁻¹): 3052, 2945, 2863, 1726, 1639, 1460, 1245, 979, 830

¹H NMR (200 MHz, DMSO-d₆): 9.25 (16H, m), 8.73 (16H, m), 7.94 (4H, s), 6.44 (4H, d, J=5Hz), 5.87 (8H, s), 4.60 (8H, m), 4.42 (12H, s), 4.03 (8H, m), 2.60 (8H, m), 1.90 (12H, s), 1.48 (8H, m)

Concentration in DMSO-d₆ too low to record a ¹³C- NMR within 1d.

Hydroxylated 2-(4-(pyridin-4-yl)-4-pyridinium)-methyl cavitand **9**

Acetylated 2-(4-(pyridin-4-yl)-4-pyridinium)-methyl cavitand **7** (0.30 g, 0.000153 mol) was dissolved in 10ml of aqueous NaOH solution (pH=10) and then stirred at 25°C for 5 h. The solution was then neutralized (final pH=7.0) using 4N HCl. The solvent was removed at normal pressure by purging with N₂ and the residue was washed 3 times with 5ml of acetone each and

dried in high vacuum. Finally, 5 ml of methanol was added to the residue and the mixture was stirred for 5 minutes and then filtered. The filtrate was collected and the solvent was removed under reduced pressure. The product was obtained as a light brown powder, yield 0.25g (91%).

FT-IR (KBr) (cm^{-1}): 3272-3626 (br), 1639, 1250, 1153, 1020, 989, 953, 553

^1H NMR (200 MHz, DMSO- d_6): δ 9.19 (8H, d, $J=7.7\text{Hz}$), 8.88 (8H, d, $J=7.7\text{Hz}$), 8.65 (8H, d, $J=7.7\text{Hz}$), 8.04 (8H, d, $J=7.7\text{Hz}$), 7.46 (4H, m), 7.32 (4H, s), 6.47 (4H, m), 5.90 (4H, m), 4.62 (8H, m), 4.47 (8H, m), 3.40 (12H, m), 1.38 (8H, m)

Concentration in DMSO- d_6 too low to record a ^{13}C - NMR within 1d.

Hydroxylated 2-(4-(4-methylpyridinium)-4-pyridinium)-methyl cavitand **10**

Hydroxylated 2-(4-(pyridin-4-yl)-4-pyridinium)-methyl cavitand **9** (0.10 g, 0.000066 mol) was dissolved in MeOH (10 mL). Then dimethyl sulfate (41.7 mg, 0.00033 mol) was added and the reaction mixture was refluxed for 1d. 0.10 mL of water was added to the mixture before the solvent was removed at normal pressure by purging with N_2 and the collected in a liquid N_2 cooled trap. The residue was washed 3 times with 5ml of water each and recrystallized from 3ml of acetone. It was then dried in vacuum. The product was obtained as a light brown powder, yield 0.14g (92%).

FT-IR (KBr) (cm^{-1}): 3426, 1644, 1112,620

^1H NMR (200 MHz, DMSO- d_6): 9.34 (16H, m), 8.83 (16H, m), 8.04 (4H, s), 6.50 (4H, d, $J=5\text{Hz}$), 6.00 (8H, d, $J=4\text{Hz}$), 4.63 (12H, m), 4.47 (12H, m), 1.37 (8H, m)

Concentration in DMSO- d_6 too low to record a ^{13}C - NMR within 1d.

TBDPS-protected 2-(4-(pyridin-4-yl)-4-pyridinium)-methyl cavitand **11**

TBDPS-protected 2-bromomethyl cavitand **6** (1.22 g, 0.00058 mol) and 4,4'-bipyridine (0.73 g, 0.00467 mol) was dissolved in DMF (10 ml) and heated to 60°C under a nitrogen atmosphere for 5 d. The solvent was removed at normal pressure by purging with N_2 and then collected in a liquid N_2 cooled trap. The residue was washed 3 times with 5ml of acetone each, then recrystallized from acetone and dried at reduced pressure. The product was obtained as a red brown powder, yield 1.30 g (82.0%).

FT-IR (KBr) (cm^{-1}): 2923, 2853, 1634, 1460, 1404, 1240, 1148, 1102, 1020, 979, 953, 815, 702, 610, 502

^1H NMR (200 MHz, DMSO- d_6): 9.14 (8H, d, $J=7.7\text{Hz}$), 8.90 (8H, d, $J=7.7\text{Hz}$), 8.76 (8H, d, $J=7.7\text{Hz}$), 8.60 (8H, d, $J=7.7\text{Hz}$), 7.97 (12H, m), 7.87 (4H, d, $J=7.4\text{Hz}$), 7.48 (16H, m), 7.34 (16H, m), 6.47 (4H, d, $J=5\text{Hz}$), 5.83 (8H, d, $J=4\text{Hz}$), 4.60 (12H, m), 3.66 (8H, m), 1.46 (8H, m), 0.80 (36H, s)

Concentration in DMSO- d_6 too low to record a ^{13}C - NMR within 1d.

Methoxylated 2-Methyl Cavitand **12**

TBDPS-protected 2-methyl cavitand **5** (0.10 g, 0.000055 mol) and methyl iodide (19.5 mg, 0.000138 mmol) was dissolved in DMF (5 mL) and heated to 50°C under nitrogen atmosphere for 2 d. The excess of methyl iodide was quenched by MeOH. The solvent was removed at normal pressure by purging with N_2 and then collected in a liquid N_2 cooled trap. The crude product was purified by column chromatography (10:1 hexanes:ethyl acetate) to yield cavitand **12** as a white solid, yield 11.4 mg (11%).

FT-IR (KBr) (cm^{-1}): 2950, 2873, 1649, 1475, 1306, 1240, 1157, 1096, 973, 671, 589, 502

^1H NMR (400 MHz, CDCl_3): 6.90 (4H, s), 5.87 (4H, d, $J=5.7\text{Hz}$), 4.76 (4H, t, $J=4.6\text{Hz}$), 4.24 (4H, d, $J=4.6\text{Hz}$), 3.47 (8H, t, $J=6.2\text{Hz}$), 3.34 (12H, s), 2.28 (8H, m), 1.96 (12H, s), 1.63 (8H, m)

^{13}C NMR (400 MHz, CDCl_3): 153.48, 137.93, 124.09, 120.76, 98.65, 76.91, 72.62, 58.60, 36.79, 28.07, 26.81, 10.46

Acetylated 2-(4-((3-methyl)-pyridin-4-yl)-4-(3-methyl)pyridinium)-methyl cavitand **13**

A: Sodium metal (20 g, 0.87 mol) was added to freshly distilled 3-picoline (150 ml, 1.54 mol), the mixture was heated to 70°C while stirring until sodium completely dissolved. A gentle air stream was directed to the surface of the resulted solution for a week. The reaction mixture was then washed twice with 100 ml hexane and the hexane layer was decanted. The crude product was purified by column chromatography (1:1 hexane : ethylacetate followed by 100% ethylacetate) yield 8.5 g (11.6%). mp 116°C

^1H NMR (200 MHz, CDCl_3): 8.56 (2H, s), 8.51 (2H, d, $J=7.7\text{Hz}$), 7.02 (2H, d, $J=8.3\text{Hz}$), 2.07 (6H, s)

B: Acetylated 2-bromomethyl cavitand **4** (0.70 g, 0.000535 mol) and 3,3'-dimethyl-4,4'-bipyridine (0.80 g, 0.00434 mol) was dissolved in DMF (6 mL) and kept at 60°C for 4 d. The solvent was removed at normal pressure by purging with N_2 and collected in a liquid N_2 cooled

trap. The residue was washed 3 times with 5ml of acetone each, then recrystallized from acetone and dried at reduced pressure. The product was obtained as a darkbrown powder, yield 0.75 g (68.2%) mp 98°C.

FT-IR (KBr) (cm⁻¹): 2935, 1726, 1460, 1465, 1245, 958, 989

¹H NMR (200 MHz, DMSO-d₆): 9.15 (4H, s), 8.90 (4H, d, J=6.4Hz), 8.64 (4H, s), 8.56 (4H, d, J=8Hz), 8.03 (8H, m), 7.98 (4H, s), 7.28 (4H, d, 8Hz), 6.46 (4H, d, J=6Hz), 5.75 (8H, s), 4.61 (12H, m), 4.03 (4H, m), 3.43 (4H, m), 2.46 (12H, s), 2.45 (12H, s), 2.14 (12H, s), 1.46 (8H, m)

Concentration in DMSO-d₆ too low to record a ¹³C- NMR within 1d.

Hydroxylated 2-(4-((3-methyl)-pyridin-4-yl)-4-(3-methyl)pyridinium)-methyl cavitand **14**

Acetylated 2-(4-((3-methyl)-pyridin-4-yl)-4-(3-methyl)pyridinium)-methyl cavitand **13** (0.20 g, 0.000098mol) was dissolved in 10ml of aqueous NaOH solution (pH=10) and then stirred at 25°C for 5 h. The solution was then neutralized (final pH=7.0) using 4N HCl. The solvent was removed at normal pressure by purging with N₂ and the residue was washed 3 times with 5 ml of acetone each and dried in high vacuum. Finally, 5 ml of methanol was added to the residue and the mixture was stirred for 5 minutes and then filtered. The filtrate was collected and the solvent was removed under reduced pressure. The product was obtained as a light brown powder, yield 0.15g (98%).

FT-IR (KBr) (cm⁻¹): 3391, 2976, 2899, 2853, 1614, 1578, 1527, 1501, 1445, 1424, 1337, 1276, 1204, 1168, 1122, 1035, 1004, 979, 871, 804

¹H NMR (400 MHz, DMSO-d₆): 9.28 (4H, m), 8.97 (4H, m), 8.67 (4H, m), 8.58 (4H, m), 8.04 (4H, m), 7.95 (4H, m), 7.33 (4H, m), 6.45 (4H, m), 5.81 (8H, m), 4.64 (12H, m), 3.49 (12H, m), 3.42 (12H, m), 2.08 (12H, m), 2.26 (12H, m), 1.42 (8H, m)

Concentration in DMSO-d₆ too low to record a ¹³C- NMR within 1d.

Hydroxylated 2-(4-((4-methyl(3-methyl)pyridinium)-4-(3-methyl(-pyridinium))))-methyl cavitand **15**

Hydroxylated 2-(4-((3-methyl)-pyridin-4-yl)-4-(3-methyl)pyridinium)-methyl cavitand **15** (0.10 g, 0.000049 mol) was dissolved in MeOH (10 mL). Then dimethyl sulfate (74.7 mg, 0.00024 mol) was added and the reaction mixture was refluxed for 1d. 0.10 mL of water was added to the mixture before the solvent was removed at normal pressure by purging with N₂ and collected in a

liquid N₂ cooled trap. The residue was washed 3 times with 5ml of water each and recrystallized from 3 ml of acetone. It was then dried in vacuum. The product was obtained as a light brown powder, yield 0.103g (100%).

FT-IR (KBr) (cm⁻¹): 3406, 3104, 2981, 2909, 1695, 1537, 1419,1342, 1163, 1122, 1035, 994, 973, 881, 830, 717, 676, 605

¹H NMR (200 MHz, DMSO-d₆): 9.36 (4H, s), 9.27 (4H, d), 9.07 (4H, s), 8.92 (4H, d), 8.14 (8H,m), 7.95 (4H, s), 6.44 (4H, d), 5.75 (8H, d), 4.68 (8H, m), 4.42 (12H, s), 4.16 (16H, m), 3.50 (12H, s), 2.82 (12H, s), 1.42 (8H, m)

Concentration in DMSO-d₆ too low to record a ¹³C- NMR within 1d.

7-Aminocoumarin (7-amino-4-methyl-2*H*-chromen-2-one) **16**

m-Aminophenol (5.0 g, 0.0459 mol) was dissolved in 200 ml of anhydrous THF. Acetic anhydride (4.4 ml, 0.0459 mol) was added to the solution. The mixture was stirred at room temperature for 2 h. The solvent was then removed at reduced pressure and the residue was recrystallized in toluene. N-acetyl-aminophenol was obtained as white needles, yield 6.90 g (100%).

N-acetyl-aminophenol (3.63 g, 0.024 mol) and ethyl acetoacetate (3.74 g, 0.029 mol) were mixed with 70% sulfuric acid (58 ml) and the mixture was stirred at room temperature for 6 h. The mixture was then poured into 250 ml ice water, allowed to remain at 4°C overnight and filtered. The white crystals recovered are the first fraction of the product N-(4-methyl-2-oxo-2*H*-chromen-7-yl)acetamide. A second fraction was obtained by extracting the mother liquor 3 times with diethyl ether (30 ml each). The diethyl ether layers were combined and the solvent removed under reduced pressure. The white solid obtained was combined with the other batch of product, yield 2.42 g (45.8%). N-(4-methyl-2-oxo-2*H*-chromen-7-yl)acetamide (1.40 g, 0.00645 mol) was refluxed in 90% sulfuric acid (10 mL) for 5h. The mixture was then poured into 250 ml ice water and allowed to remain at 4°C overnight. The solution was then carefully neutralized using 50% NaOH. The white precipitate was filtered and washed with 3ml of ice water and dried at normal pressure using N₂, yield 1.0 g (88.5%) of the hydrogen sulfate salt of the protonated product!

The latter was dissolved in as little DMF as possible (usually 4 mL). Anhydrous K₂CO₃ (0.90g) was added, which resulted in a suspension. After stirring for 2 h at room temperature, the

mixture was cooled to 0°C and then filtered. The solvent of the filtrate was removed at room temperature in high vacuum, yield 0.35 g (98%).

3-(4-methyl-2-oxo-2*H*-chromen-7-yl carbamoyl) propanoic acid **17**

7-amino-4-methyl-2*H*-chromen-2-one **16** (0.35 g, 0.0020 mol) and succinic anhydride (0.20 g, 0.0020 mol) were dissolved in DMF (5 ml) and stirred at room temperature overnight. The solvent was removed at normal pressure by purging with N₂ and collected in a liquid N₂ cooled trap. The residue was sonicated in ethanol (100%, 20 mL) for 1 min and then filtered. A white powder was obtained, yield 0.47 g (85.4%) mp 170°C.

FT-IR (KBr) (cm⁻¹): 3493, 3421, 3308, 2930, 1742, 1711, 1670, 1624, 1583, 1537, 1398, 1363, 1229, 1178, 871, 815, 717

¹H NMR (200 MHz, DMSO-d₆): 10.35 (1H, s), 7.64 (2H, m), 7.40 (1H, d, J=5.9Hz), 6.18 (1H, s), 2.49 (4H, m), 2.33 (3H, s)

¹³C NMR (200 MHz, DMSO-d₆): 173.05, 170.23, 159.37, 153.04, 152.45, 141.89, 125.26, 114.27, 111.43, 104.63, 30.53, 27.88, 17.29

Hydroxylated 2-(4-(pyridin-4-yl)-4-pyridinium)-methyl cavitand (3-(4-methyl-2-oxo-2*H*-chromen-7-yl carba-moyl)propanoic acid)monoester **18**

Hydroxylated 2-(4-(pyridin-4-yl)-4-pyridinium)-methyl cavitand **9** (0.16 g, 0.00011 mol), 3-(4-methyl-2-oxo-2*H*-chromen-7-yl carbamoyl) propanoic acid **17** (0.030 g, 0.11 mmol) and TPP (0.0058 g, 0.00022 mol) was dissolved in DMF (5 mL) under a nitrogen atmosphere. DEAD (38 ul, 0.00022 mmol) was added and the mixture was kept at 60°C for 12 h. The solvent was removed at normal pressure by purging with N₂ and collected in a liquid N₂ cooled trap. The residue was washed 3 times with 5 ml of acetone and the recrystallized from acetone. A light brown powder was obtained, yield 0.15 g (79.9%).

FT-IR (KBr) (cm⁻¹): 3631-3308 (br), 1745, 1710, 1639, 1460, 1250, 1163, 1112, 984, 958, 820, 723, 538

¹H NMR (400 MHz, DMSO-d₆): 9.17 (8H, m), 8.89 (8H, m), 8.04 (8H, m), 7.90 (8H, m), 7.79 (3H, m), 7.38 (1H, m), 6.46 (4H, m), 5.88 (8H, m), 4.64 (4H, m), 4.08 (2H, m), 3.62 (6H, m), 2.40-2.45 (16H, m), 2.30 (4H, m), 1.4-1.75 (11H, m)

Concentration in DMSO-d₆ too low to record a 1 D ¹³C- NMR.

Hydroxylated 2-(4-((3-methyl)-pyridin-4-yl)-4-(3-methyl)pyridinium)-methyl cavitand (3-(4-methyl-2-oxo-2*H*-chromen-7-yl)carbamoyl)propanoic acid)monoester **19**

Hydroxylated 2-(4-((3-methyl)-pyridin-4-yl)-4-(3-methyl)pyridinium)-methyl cavitand **15** (0.18 g, 0.00011 mol), 3-(4-methyl-2-oxo-2*H*-chromen-7-yl) carbamoyl) propanoic acid **17** (0.03 g, 0.11 mmol) and TPP (0.0058 g, 0.00022 mol) were dissolved in DMF (5 mL) under a nitrogen atmosphere. DEAD (38 μ l, 0.00022 mmol) was added and the mixture was kept at 60°C for 12h. The solvent was removed at normal pressure by purging with N₂ and collected in a liquid N₂ cooled trap. The residue was washed 3 times with 5ml of acetone and then recrystallized from acetone. A light brown powder was obtained, yield 0.164 g (81%).

FT-IR (KBr) (cm⁻¹): 3401, 2991, 2899, 1608, 1537, 1501, 1429, 1347, 1286, 1204, 1173, 1127, 1030, 1000, 979, 886, 804

¹H NMR (400 MHz, DMSO-d₆): 9.32 (4H, m), 8.96 (4H, m), 8.65 (4H, m), 8.56 (4H, m), 8.03 (8H, m), 7.77 (1H, m), 7.64 (1H, m), 7.46 (1H, m), 7.33 (4H, m), 6.53 (4H, m), 6.21 (1H, m), 5.84 (8H, m), 4.66 (8H, m), 4.39 (4H, m), 4.08 (4H, m), 2.56 (4H, m), 2.38 (3H, m), 2.26 (8H, m), 2.07 (24H, m), 1.41 (8H, m)

Concentration in DMSO-d₆ too low to record a 1 D ¹³C- NMR.

Quaternization procedure with dimethyl sulfate **20**

Hydroxylated 2-(4-(pyridin-4-yl)-4-pyridinium)-methyl cavitand (3-(4-methyl-2-oxo-2*H*-chromen-7-yl)carbamoyl) propanoic acid)monoester **18** (0.080g, 0.000045mol) and dimethyl sulfate (0.028 g, 0.000225 mol) was dissolved in DMF (4 mL) under nitrogen atmosphere and heated to 50°C for 1 d. The precipitation was collected, washed with 3ml of acetone for 3 times and dried under reduced pressure. A light brown powder was obtained, yield 0.075 g (78%).

FT-IR (KBr) (cm⁻¹): 3442, 1639, 1189, 1122, 620

¹H NMR (200 MHz, DMSO-d₆): 9.26 (16H, m), 8.72 (20H, m), 8.20-7.62 (3H, m), 6.42 (4H, m), 5.86 (8H, m), 4.60 (12H, m), 4.42 (16H, m), 3.73 (3H, m), 3.31 (4H, m), 2.45-2.48 (11H, m), 1.44 (8H, m)

Concentration in DMSO-d₆ too low to record a 1 D ¹³C- NMR.

Quaternization procedure with dimethyl sulfate **21**

Hydroxylated 2-(4-((3-methyl)-pyridin-4-yl)-4-(3-methyl)pyridinium)-methyl cavitand (3-(4-methyl-2-oxo-2*H*-chromen-7-ylcarbamoyl)propanoic acid)monoester **19** (0.08 g, 0.00004 mol) and dimethyl sulfate (0.025 g, 0.00020 mol) was dissolved in DMF (4 mL) under nitrogen atmosphere and heated to 50°C for 1 d. The precipitation was collected, washed with 3ml of acetone for 3 times and dried under reduced pressure. A light brown powder was obtained, yield 0.071 g (75%).

FT-IR (KBr) (cm⁻¹): 3404, 3063, 2905, 1639, 1475, 1250, 1152, 1060, 1014, 989, 769, 620, 589

¹H NMR (400 MHz, DMSO-d₆): 9.28 (4H, m), 9.19 (4H, m), 9.02 (4H, m), 8.90 (4H, m), 8.13 (8H, m), 8.10 (4H, m), 7.86 (4H, m), 7.51 (4H, m), 6.41 (4H, m), 5.71 (8H, m), 4.64 (8H, m), 4.51 (4H, m), 4.37 (12H, m), 3.45 (3H, m), 2.73 (12H, m), 2.46 (19H, m), 2.20 (8H, m), 2.12 (4H, m), 1.99 (4H, m)

Concentration in DMSO-d₆ too low to record a 1D ¹³C- NMR.

CHAPTER 3 - Gold Nanoparticle-binding Resorcin[4]arene Cavitand

Introduction

Expression of MspA Porin Mutants in *M. smegmatis*

The discovery of the porin MspA and of three very similar proteins of *M. smegmatis* has been described.^{xliv,xlv} All four *msp* genes partially or fully complement the permeability defects of porin mutants, demonstrating that they encode porins of *M. smegmatis*.^{xlvi} To achieve a preparation of pure MspA protein, all four *msp* porin genes of *M. smegmatis* were consecutively deleted by the Bossmann group. The strains **ML16** ($\Delta mspA \Delta mspC \Delta mspD$) and **ML59** ($\Delta mspA \Delta mspB \Delta mspC \Delta mspD$, *attB:loxP*-*p_{imyc}*-*mspA*-*loxP*) allow our group to express mutant MspA proteins with little or no background expression of endogeneous porins of *M. smegmatis*. Expression of functional porin genes will be achieved by replacing wild-type *mspA* by a mutated *mspA* gene by temporarily expressing the L5 recombinase as demonstrated for other genes according to a published method.^{xlvii} These strains have been used for extraction and purification of over 100 MspA mutants so far.^{xlviii} Expression of correctly folded and fully functional MspA pores has been achieved in *E. coli* and may be used as an alternative expression system.⁴⁸

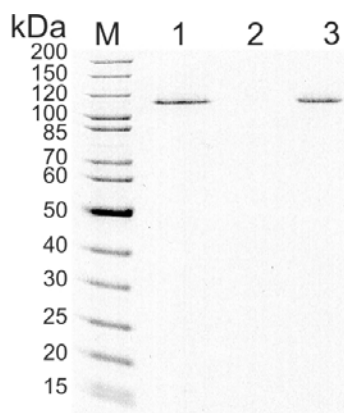


Figure 3.1: Expression of MspA mutants in the mutant *M. smegmatis* ML10.

A 10% polyacrylamide gel was used to separate proteins in detergent extracts of the following *M. smegmatis* strains: lane 1: ML10/*pMN016* (wt MspA), lane 2: ML10/*pMS2* (no MspA), lane 3: ML10/*pMN016-mspAG44C*.

The plasmids *pMN016* and *pMS2* are an *mspA* expression vector and an empty vector, respectively.

Purification of MspA from *M. smegmatis*

The aforementioned procedure exploits the extreme thermal stability of MspA by heating *M. smegmatis* cells to 100 °C in the presence of 0.5% of the non-ionic detergent *n*-octylpolyoxyethylene and yields mainly Msp porins with very little contamination by other proteins. Using the ML59 strain or *E. coli* as a host system can eliminate the presence of a small number of other Msp porins. Expression of the *mspA* gene using the plasmid pMN016 yields wild-type levels of MspA in the ML10 strain demonstrating that more than 95% of all extractable porin is made from the *mspA* gene on pMN016 (Figure 3.1, lane 1). The purity of MspA, with respect to other proteins, in these detergent extracts is already greater than 85% as determined by quantitative image analysis (not shown). MspA mutants are expressed on the same level as wild-type MspA as shown for the cysteine mutant MspAG44C (Figure 3.1, lane 3) or on lower levels as shown for other cysteine mutants.^{xlix} To remove contaminating minor proteins and small molecules, a purification method based on subsequent anion exchange and gel filtration chromatography has been developed.¹ The group of Prof. Dr. Michael Niederweis at the University of Alabama at Birmingham, with whom we collaborate, has used the ML10 and ML16 strains of *M. smegmatis* for the isolation of 48 MspA cysteine mutants in detergent extracts and for the chromatographic purification of 30 MspA constriction zone mutants with yields of up to 750 µg MspA per liter culture of *M. smegmatis*.⁴⁴ Their results have shown that they have developed an efficient expression and purification system for MspA mutants in *M. smegmatis*.

MspA is a Very Stable Pore Protein with a Unique Structure

MspA is an extremely stable membrane protein, which withstands organic solvents, heating to 100 °C for 30 min in the presence of detergents or 1 M HCl or NaOH.^{33a} This extraordinary stability has many advantages including a long-term durability of the protein (fully functional MspA pores have been stored for longer than three years) and the possibility to use organic solvents, which is often helpful in technical processes. The unique protein architecture is probably one reason for the stability of MspA. The crystal structure of MspA reveals a new all beta-fold: eight monomers span the membrane twice and have a very large interaction area to

form a central channel.^{33b} The constriction zone has a diameter of 1.0 nm and is defined by two rings of aspartates D90 and D91 (Figure 3.2).

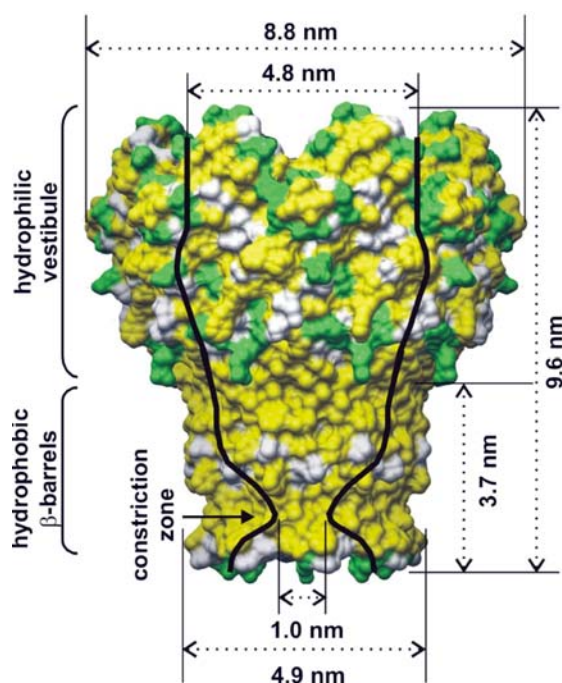


Figure 3.2: Dimensions of the MspA-homopore^{33b}: yellow (medium gray): hydrophobic amino acids, green (dark gray): hydrophilic amino acids. The hydrophilic vestibule of MspA is funnel-shaped and has a water-accessible volume of approximately 96 nm^3 ^{33b}

Preliminary SPR-Measurement of MspA on Gold

Conventional SPR-measurements monitor the changes in thickness and/or refractive index of ultrathin films on noble metal surfaces.⁵⁰ When an incident beam of p-polarized light (p: in plane) of a defined wavelength strikes the surface at a given angle through a prism, photon-plasmon surface electromagnetic waves (surface plasmon polaritons) are created at the metal(usually Au or Ag)/dielectric interface. The typical film thickness of the metal surface on glass is 50nm. These waves propagate parallel to the metal/dielectric interface. Typically, they decay exponentially exhibiting a typical decay length (1/e) of approximately 200nm. The measurable consequence of the occurrence of surface plasmon polaritons is a reduced intensity of the reflected light under the incident angle Θ . The reflectance R of the incident light is usually calculated by using a three-layer Fresnel equation relating p-polarization.^{li} The reflectance varies as a function of the dielectric constant (ϵ_p) of the sensing layer, which is the square of the refractive index n. A typical model for the quantitative interpretation of SPR-data takes into

account N absorption oscillators per unit of volume that depend on the concentration of the proteins on the metal/dielectric interface. Conventional SPR-biosensors (e.g. the BiaCore instrument that will be used in this study) use monochromatic light and vary the distribution of the incident angles. The corresponding reflected beams with reduced intensity are detected and the SPR angles of reflected light continuously calculated. The change in SPR angle Θ of reflected light at a given incident wavelength can be calculated according to Equation (3.1)⁵⁰:

$$\Delta\Theta(\lambda) = c_1\Delta n + c_2\Delta d \quad (3.1) \quad c_1, c_2: \text{constants, } n: \text{refractive index, } d: \text{thickness of the layer}$$

According to the Lorentz-Lorenz relation, any change in the thickness of the adsorbed protein-layer (Δd) will result in a refractive index change (Δn).

$$\Delta n = -\frac{1}{6n} (n^2 + 2)^2 \left(\frac{n^2 - 1}{n^2 + 2} - \frac{n_w^2 - 1}{n_w^2 + 2} \frac{V_p}{V} \right) \frac{\Delta d}{d} \quad (3.2)$$

n_w : refractive index of water ($n_w=1.333$)
 V_p : volume of the adsorbed protein
 V_w : volume of water in the adsorbed layer
 $V=V_p+V_w$: volume of the protein layer

SPR angles are reported in resonance units (RU). A response of 10^3 RU corresponds to an angle change of 0.1 degree, the typical value for binding 1ng/mm^2 of protein. According to Equation (3.1), the SPR-angle of the reflected light should vary linearly with increasing thickness of the protein layer on the surface if the changes in the refractive index occurring during adsorption remain small. We have adsorbed the myco-bacterial porin MspA on a gold-chip ($d_{Au}=50$ nm) and observed the changes in the SPR angles Θ of reflected light and the corresponding RU-units. It becomes immediately clear that the change of Θ is not monotonous when adsorbing MspA. The main reason for this deviation is easily found in the geometric shape of MspA, which is approximately 9.6 nm in height and 8.6 nm in diameter. However, once a monolayer of MspA on gold is formed, the theoretical and the measured angles Θ intercept, indicating that indeed a monolayer of MspA is formed. Corroborating AFM (Atomic-Force-Microscopy) results were obtained in the PI's group, indicating that MspA can act as stable "stand-alone" porin on mica and gold.

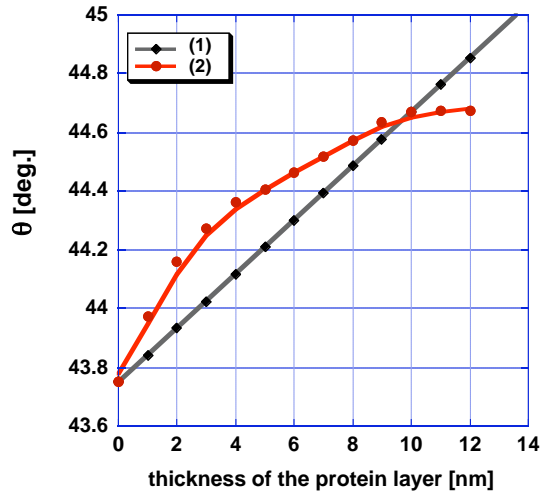


Figure 3.3: Adsorption of *MspA* (wt) on gold, measured by SPR (BiaCore 3000). In each step, a tenth of the required amount of the cysteine-containing *MspA*-P97C-mutant to form a monolayer was added. The measurement was performed by Dr. Stefan Bossmann at the University of Kansas

(1) Theoretical straight line of the dependence of the SPR reflected angle (Θ) on the diameter of the adsorbed protein layer, (2) experimentally obtained curve for *MspA* adsorption

Localized Surface Plasmon Resonance with Gold Nanoparticles in Solution

Despite their high popularity and abundance in laboratories, SPR-based detection methods have a major drawback in that their detection limit is approximately 1 nM of a 200kDa protein.⁵² Other drawbacks are the relatively high costs of the SPR-chips and that these measurements are relatively slow, not allowing their use in clinical high-throughput facilities.

Based on the earlier work of *P. Englebienne* and coworkers^{liii} the Bossmann group has revisited the use of gold nanoparticles in SPR-experiments. The PI's spectral simulations (see Figure 3.4) indicate that a higher sensitivity could indeed be achieved when the phenomenon of localized surface plasmon resonance (LSPR) is applied.⁵² The optical extinction $E(\lambda)$ of nanoparticles being smaller than the wavelength of the exciting light source, is given by Equation (3.3).

$$E(\lambda)L_t = S(\lambda) + A(\lambda)L_t \quad (3.3) \quad \lambda: \text{wavelength, } S: \text{scattering, } A: \text{absorbance, } L_t: \text{optical path length}$$

The particle polarizability $\alpha(\nu)$ is a function of the effective complex dielectric constants of the

metal nanoparticle ϵ_m and the medium ϵ_0 . The optical extinction cross-section $C_{E(\lambda)}$ for a single

$$\alpha(\nu) = f_m \left(\frac{\epsilon_m - \epsilon_0}{\epsilon_m + K\epsilon_0} \right) \quad (3.4) \quad \begin{array}{l} f_m: \text{volume fraction of the metal in the mixture, } K: \\ \text{geometric factor (K=2 for spheres)} \end{array}$$

nanoparticle is related to the particle polarizability $\alpha(\nu)$ via its absorbance and scattering cross sections, as expressed in Equation (3.5).

$$C_{E(\lambda)} = ki\alpha(\nu) + \frac{k^4}{6\pi} |\alpha(\nu)|^2 \quad (3.5) \quad k = \frac{2\pi r \sqrt{\epsilon_0}}{\lambda}, \quad r, \text{ particle radius}$$

Finally, the transmittance T follows from the extinction cross section $C_{E(\lambda)}$ by means of Equation (3.6).

$$T = e^{-NC_{E(\lambda)}L_t} \quad (3.6) \quad N: \text{number density of particles}$$

Noble metal nanoparticles are especially attractive for SPR-measurements in solution because the real part ϵ'_m of the complex dielectric constant ϵ_m decreases monotonically with λ in the visible range of the spectrum, whereas the imaginary part ϵ''_m is small and first-order independent on λ . Hence, $C_{E(\lambda)}$ will become very large when the sum of ϵ'_m and $K\epsilon'_0$ approaches zero when the LSPR of the metal nanoparticles is approached.

$$\epsilon_m = \epsilon_m^\infty - \frac{\omega_p^2}{\omega(\omega + i\omega_\tau)} = \epsilon'_m + i\epsilon''_m \quad (3.7) \quad \begin{array}{l} \epsilon_m^\infty: \text{contribution from bound electrons} \\ \omega_p: \text{plasmon frequency} \\ \omega_\tau: \text{damping frequency} \\ \omega: \text{angular frequency of the incident light} \end{array}$$

By solving Equation 3.3-3.7, we were able to simulate the wavelength changes of the LSPR of 50nm gold nanoparticles in dependence to the refractive index at the metal/dielectric interface. As it becomes apparent from Figure 3.4, any minuscule change in the dielectric constant/refractive index ($n_0 = \sqrt{\epsilon_0}$) results in a discernible shift of the LSPR! According to this model, a red-shift of approximately 0.5nm occurs for every 0.01 unit increment in n .

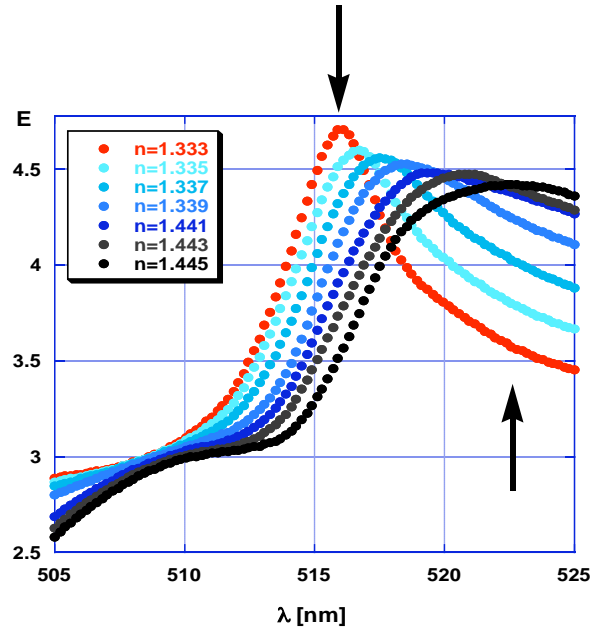
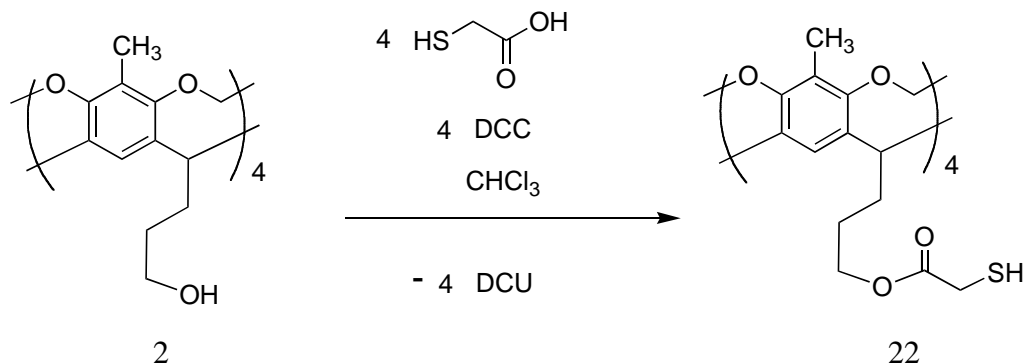


Figure 3.4: Simulated absorption spectra of 50nm spherical gold nanoparticles in aqueous solution, simulated according to eqn. (3.3) - (3.7). The two arrows mark the regions of the spectrum where pseudo-linear dependencies of the optical absorption (A) from the refractive index of the metal/dielectric interface can be discerned. These wavelengths ($\lambda = 516\text{nm}$ and 523 nm) are especially suitable for a simple detection setup by monitoring the absorption of one wavelength. This simulation was performed by Dr. Stefan Bossmann.

It is noteworthy that LSPR-detection does not only work by using gold nanoparticles of 50nm in diameter, but with virtually any size between 20 nm and 100 nm. Since the LSPR-maxima are a linear function of the diameters of gold nanoparticles^{liii}, several measurements can be performed in the same cuvette/vial by attaching one specific antibody or antibody-fragment to one particular size of nanogold. The major drawback of using monoclonal antibodies or antibody-fragments chemically linked to gold- nanoparticles is their lack in long-term stability.^{liv} This effect causes relatively fast changes of n at the metal-/dielectric(antibody) – interface, which can be the source of many artifacts. We anticipate that the solution to this problem will be the use of MspA-scFv-fragment fusion proteins at the metal/dielectric - interface. Due to the stability of MspA, we expect the chemisorbed layer of fusion proteins to be very long-term stable.

Synthesis of Resorcin[4]arenes Designed for the Binding on Gold



Scheme 3.1

The product of this reaction is very air sensitive. After work up procedure and one quick column chromatography, most of the product was lost. The remaining material couldn't afford further purification in air. Therefore, only impure cavitand products mixed with DCC and DCU was obtained. The ¹HNMR of the product possess typical pattern of resorcin[4]arene cavitands and it's featured peaks have different chemical shifts from starting material **2**. Also, the product's room temperature solubility in CDCl₃ is very different from the starting material **2**. Combining the information from the NMR spectra and the result of gold nanoparticle binding studies, I propose that **22** was one of the products, possibly mixed with some tris-functionalized cavitand.

Binding of the Tetra-thiol-substituted Resorcin[4]arene to the Surface of Gold-Nanoparticles.

A) Plasmon Absorption

I have attempted to verify the photophysical behavior of gold nanoparticles that is described by equations 3.1-3.7 with the following sequence of experiments: Gold nanoparticles (a precious gift from NanoScale Materials Inc.) possessing a spherical shape and a diameter of 47+/-5 nm underwent ligand exchange in toluene. This process is thermodynamically favored due to the formation of four thiol-gold bonds per resorcin[4]arene. The binding enthalpy of 4 x -5 to -6 kcal mol⁻¹, which is typical for the binding of alkanethiols to gold^{lv}, is sufficient to displace the organic coating used (undisclosed information) for the stabilization of the gold nanoparticles. As it becomes clear from Figure 3.5, the process of ligand exchange did not lead to a significant change in the diameter of the gold nanoparticles, otherwise the observed plasmon-absorption spectrum would have indicated that. The maximum of the plasmon absorption of the gold nanoparticle in the absence of the tetra-thiol-substituted resorcin[4]arene

is 508 nm. It then moves stepwise to approximately 510, 512, 513 and 515 nm upon addition of four aliquots of thiol-footed resorcin[4]arene. It is noteworthy that the concentration of gold nanoparticles in toluene is 3.85×10^{-10} M ($\epsilon=7.8 \times 10^9$ at 508nm, according to NanoScale) and the concentrations of thiol-footed resorcin[4]arene are 0.5×10^{-7} M, 1.0×10^{-7} M, 1.5×10^{-7} M and 2.0×10^{-7} M. The spherical gold nanoparticles feature a surface of approximately 6940 nm^2 , whereas the effective surface of the thiol-footed resorcin[4]arene is approximately 3.25 nm^2 , according to molecular modeling (MM2, PM3). According to these approximations, the maximum number of bonded thiol-footed resorcin[4]arene macrocycles at the surface of one gold nanoparticle is 2125. These measurements show that the measurement concept relying on the surface plasmon of a nanoparticle instead of an ultraflat surface, as discussed in this chapter is valid. We have found at least a qualitative agreement of the measurements reported here and the predicted absorption behavior of the surface-plasmon of a gold nanoparticle. Note that increasing the resorcinarene's concentration to 2.5×10^{-7} M did not lead to a discernible change of the UV/Vis-spectrum. Therefore, we have concluded that at that concentration no further surface coating occurs. However, our measurements did not allow us to conclude, whether the surface coverage was complete or not. TEM (Transmission electron microscopy) imaging did not lead to a conclusive result either because of problems with the sample preparation. Our TEM samples indicated that clustering and/or coagulation of the samples. However, from the comparison of the maximal number of resorcinarenes at the surface of the gold nanoparticles and the concentration added in this experiment, it appears that the number of surface-bound organic ligands is approximately 4 times less than a perfect surface coverage.

Note that addition of thiol-footed resorcin[4]arene beyond $c = 2.5 \times 10^{-7}$ M led to the precipitation of the coated gold nanoparticles.

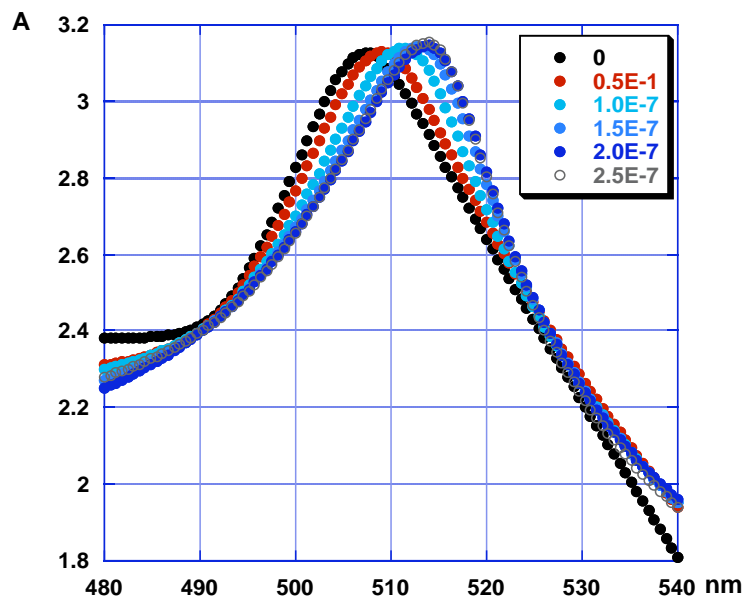


Figure 3.5: Absorption spectra of gold nanoparticles ($d=47\pm 5$ nm, $c=3.85 \times 10^{-10}$ M) in toluene (black curve) and upon addition of thiol-footed resorcin[4]arene. The concentration of the macrocycle were 0.5×10^{-7} M (red curve), 1.0×10^{-7} M (light blue curve), 1.5×10^{-7} M (blue curve), 2.0×10^{-7} M (dark blue curve) and 2.5×10^{-7} M (grey curve).

B) Plasmon Emission

After a qualitative agreement of the light absorption and scattering theory and my experiments had been achieved, we have investigated the emission behavior of the assemblies of the gold nanoparticles and the thiol-footed resorcin[4]arene in toluene.

I would like to thank Mrs. Thilani N. Samarakoon for her help concerning the fluorescence measurements. The emission of the thiol-footed resorcin[4]arene has a maximum of 320 ± 3 nm and is most likely an monomer-peak occurring from one of the four neighboring and chemically linked benzene units of the macrocycle.^{lvi}

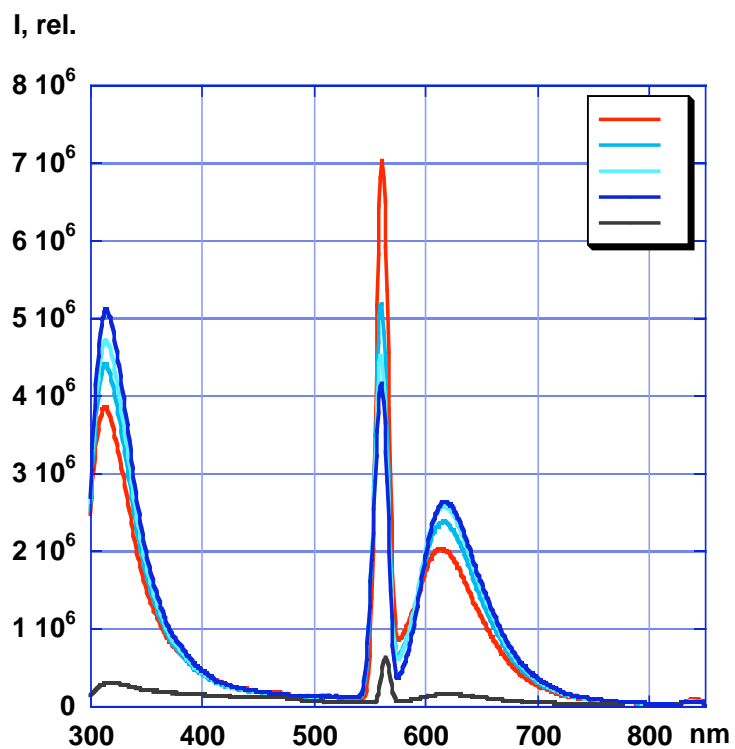


Figure 3.6: Emission spectra of gold nanoparticles ($d=47\pm 5$ nm, $c=3.85 \times 10^{-10}$ M) in toluene (black curve) and upon addition of thiol-footed resorcin[4] arene. The concentration of the macrocycle were 0.5×10^{-7} M (red curve), 1.0×10^{-7} M (light blue curve), 1.5×10^{-7} M (blue curve), 2.0×10^{-7} M and (dark blue curve).

Note that the strong peak at 560 nm is an artifact due to excitation at $\lambda = 280$ nm.

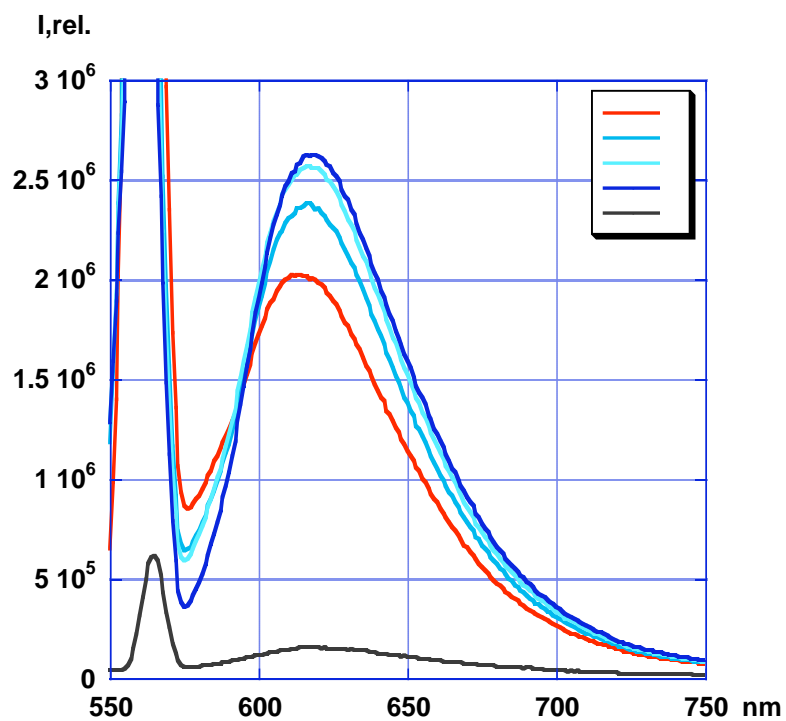


Figure 3.7: Emission spectra of gold nanoparticles ($d=47\pm 5$ nm, $c=3.85 \times 10^{-10}$ M) in toluene (black curve) and upon addition of thiol-footed resorcin[4]arene. The concentration of the macrocycle were 0.5×10^{-7} M (red curve), 1.0×10^{-7} M (light blue curve), 1.5×10^{-7} M (blue curve) and 2.0×10^{-7} M (dark blue curve).

Note that the strong peak at 560 nm is an artifact due to excitation at $\lambda = 280$ nm.

It is most interesting that the fluorescence occurring from the surface plasmon of the gold nanoparticle is enhanced with increasing concentration of the thiol-footed resorcin[4]arene. Since the excitation wavelength is $\lambda = 280$ nm, it is our mechanistic hypothesis that the photoexcited resorcin[4]arene is able to transfer its electronic excitation to the chemically attached gold nanoparticle. The higher the surface coverage, the higher the resulting emission from the surface plasmon. The increase of the fluorescence is leveling off at a resorcinarene-concentration of 2.0×10^{-7} M. This is the same threshold that was observed in the Vis-absorption experiment. Apparently, this method is more sensitive than studying the VIS-absorption of the surface plasmon!

Addition of Hexachlorobenzene

Further proof for this measurement concept has been obtained by adding defined amounts of hexachlorobenzene to the toluene-solution containing 3.85×10^{-10} M mol gold nanoparticles and 2.0×10^{-7} M of thiol-footed resorcin[4]arene. As Figure 3.8 indicates, the thiol-footed resorcin[4]arene is able to bind one hexachlorobenzene-molecule per macrocycle when in the vase conformation. The latter is ensured by the simultaneous binding of the four thiol-units to the gold surface. Note that the surface of the gold-nanoparticle ($d = 47 \pm 5$ nm) appears quite flat with respect to the resorcin[4]arene ($d=1.18$ nm).

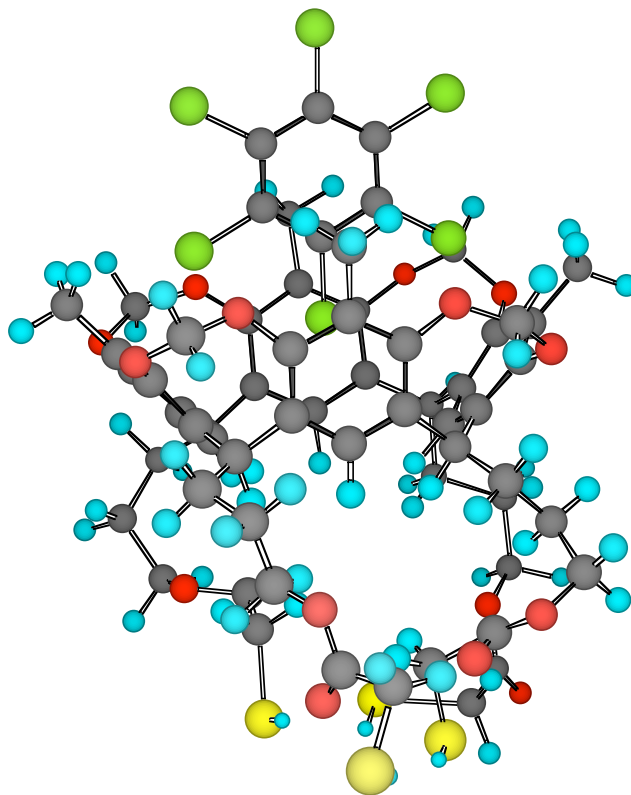


Figure 3.8: Supramolecular complex between the thio-footed resorcin[4]arene and hexachlorobenzene. I constrained the macrocycle in the “vase”-conformation to simulate the binding of the four “thiol-feet” on a gold surface.

Figure 3.9 and 3.10 indicate that again a characteristic red-shift of the emission occurring from the surface plasmon is observed. It is our hypothesis that the toluene solvent molecule that is usually bound within the cavity of the resorcinarene-macrocycle is replaced by the more hydrophobic and electron-poor hexachlorobenzene. This causes a change in the refractive index of the resorcinarene-layer that is chemically attached to the surface of the gold nanoparticle. Consequently, the emission maximum shifts from 618 to 632 nm. Once a hexachlorobenzene-concentration of 4×10^{-7} M is reached, no more changes of the emission maximum can be observed. However, the emission peak decreases due to parasitic absorption of the incident light at the excitation wavelength by hexachlorobenzene.

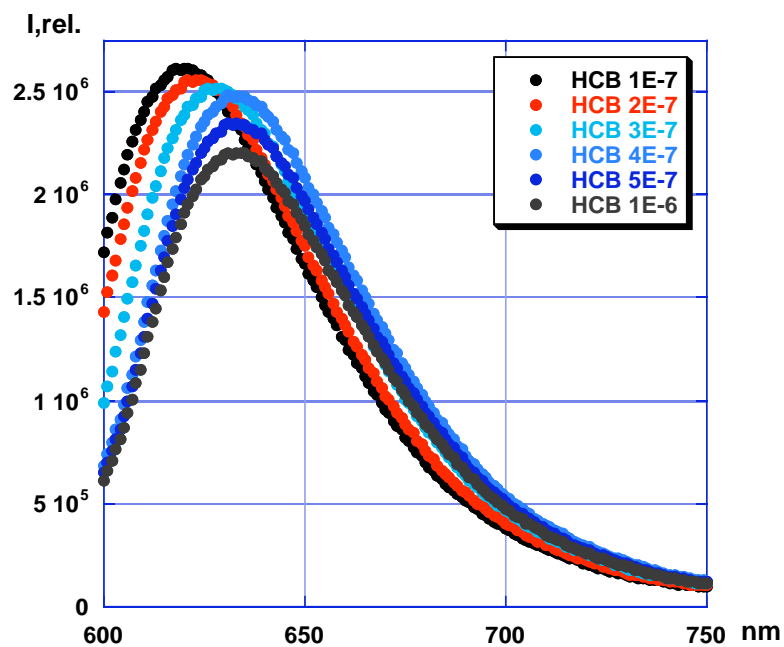


Figure 3.9: Plasmon-emission occurring from thiol-ferrocene-resorcin[4]arene-covered gold nanoparticles.

$$\lambda_{exc}=280 \text{ nm}$$

[Au-nanoparticles]:

$$3.85 \times 10^{-10} \text{ M}$$

[resorcinarene]:

$$2.0 \times 10^{-7} \text{ M}$$

the HCB (hexachlorobenzene) concentration was varied from $1 \times 10^{-7} \text{ M}$ to $1 \times 10^{-6} \text{ M}$

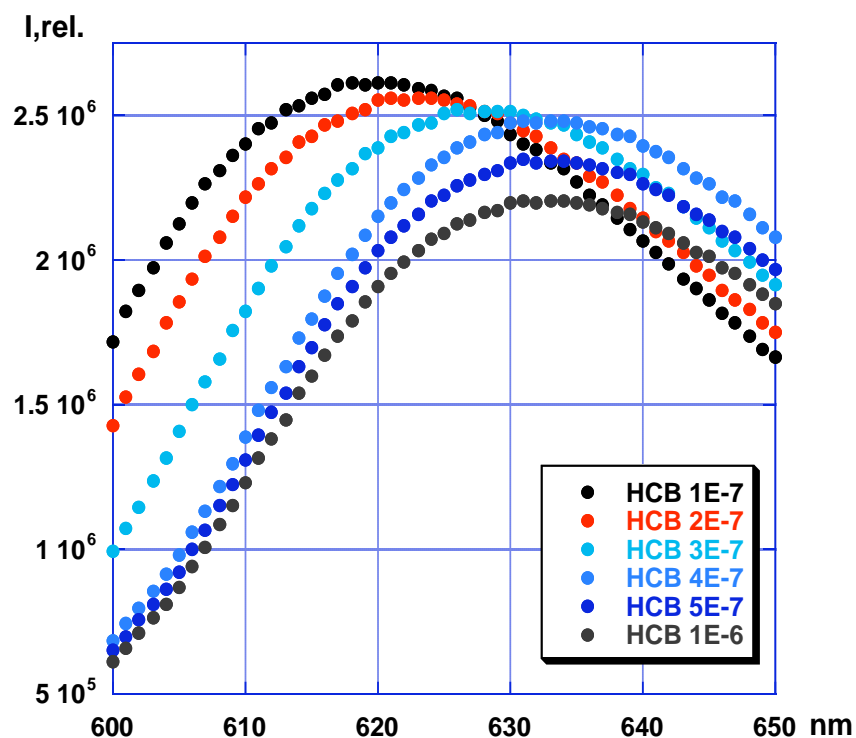


Figure 3.10: Enlargement of Figure 3.5.

I would like to emphasize again that we regard these measurements as a proof of concept for utilizing the emission of gold nanoparticles in chemical sensors after covering their surface with thiol-footed resorcin[4]arenes.

Experimental Session:

Synthesis of 2,20:3,19-Dimetheno-1H,21H,23H,25H-bis[1,3]dioxocino[5,4-i:5',4'-i']benzo[1,2-d:5,4-d']bis[1,3]benzodioxocin-1,21,23,25-tetra(propyl 2-mercaptoacetate), 7,11,15,28-tetramethyl **22**

A: Sodium-2-mercaptoacetate (1.0 g, 0.0087 mol) was suspended in 50 ml of diethyl ether. Then, 10 mL of 1N HCl was added and the two-phase mixture shaken for one minute. The diethyl ether phase was dried by using molecular sieves and then the ether was removed in medium vacuum using a rotavap. 2-mercaptoacetic acid (0.66 g, 82%) was obtained as product.

B: 2,20:3,19-Dimetheno-1H,21H,23H,25H-bis[1,3]dioxocino[5,4-i:5',4'-i']benzo[1,2-d:5,4-d']bis[1,3]benzodioxocin-1,21,23,25-tetrapropanol, 7,11,15,28-tetramethyl (1.0 g, 1.21 mmol) and 2-mercaptoacetic acid (0.56 g, 6.06 mmol) were dissolved in 100ml anhydrous

chloroform at 60°C. Solid DCC (dicyclohexyl-carbodiimide) (1.25 g, 6.05 mmol) was added to the mixture. The mixture was refluxed under nitrogen over night. A white solid was formed on top of the CHCl₃. The solution was allowed to cool to room temperature and the white solid (dicyclohexylurea, DCU) was filtered off. The solvent was removed under reduced pressure and the brownish residue was washed in 10ml of hexane for 3 times. Column chromatography with CH₂Cl₂ yielded a yellow powder as product. Yield: (0.01g, <0.92%)

CHAPTER 4 - Towards an Organic Reduction Catalyst Based on a Resorcin[4]arene Featuring Four Viologene Units

Introduction

Resorcinarenes have been very successfully used to bind small molecules^{lvii,lviii} to create capsules^{lix}, hemicarcerands^{16,lx} and carcerands^{14,60,78} in order to entrap and deliver larger molecules (e.g. drugs)^{lxi,lxii}, and to study organic reactions in confined space and a very controlled reaction environment.¹⁴ The work described here is directed towards the design of an organic reduction catalyst for chlorinated aliphatic and aromatic hydrocarbons. It is well known that oligochlorinated hydrocarbons, such as the insecticide DDT^{lxiii} and hexachlorobenzene (HCB)^{lxiv} and oligochlorinated dibenzodioxins and dibenzofurans^{lxv}, which are formed during from pyrolysis or incomplete incineration of chlorine-containing waste^{lxvi}, are a major environmental problem. This is also true for chlorinated warfare agents, such as “Agent Orange”, which was used in the Vietnam War as defoliant agent and contains very high amounts of polychlorinated biphenyls (approx. 10%) and traces of chlorinated dibenzodioxins.^{lxvii} Their reduction to “simple” aliphatic and aromatic hydrocarbons or at least the partial removal of the organically bound chlorine atoms would greatly diminish their environmental impact. On a technical scale, this is achieved by their reaction with elementary (molten) sodium.^{lxviii} However, this technology cannot be regarded as safe due to the great fire and explosion risks of liquid sodium. Therefore, organic reduction catalysts, which can be coupled with reductive redox-processes, would be of an enormous advantage. They would operate much safer (due to the absence of chemical reduction reagents) and would rely on electrodes to supply the electrons needed for the reduction processes. A major challenge is to design organic reduction catalysts that are capable of multi-electron reduction processes. Another challenge is to realize sufficiently negative standard-reaction potentials in order to reductively attack the stable carbon-chlorine bonds. Depending on the chlorinated molecule, standard-reaction potentials lower than -2.0 V (vs. SHE) (standard hydrogen electrode) should be accomplished.^{lxix}

Results and Discussion

I have already described the synthesis of methylene-bridged resorcin[4]arenes featuring 4,4'-bipyridinium or 3,3'-dimethyl-4,4'-bipyridinium units, chemically linked to the “rim” of the cavitand.^{lxx} Both cavitands have been employed in the studies described in this chapter as well.

As it is apparent from Figure 4.1, the charge-repulsion between the four bipyridinium units, which are connected to methylene-groups permitting them relatively unhindered rotation, causes a flower-like opening of the resorcin[4]arenes' rims (kite-conformation⁵⁷). When reduced, it can be expected that the electrostatic repulsion first diminishes (+8 -> +4) and then disappears (+4 -> 0), causing the macrocycle to adopt different conformations. Doubly reduced viologens are not charged and, therefore, hydrophobic in nature. They can form supramolecular aggregates by hydrophobic interaction. For example, Willner and coworkers have shown that they can be bound in the hydrophobic interior of beta-cyclodextrines.^{lxxi,lxxii} Therefore, we have anticipated before starting this work that the doubly-reduced bipyridinium-modified methylene-bridged resorcin[4]arenes will form deep cavitands⁵⁷ for uncharged halogenated compounds. Furthermore, we expect that electron-transfer from the singly- or doubly-reduced viologens to the chlorinated compounds^{lxxiii} will take place inside such a deep cavitand.

The (3,3'-dimethyl)-4,4'-bipyridinium units are very suitable electron-relays, which can be reduced stepwise to viologen-monoradical cations and then to the uncharged viologen diradicals.^{lxxiv} Their highly negative redox potentials allow them to reduce and detoxify chlorinated toxic hydrocarbons, such as tetrachlorocarbon, tetrachloroethylene^{lxxv} and hexachlorobenzene.⁶⁹ Viologens are widely used as electron relays in artificial photolysis, because they are very stable in the absence of metal catalysts.⁷⁴

In Figure 4.1 to 4.4, the two resorcin[4]arenes used in this study and their main-conformations in the unreduced (+8)-state are shown. It is apparent that the charge-repulsion between the bipyridinium (viologen) groups is causing the macrocycle to adopt the kite formation, in which the four viologen-petals open like a flower.

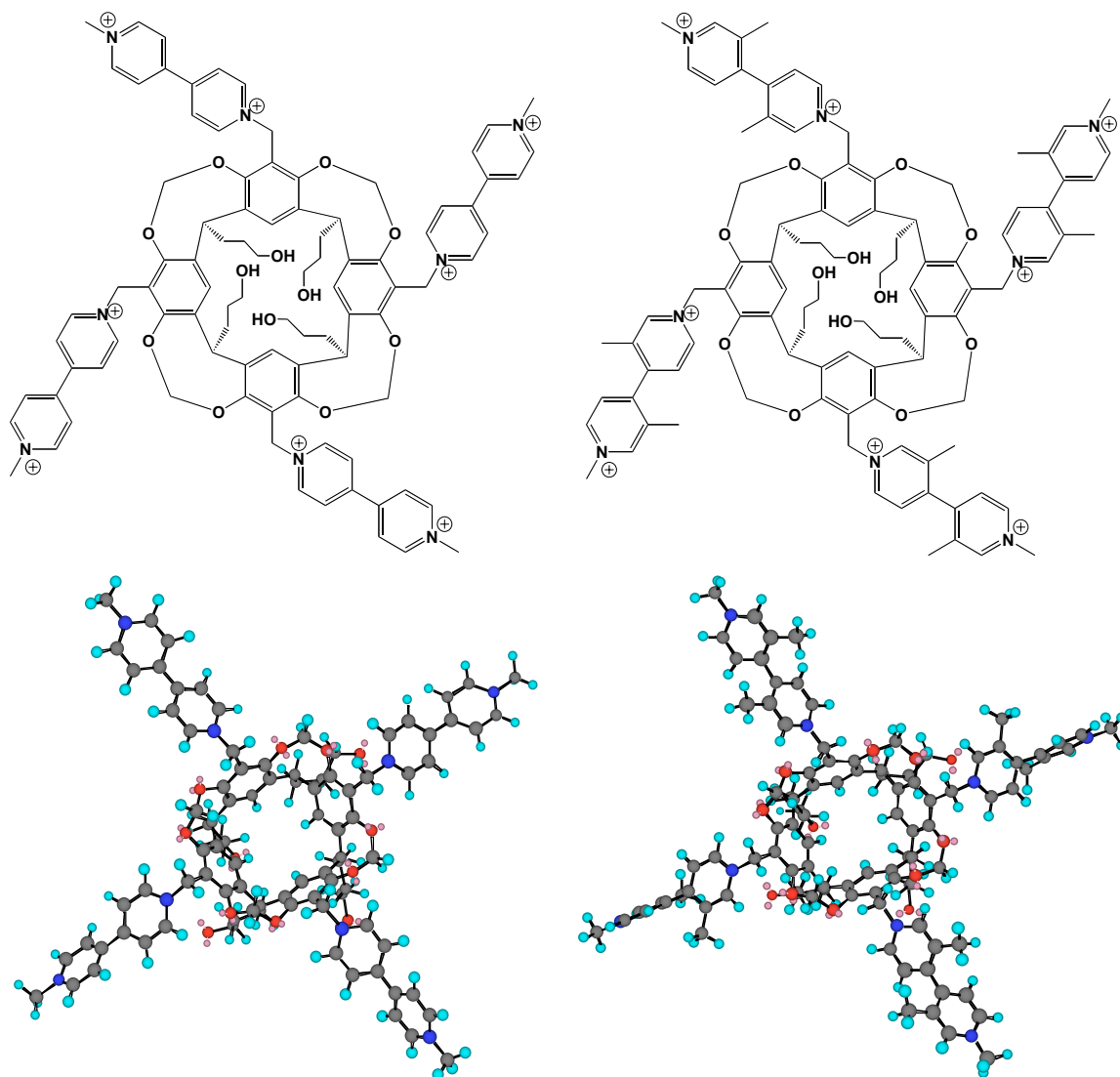


Figure 4.1: Redox-active viologen-resorcin[4]arene (left) and dimethylviologen-resorcin[4]arene (right).

The electrochemical properties of the viologen-resorcin[4]arene and dimethyl-viologen-resorcin[4]arene have been investigated by using the electrochemical method of Differential-Pulse-Voltammetry (DPV).

Differential pulse voltammetry is working as follows^{lxxvi}: A series of voltage pulses (duration: 1-500 milliseconds) is superimposed on a potential linear sweep or “stair steps” in which the potential is raised in (many) steps. The current is measured before each potential change (at the end of the plateau/just before the potential is raised), and the current difference is plotted as a function of the applied potential. This strategy has the enormous advantage that the

effect of the charging current can be decreased and the measurements are not clouded by this effect! Another advantage is that also non-reversible redox transitions can be discerned. The results obtained with the viologen-resorcin[4]arene in anhydrous acetonitrile (electrolyte: LiF) are shown in Figure 4.2:

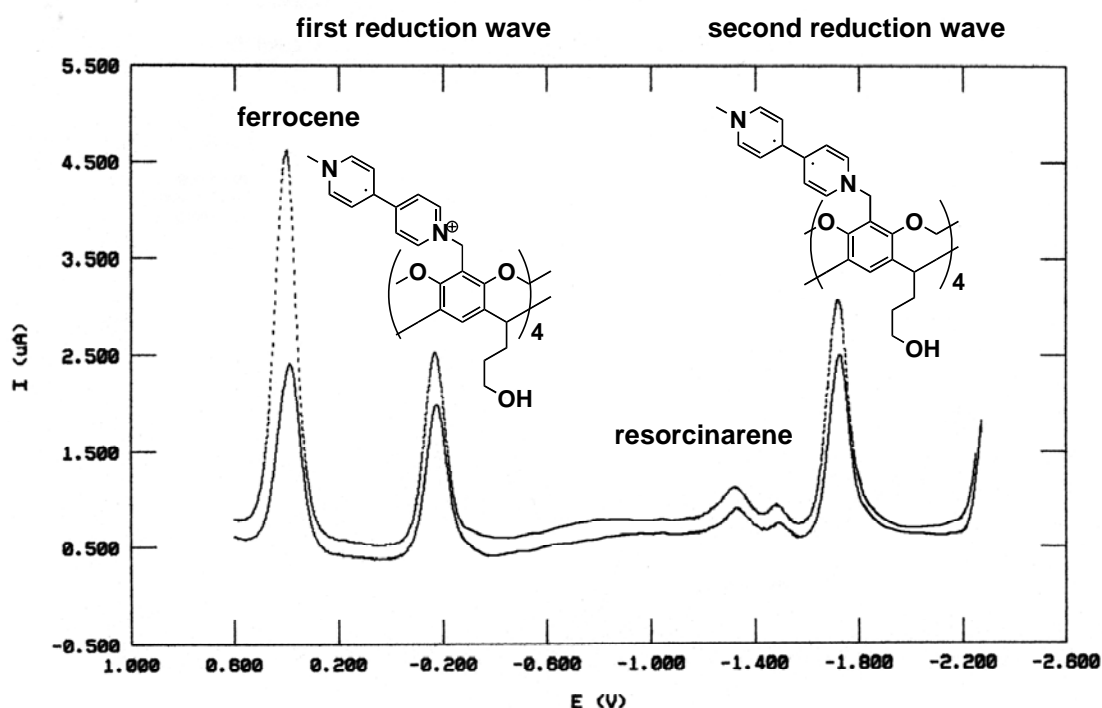


Figure 4.2: DPV of viologen-resorcin[4]arene ($1.0 \times 10^{-6} M$) in anhydrous acetonitrile ($0.50 M$ of LiF) under argon. (scan time: 2 min, step-width: 50 microseconds, working electrode: Pt). Shown are two consecutive scans. Ferrocene ($E_0=0.51$) vs. SCE (saturated calomel electrode) has been used as internal redox standard.

At standard conditions, the potential of the saturated calomel electrode is +0.241 V versus the SHE. At our concentrations, and using ferrocene as standard we have determined the electrochemical potential of the reference electrode to +0.058V. *All electrochemical potentials are given vs. SHE.*

As Figure 4.2 shows, there are two major reduction waves when studying viologen-resorcin[4]arene. We have attributed the two big reductive peaks (4 electrons each) to the first and second reduction wave of the four viologen-units that are covalently attached to the

resorcin[4]arene. In the first wave, occurring at - 0.16 V, the monoradical-cation of each viologen is created. The observed reduction potential less negative than that of methylviologen (- 0.45 V).⁷⁴ This shift could be caused by the presence of four viologens that are chemically attached to the resorcin[4]arene, which leads to a tremendous increase of the local concentration. According to the classic Nernst equation, we observe a shift towards a higher electrochemical potential, if the concentration of the electron acceptor (Ox) is enhanced.

$$E = E^0 - \frac{RT}{nF} \ln \frac{c_{Red}}{c_{Ox}} \quad (4.1)$$

E^0 : Standard electrode potential; R: universal gas constant (8.314510 J K⁻¹ mol⁻¹);

T: absolute temperature. (TK = 273.15 + T°C.), $c()$: concentrations of the reduced (Red) and the oxidized (Ox) species that form the redox couple (Ox/Red); F: Faraday constant (9.6485 × 10⁴ C mol⁻¹); n: number of electrons transferred in the electrochemical reaction.

In the second wave, the viologen-diradical, which is neutral, is formed at -1.71 V. The difference of approximately 1.55 V between the monocation-radical and the double-reduced viologen is typical for many viologen systems that originate from 4,4'-bipyridinium.⁷⁴ At approximately -1.24 V and -1.41 V, two one-electron transitions could be detected, which we attribute to reductive events in the resorcin[4]arene's ring structure.

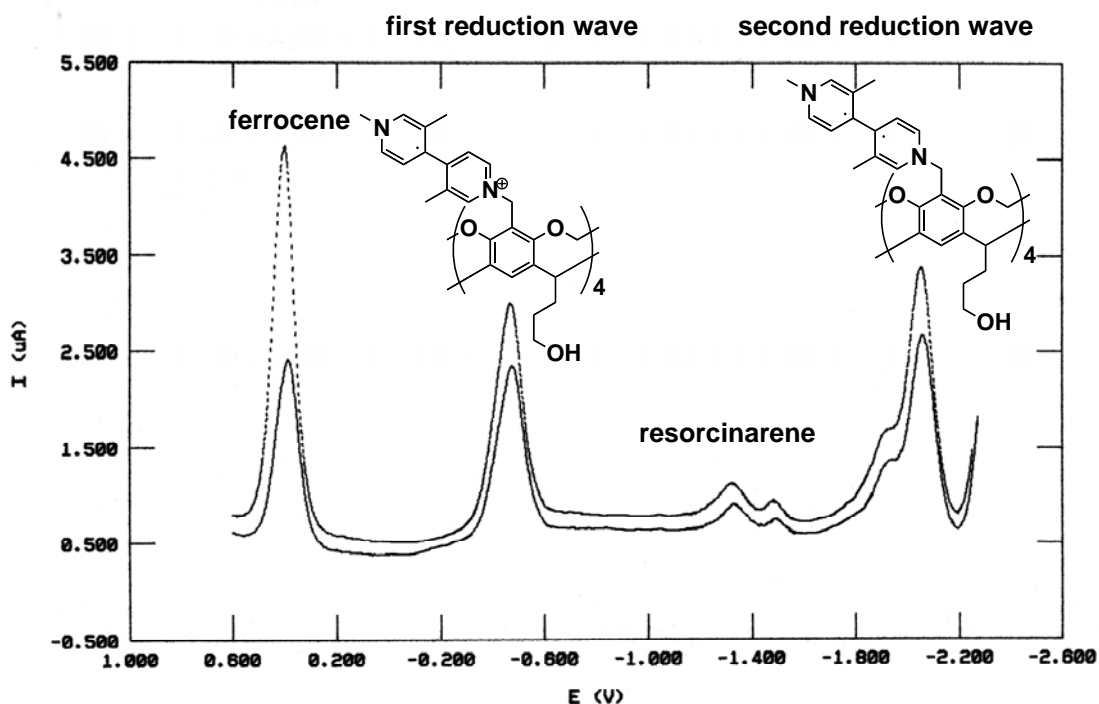


Figure 4.3: DPV of dimethyl-viologen-resorcin[4]arene ($1.0 \times 10^{-6}M$) in anhydrous acetonitrile ($0.50M$ of LiF) under argon. (scan time: 2 min, step-width: 50 microseconds), shown are two consecutive. Ferrocene ($E_0=0.51$) vs. SCE (saturated calomel electrode) has been used as internal redox standard.

As Figure 4.3 summarizes, we have found two major reduction waves of dimethylviologen-resorcin[4]arene as well (4 electrons for the first wave, 1 plus 3 electrons for the second wave). They arise from the first and second reduction wave of the four dimethylviologen-units that are covalently attached to the resorcin[4]arene. In the first wave, occurring at -0.40 V, the monoradical-cation of each dimethylviologen is created. Also in this case, the observed reduction potential is less negative than that of 3,3'-dimethylmethylviologen (-0.79 V).⁷⁴

The second peak splits in two peaks at -1.75 (1 electron) and at -1.97 (3 electrons). From semiempirical calculations (PM3), we have obtained some evidence for the most stable conformation (see below) which would corroborate this result. Again, the potential difference between the monocation radical and the double-reduced viologen is approximately 1.5V, as it is typical for viologens.

The newly synthesized (dimethyl)viologen-resorcin[4]arenes possess very suitable electrochemical reduction potential, which should enable them to reduce a variety of halogenated aliphatic and aromatic hydrocarbons.

Unfortunately, a fraction of the (dimethyl)viologen-resorcin[4]arenes decomposed or polymerized on the platinum working electrode. Therefore, I could not perform long-term electrolyses in combination with the GC- or HPLC-analysis of the products formed. The optimization of the redox electrode is a major challenge and a task for one of the new graduate students coming to the research group of my advisor.

Semiempirical Calculations (PM3)

I have used the semi-empirical method PM3^{lxxvii} to visualize the change in conformation, which is expected to occur during the stepwise reduction of the resorcin[4]arene. The results are summarized in Figure 4.4.

In the first row, the resorcinarenes possessing four chemically linked mono-radical cation viologens (total charge: +4) are shown, in the second row the completely reduced macrocycles. A stepwise folding from the kite-conformation (see Figure 4.4) to a “semi-kite/semi-vase”-conformation can be discerned: the mono-reduced viologen-units are alternating “in” and “out”. Interestingly, both completely reduced macrocycles do not form a “vase” as most stable conformer. Furthermore, three completely reduced viologens are oriented “inside”, whereas one group remains to be directed to the “outside”. This finding is somewhat surprising, because one would have expected⁵⁷ that a completely reduced macrocycle would form an undistorted “vase”-conformer. Obviously, these calculations were performed at zero K and not with the most sophisticated software. However, PM3 calculations are known to get the principal structures right.⁷⁷ That’s why they are used as a relatively fast calculation method in our laboratories. For the case of the completely reduced dimethyl-viologen-resorcin[4]arene, our findings from PM3 are supported by the electrochemical results. A one to three integration of the last reduction step is observed. This electrochemical behavior that I have observed could originate from a main conformer that is not symmetrical. However, further calculations and experiments will have to be done before a) the electrochemical behavior of these systems is completely understood and b) an efficient electrocatalytic system for the reductive dehalogenation of organic compounds is available.

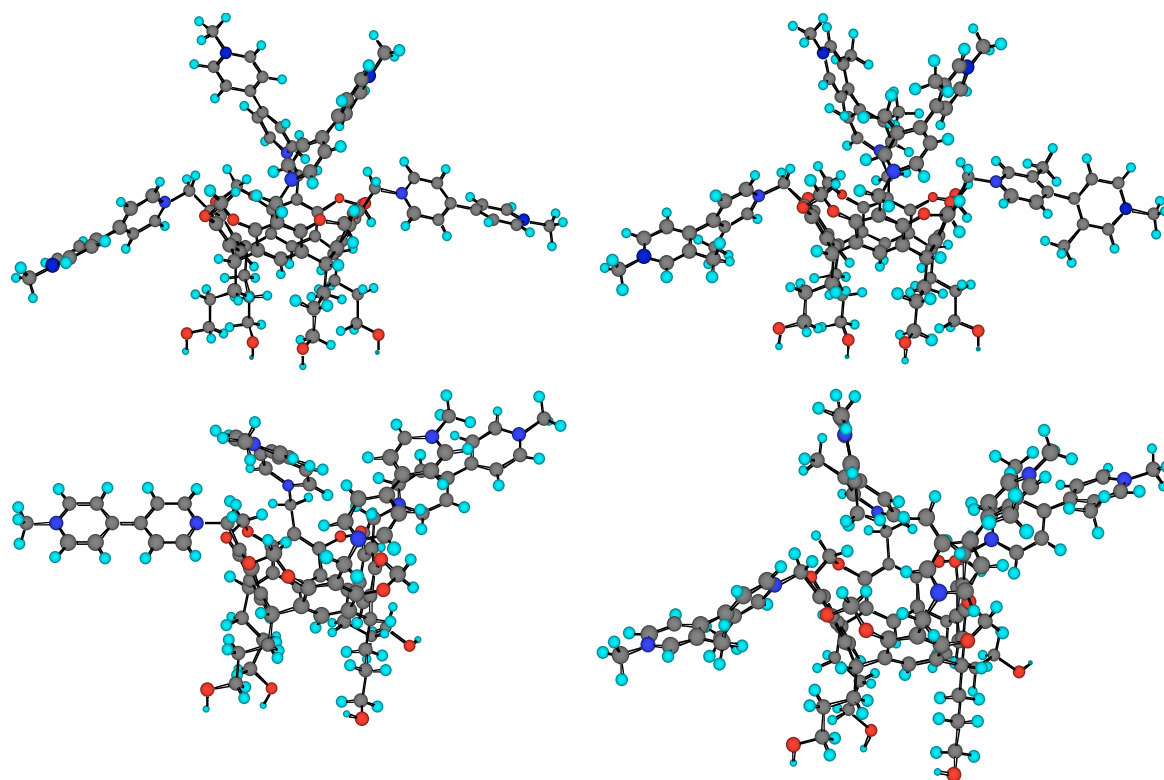


Figure 4.4: PM3-calculations of the most stable conformations of viologen-resorcin[4]arene (left) and dimethyl-viologen-resorcin[4]arene (right).

first row: macrocycles possessing a total charge of plus four

second row: macrocycles possessing a total charge of zero

CHAPTER 5 - DNA-intercalating Heterocyclic Resorcin[4]arene Cavitands

Introduction

The use of resorcin[4]arenes^{57,58}, hemicarcerands^{16,60} and carcerands^{14,lxxviii} as drug-containers⁵⁹ and drug-release systems^{61,62} has been studied extensively. The resulting supramolecular complexes of proven drugs and other small molecular weight components with these macrocyclic structures, as well as co-crystals of resorcin[4]arenes and these molecules are under intense investigation. Carcerplexes (the complexes of small molecules within carcerands) are often extremely stable and, therefore, their release is extremely slow.^{lxxix} It is noteworthy that the use of resorcin[4]arenes as anticancer drugs has not been attempted to date, to my best knowledge. At a first glance, this might not be surprising, since most of the resorcin[4]arenes are symmetric (when neglecting their various conformations)⁵⁷ and do not possess specific sites for binding to metabolic enzymes^{lxxx}, transmembrane channels^{lxxxi}, or specific DNA-sequences.^{lxxxii} When looking at DNA-binding drugs, there are numerous examples that bind to DNA and block the activity of various enzymes, such as DNA-polymerase, DNA-ligase and the topoisomerases I and II.^{lxxxiii,lxxxiv} For instance, doxorubicin, that is prescribed against numerous cancers including lymphoma and breast cancer^{lxxxv}, binds to the DNA and blocks the DNA function by DNA drug binding interactions. DNA topoisomerase II is the primary target of Doxorubicin molecules. Topoisomerase II is an enzyme in human cells, which unwinds DNA for transcription. According to the generally accepted mechanism, doxorubicin forms a DNA-enzyme-drug complex which restrains the enzyme and, therefore, the unwinding process of DNA.^{lxxxvi} The cell-division cycle (CDC), in eukaryotic cells consists of four distinct phases^{lxxxvii}: G1 phase, S phase, G2 phase (collectively known as interphase) and M phase. During G1 (growth phase 1) the cell creates organelles and begins its metabolism, during the S-phase, DNA-synthesis and copying of the chromosomes is completed and during G2 (growth phase 2) the cell grows in preparation for cell division). The M phase is itself composed of two tightly coupled processes: mitosis, in which the cell's chromosomes are divided between the two daughter cells, and cytokinesis, in which the cell's cytoplasm physically divides. Stopping the DNA replication leads

to apoptosis^{lxxxviii} (programmed cell death), because the cell cannot leave the S-phase of the cell division cycle and, therefore, enters a cascade of termination events (e.g. caspase activation⁹⁶).

It was my approach to modify water-soluble resorcin[4]arenes with DNA-intercalating heterocyclic units and probe their DNA-binding properties. Starting from three-fold bridged resorcinarenes, I have selected two DNA-intercalating aromatic heterocycles (pyrazine and quinoxaline) as forth bridge. Quinoxaline-antibiotics are known to bind to DNA via intercalation of the electron-poor heterocycle between two DNA-base pairs.^{lxxxix,xc,xcii} It is our hypothesis that intercalation or surface binding of the heterocycles will sterically impede the attack of DNA-maintaining enzymes due to the presence of the attached resorcinarenes. The aim of our research was to provide the proof-of-principle. The first steps of this endeavor consists in establishing evidence that the unsymmetrical resorcin[4]arenes are indeed capable of binding to B-DNA via intercalation. I do not claim that the macrocycles reported here are suitable for any animal testing in the near future. However, we regard this finding as a stepping-stone towards new drug developments.

Results and Discussion

Calf-Thymus (CT) DNA has been used in our binding experiments, because it is a model for B-DNA, because of its almost statistical distribution of AT- and CG-base pairs. Most of the natural DNA (in the absence of protein or RNA-binding) has the structure of B-DNA, which possesses a more elongated double-helix than A-DNA, well accessible major groove and a rather narrow, but hydrated minor groove. In fact, hydration of the DNA's minor groove appears to be a major factor in thermodynamically stabilizing B-DNA. Its desoxyribose-sugars pucker C2'-endo, the AT- and CG-base pairs are almost perpendicular to the helix axis.^{xcii} Therefore, intercalative binding, which consists of a complete or partial insertion of a usually aromatic molecule between two DNA-base pairs, is favored to B-DNA, compared to A- and Z-DNA.

Table 5.1: Structural Features of A-, B-, and Z-DNA¹⁰² (quoted from ref. 93)

	A	B	Z
Helix sense	Right handed	Right-handed	Left handed
Repeating unit	1 bp	1bp	2 bp
Rotation/bp	33.6°	35.9°	60°/2
Mean bp/turn	10.7	10.0	12
Inclination of bp to axis	+19°	-1.2°	-9°
Rise/bp along axis	2.3Å	3.32Å	3.8Å
Pitch/turn of helix	24.6Å	33.2Å	45.6Å
Mean propeller twist	+18°	+16°	0°
Glycosyl angle	anti	anti	C: anti, G: syn
Sugar pucker	C3'-endo	C2'-endo	C: C2'-endo, G: C2'-exo
Diameter	26Å	20Å	18Å

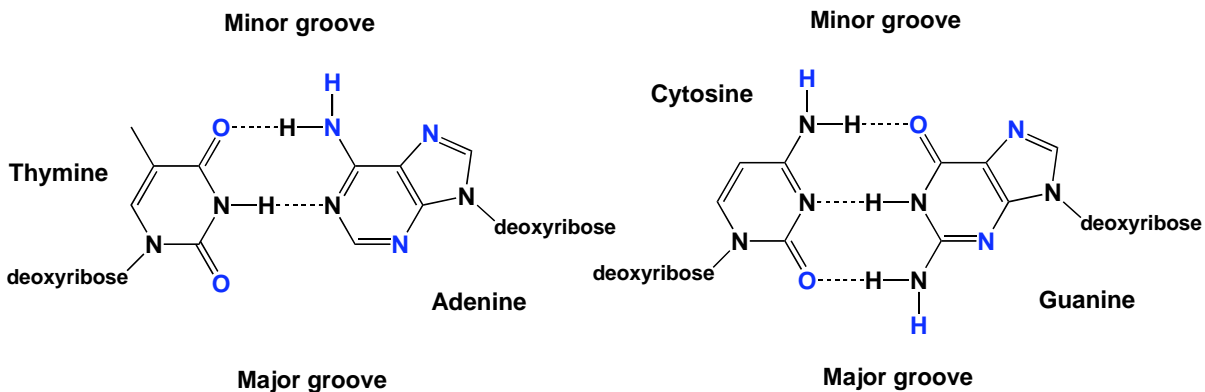


Figure 5.1: Occurrence of Major and Minor Grooves in the structure of B-DNA: Both base pairs feature three potential hydrogen binding sites in the Major Groove areas, whereas only two hydrogen binding sites are available in the Minor Groove.

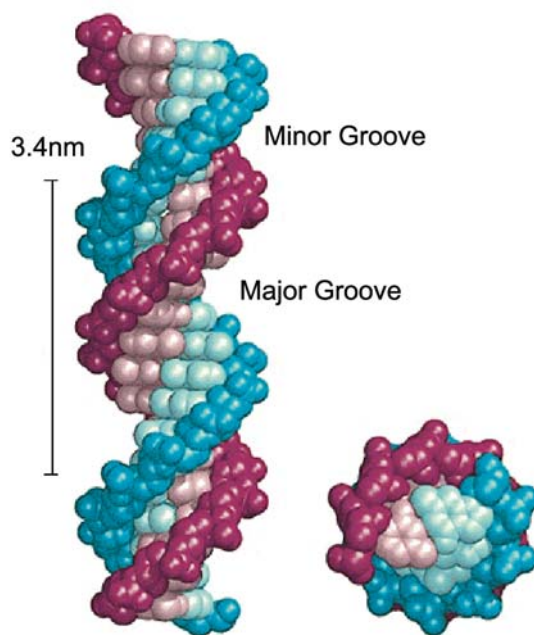


Figure 5.2: Major and Minor Groove in B-DNA. The model was generously provided by the Prof. Dr. Jacqueline K. Barton, California Institute of Technology.

DNA-Binding

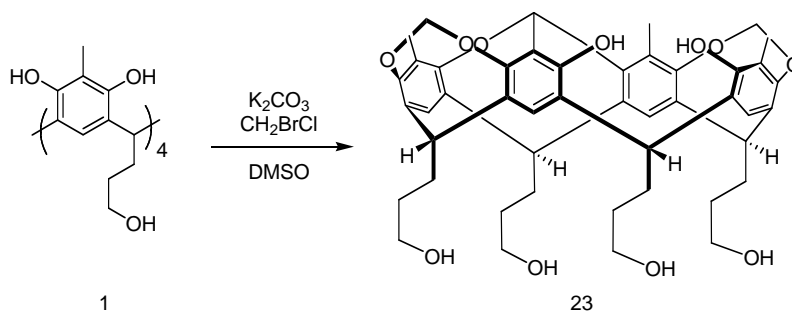
Intercalation requires that the DNA open the space required between two base-pairs by partial unwinding. This opening is a dynamical process, which has to occur within the time-frame of the DNA-motion. Depolarized dynamic light scattering measurements of DNA [CG]₆-

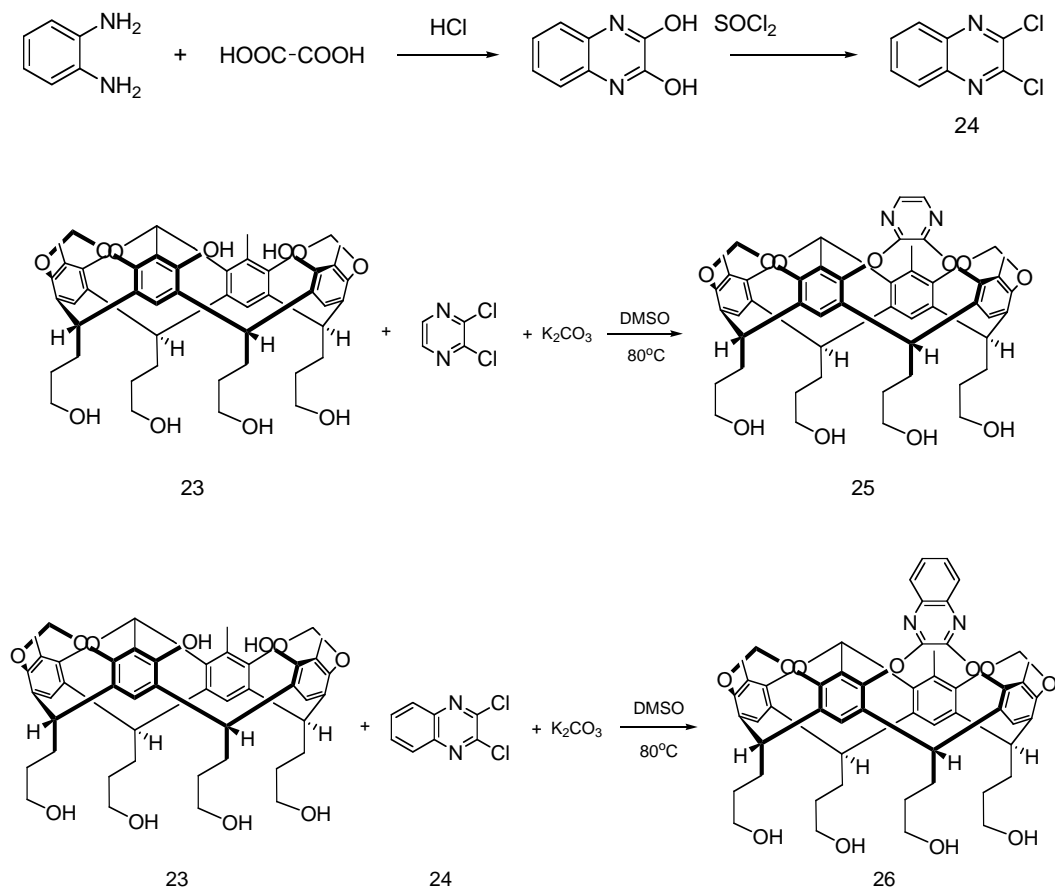
dodecamers have shown that the time constant for the rotational motion of such oligomers is in the nanosecond range.^{xciii} Extrapolation of these measurements to B-DNA, possessing a length of approximately 10,000 bp^{xciv}, leads to a window region between 50 ns and 100 ns for the expected time constant for the rotational motion of this bigger macromolecule, depending on the chemical composition (AT vs. CG) and the temperature. The degree of unwinding is typically a function of the intercalator. Unwinding creates a maximum extra space of approximately 0.34 nm 3.4 (Å). The mechanism of intercalation was first proposed by L. Lerman in 1961.^{xcv,xcvi}

Besides intercalation, surface binding is the second mode of binding to DNA. It is comparable to the binding of many molecules to other microstructures, which do not permit binding via intercalation. In many cases, binding to microstructures involves electrostatic attractions, since DNA is a negatively charged polyelectrolyte (two negative charges per base pairs). Since the resorcin[4]arenes do not possess any charges, hydrophobic and dipole-dipole interactions, as well as hydrogen-bonding to the resorcin[4]arene's pendant groups (feet), which possess hydroxy-functions, are most likely the driving forces of the binding of the resorcin[4]arenes to B-DNA surface.

Synthesis

The synthesis of a tetrabridged symmetrical resorcin[4]arene featuring methyl-, ethyl- and pyridine-dicarboxylic ester-bridged pendent groups have been described in the literature.^{xcvii,xcviii,xcix} The presence of hydroxy- groups at the “feet” must be regarded as a complication, because it can be deprotonated as well and react as nucleophile, which is able to attack the electron-deficient cis-dichloro-pyrazine and – quinoxaline. I was able to optimize the amount of base (potassium carbonate) added. Under optimized conditions, the phenolic groups, which are far more acidic than the aliphatic hydroxyl groups^c, react preferentially.





Scheme 5.1

UV/Vis-Absorption of 25 and 26

In Figure 5.3, the absorption spectra of **25** and **26** ($c = 4.76 \times 10^{-5}$ M) are shown. One can discern the presence of one $n\text{-}\Pi^*$ -transition for each electron-poor aromatic heterocycle. According to the literature, these $n\text{-}\Pi^*$ -transitions are of a special importance, because they facilitate a very rapid intersystem crossing from the excited singlet to the lowest triplet state.^{ci} Therefore, the major fraction of the luminescence occurring from pyrazine and quinoxaline is phosphorescence. Whereas the fluorescence lifetime for both compounds is in the 100-200 ps range, the spin-forbidden phosphorescence has much higher lifetimes (pyrazine: Φ_{isc} (quantum yield of intersystem crossing) = 0.87, τ_P (phosphorescence lifetime) = 4.5×10^{-6} s (in acetonitrile at 298K); quinoxaline: $\Phi_{isc} = 0.99$, $\tau_P = 0.294$ s (in acetonitrile at 298K)).^{cii}

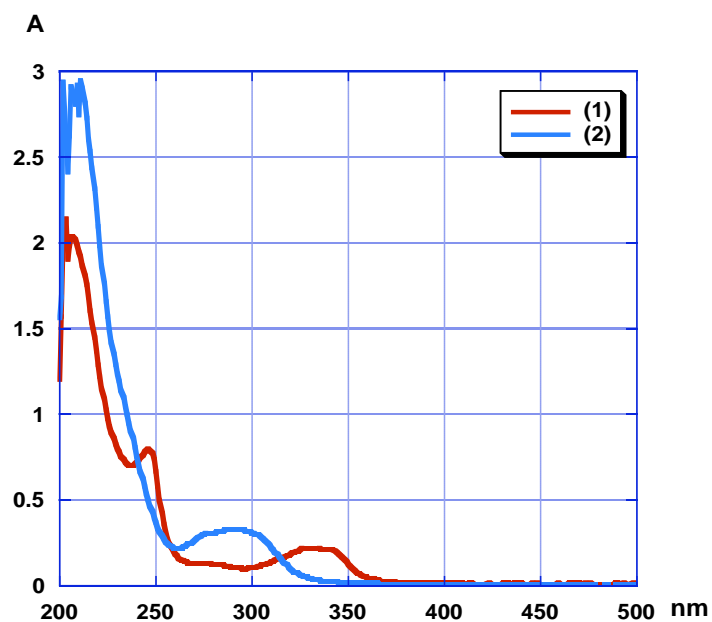


Figure 5.3: Absorption spectra of 25 (blue) and 26 (red) in MeOH/buffer (see below)
(c = 4.76 x 10⁻⁵ M)

Table 5.2: Absorption coefficients of 25 and 26

25	Π - Π^*	Π - Π^*	n - Π^*
	$\lambda_{\max}=224$ ϵ (M ⁻¹ cm ⁻¹)	$\lambda_{\max}=246$ (sh) ϵ (M ⁻¹ cm ⁻¹)	$\lambda_{\max}=284$ ϵ (M ⁻¹ cm ⁻¹)
	63,100	27,600	11,000
26	Π - Π^*	Π - Π^*	n - Π^*
	$\lambda_{\max}=212$ ϵ (M ⁻¹ cm ⁻¹)	$\lambda_{\max}=246$ ϵ (M ⁻¹ cm ⁻¹)	$\lambda_{\max}=328$ ϵ (M ⁻¹ cm ⁻¹)
	42,000	16,400	6350

Fluorescence Studies

There are two complications regarding the phosphorescence lifetimes of **25** and **26**: a) Since our resorcin[4]arenes are new compounds, there is no photophysical characterization available as of yet. Obviously, the photophysical behavior of pyrazine and quinoxaline is only able to approximate the photophysical behavior of the macrocycles **25** and **26** possessing pyrazine- and quinoxaline-bridges. b) The phosphorescence occurring from pyrazine- and quinoxaline is quenched by dissolved triplet oxygen.^{ciii} According to the experience of Dr. Stefan Bossmann with B-DNA, attempts to remove the oxygen by purging with N₂ or Ar, as well as freeze-pump-thaw cycles lead to unpredictable and not reproducible structural changes. Therefore, it is advantageous to allow the oxygen to remain in the system. We have found a concentration range, in which meaningful fluorescence measurements are possible (see below).

The fluorescence studies were conducted in the following manner: stock solutions of
a) dialyzed DNA in aqueous buffer (0.050 phosphate buffer, pH=7.0)

b) solutions of **25** and **26** in MeOH/(0.050 phosphate buffer, pH=7.0) (30/70 v/v), due to the inferior solubility of the resorcin[4]arenes in water.

2 mL of the aqueous DNA stock solution was mixed with aliquots of 0.10 mL of the resorcinarenes' stock solutions. The fluorescence measurements were taken after 20min. equilibration after each addition.

a) Concentration Dependence of **25**

In Figure 5.4, the concentration dependence of the phosphorescence of **25** in MeOH/buffer is shown. Apparently, strong self-quenching is observed. In Figure 5.5, a Stern-Volmer-plot of the self-quenching process is shown. According to Stern and Volmer^{civ}, the quotient of I⁰ (fluorescence or phosphorescence intensity in the absence of a quencher) and I (fluorescence or phosphorescence intensity in the presence of a quencher) is equal to the product of the quenching constant k_q (M⁻¹ s⁻¹), the fluorescence or phosphorescence lifetime τ in the absence of the quencher (s) and the concentration of the quencher (M), plus one.

$$\frac{I^0}{I} = 1 + k_q \tau c(q) \quad (5.1)$$

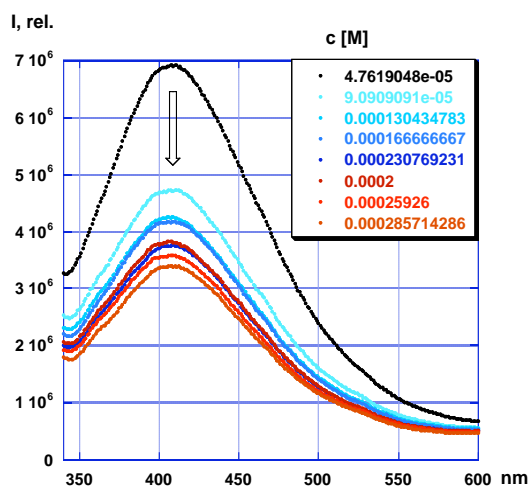


Figure 5.4: Concentration-dependence of the phosphorescence of 25 in MeOH/buffer, $\lambda_{exc}=320$ nm.

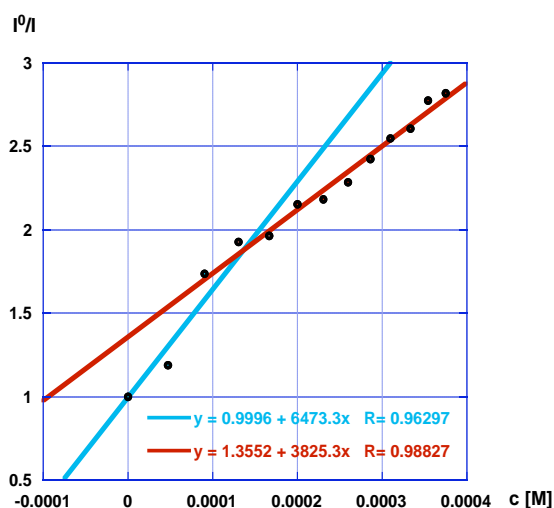


Figure 5.5: Stern-Volmer plot of the self-quenching of 25 in MeOH/buffer, $\lambda_{exc}=320$ nm. I^0 has been obtained by interpolation to $c=0$ M.

As it appears from Figure 5.5, the slope of the Stern-Volmer-plot is downwards curving and two regions of quenching can be discerned. In the lower concentration range ($0 - 1.5 \times 10^{-4}$ M) a slope of 6473 was obtained, which is equal to the product of the phosphorescence lifetime τ and the quenching constant k_q . Assuming a typical value for $k_q = 5 \times 10^9 \text{ M}^{-1} \text{ s}^{-1}$ (calculated from Equation 5.1 and $\tau_P = 4.5 \times 10^{-6}$ s), we obtain an (estimated) value for $\tau = 1.3 \times 10^{-6}$ s, which would be a typical triplet lifetime of an azine in an aerated solution. Assuming the same lifetime τ , the second quenching process would then have a quenching constant of $k_q = 2.95 \times 10^9 \text{ M}^{-1} \text{ s}^{-1}$. Since we do not have any knowledge about the possible aggregation of the asymmetric pyrazine-bridged resorcin[4]arenes with increasing concentration in solution or on the influence of these possible aggregation on the rate of intersystem crossing, we cannot assign the observed quenching behavior to two distinct quenching processes. Only a detailed time-resolved laser absorption and emission study will be able to shed some light into this complicated system.

b) Concentration Dependence of 26

The influence of the concentration of the asymmetric quinoxaline-bridged resorcin[4]arene on its steady-state phosphorescence is quite different from the behavior of the asymmetric pyrazine-bridged resorcin[4]arene, as the comparison of Figure 5.6 and 5.7 and Figure 5.4 and 5.5 indicates. The most distinct difference is that - after a plateau region has been passed - a linear increase (and not a decrease) of the phosphorescence intensity can be found.

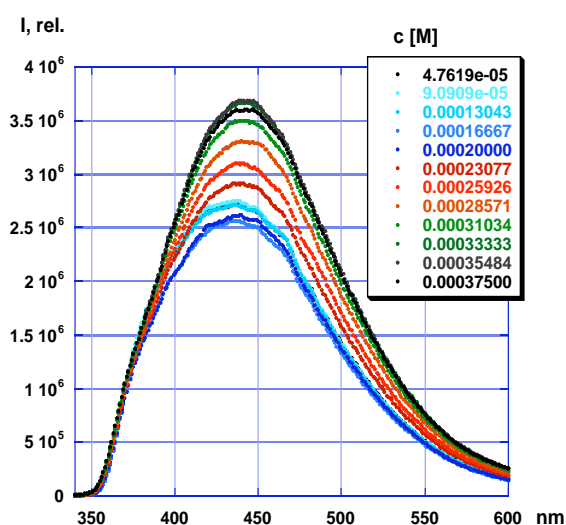


Figure 5.6: Concentration-dependence of the phosphorescence of 26 in MeOH/buffer, $\lambda_{exc} = 310$ nm.

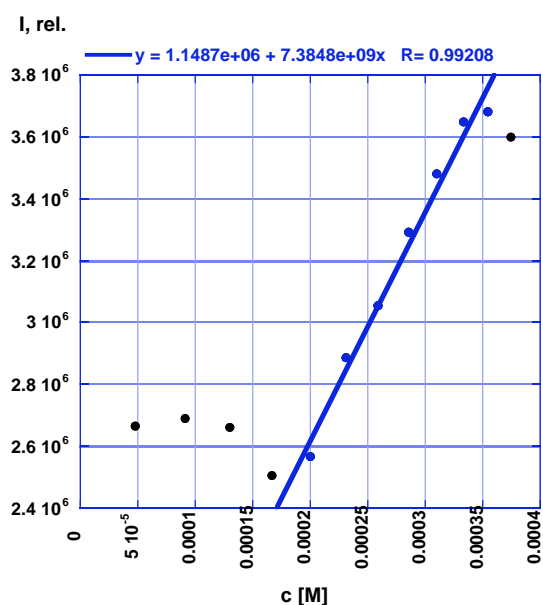


Figure 5.7: Phosphorescence intensity of 26 in MeOH/buffer, $\lambda_{exc} = 310$ nm.

Assuming that the quinoxaline-bridged resorcin[4]arene is forming clusters or micelle-analog aggregates, we can estimate a cmc (critical micelle concentration^{cv}), defined as the concentration of surfactants above which micelles spontaneously form, to 1.75×10^{-4} M.

DNA Intercalation Studies

Figure 5.8 and 5.9 shows that in the presence of CT-DNA, the phosphorescence from 25 steadily increases upon addition, until a maximum at 3.3×10^{-4} M is reached. We attribute the

observed phosphorescence increase to the binding of the pyrazine-bridged resorcin[4]arene to CT-DNA ($c = 6.25 \times 10^{-8}$ M in base pairs) via either intercalation or surface binding. Both processes are known to lead to luminescence increase, most likely due to the (partial) shielding from the surrounding water-molecules. Water, or in general, protic solvents cause the deactivation of the diazine's excited triplet-states by photodriven protonation-deprotonation processes (proton quenching).

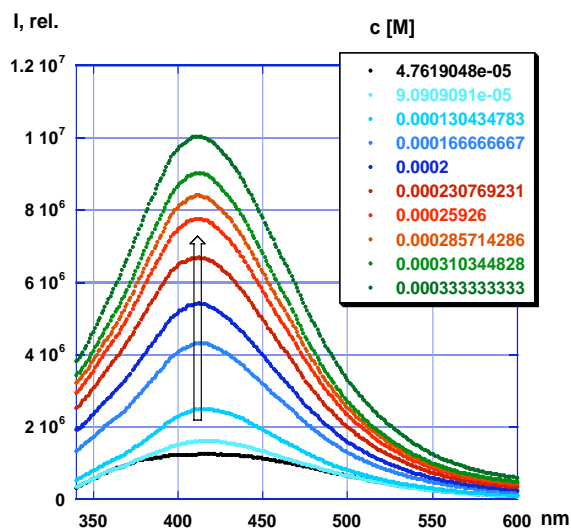


Figure 5.8: Phosphorescence increase of 25 in the presence of DNA ($c = 6.25 \times 10^{-8}$ M in base pairs) in MeOH/buffer, $\lambda_{exc} = 320$ nm.

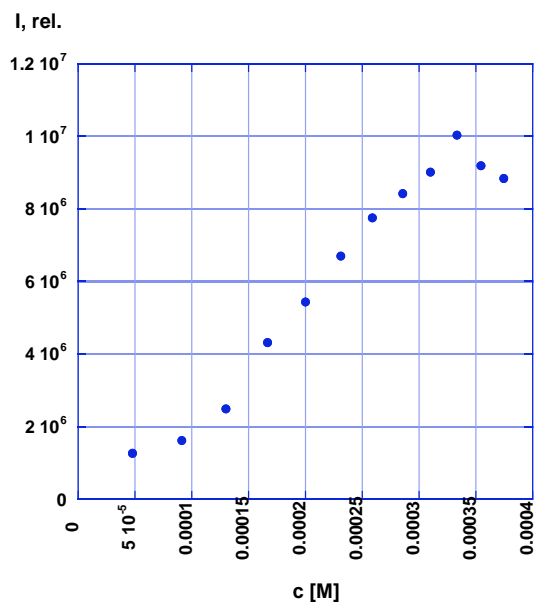


Figure 5.9: Intensity in the phosphorescence maxima, the data are taken from Figure 5.8: (left)

Before we could attempt to estimate the binding constant of **25** and **26** to CT-DNA via Scatchard-plots, computer-modeling of the resorcin[4]arenes by using the semiempirical method PM3 was performed (Figure 5.10 and 5.11). The rationale for this approach is that both macrocycles cover four base-pairs due to their geometric extensions when binding via intercalation or surface binding. Therefore, the concentration of DNA must be divided by the factor four when doing Scatchard plots in order to compensate for the real size of the macrocycles.

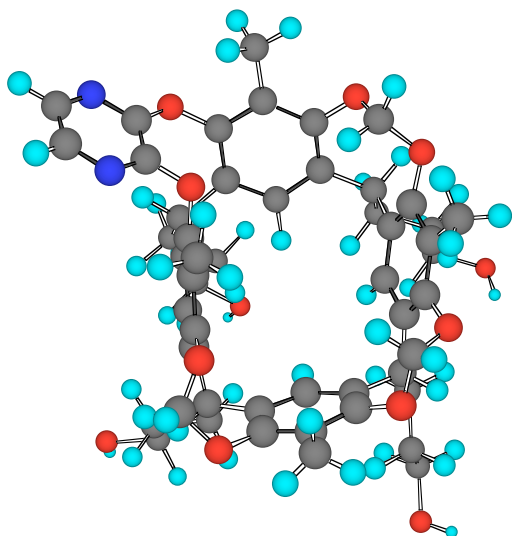


Figure 5.10: PM3 of the asymmetric pyrene-bridged resorcin[4]arene: geometric dimensions: 1.29nm x 1.08nm x 1.64 nm

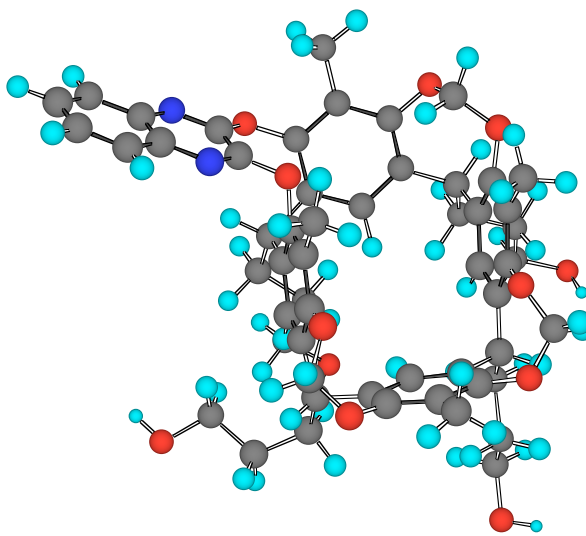


Figure 5.11: PM3 of the asymmetric quinoxaline-bridged resorcin[4]arene: geometric dimensions: 1.43nm x 1.08nm x 1.64 nm

Scatchard-Plots

Scatchard plots are a standard method to determine the binding constant(s) of organic ligands to DNA.^{cv} In the case of fluorescent ligands, Equation 5.2 is used.

$$\frac{[M]_{total}}{f} = \frac{1}{Nk_f(1-f)} + \frac{[L_{total}]}{N} \quad (5.2)$$

$[M]_{total}$: DNA concentration (in base pairs and M) over the course of titration

$[L]_{total}$: ligand (resorcinarene) concentration (M) over the course of titration

N = total number of binding sites

k_f : binding constant determined by a fluorescence (or phosphorescence) titration

$$f = \frac{F_{observed} - F_L}{F_{max} - F_L} \quad (5.3)$$

f: fraction of the ligand bound to DNA

F_L : fluorescence of the free ligand

$F_{observed}$: fluorescence observed after the addition of DNA

F_{max} : maximum fluorescence (occurring when all possible ligands are bound to DNA)

The plot of $([M]_{total}/f)$ vs. $(1/(1-f))$ provides information about the quotient of $[L]_{total}$ and N, which serves as a correction factor and yields k_f .

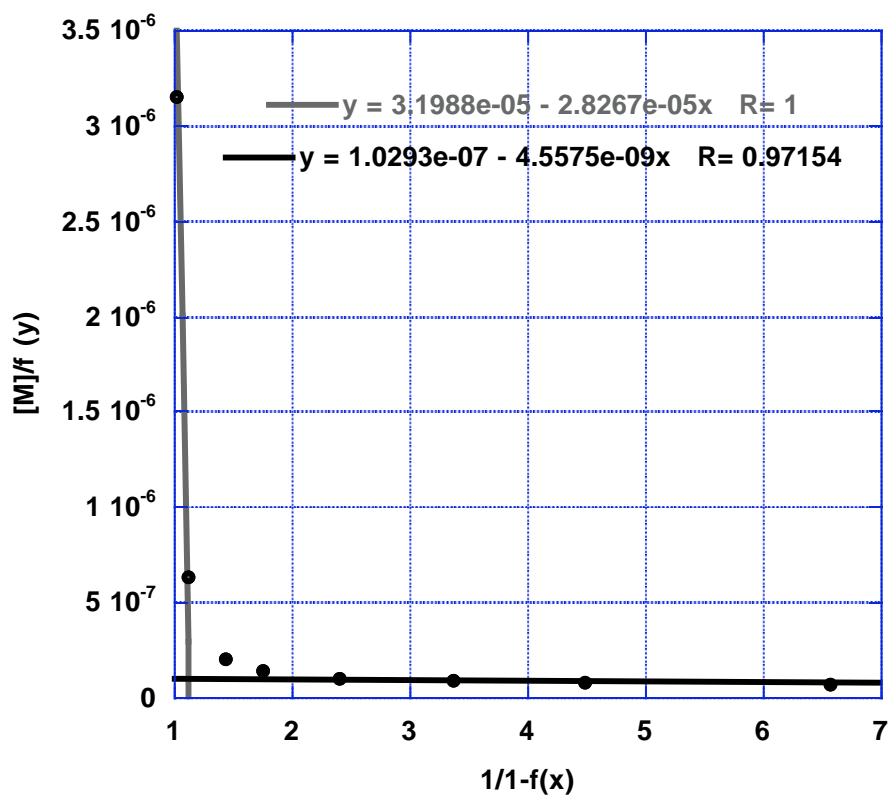


Figure 5.12: Scatchard-plot generated from data shown in Figure 5.8.

Calculations

A) Interval from 0 to 9.09×10^{-5} M of **25**; 6.25×10^{-8} M in base pairs of CT-DNA

$$[L]_{total}/N = 3.2 \times 10^{-5} \text{ M}$$

$$N=2.84$$

$$k_f = 1.25 \times 10^4 \text{ M}^{-1}$$

B) Interval from $9.09 \times 10^{-5} \text{ M}$ to $4.0 \times 10^{-4} \text{ M}$ of **25**; $6.25 \times 10^{-8} \text{ M}$ in base pairs of CT-DNA

$$[L]_{\text{total}}/N = 3.2 \times 10^{-5} \text{ M}$$

$$N=11.72$$

$$k_f = 1.87 \times 10^7 \text{ M}^{-1}$$

The occurrence of two binding constants can be interpreted as follows:

There could be two kinds of binding of **25** to DNA, for instance intercalation, possessing the bigger binding constant and surface binding, possessing the smaller binding constant.

Without further measurements, such as time-resolved luminescence and the use of spin-labeled macrocycles, there is no possibility to positively identify the mode of interactions between the resorcin[4]arene and DNA. However, it could be positively proven that a positive interaction (binding) of the resorcinarene and DNA occurs.

In Figure 5.13, the phosphorescence spectra obtained with **26** as binding ligand and otherwise unchanged experimental conditions are shown. The phosphorescence increases with increasing concentration of **26**, until a maximum at $2.8 \times 10^{-4} \text{ M}$ is reached.

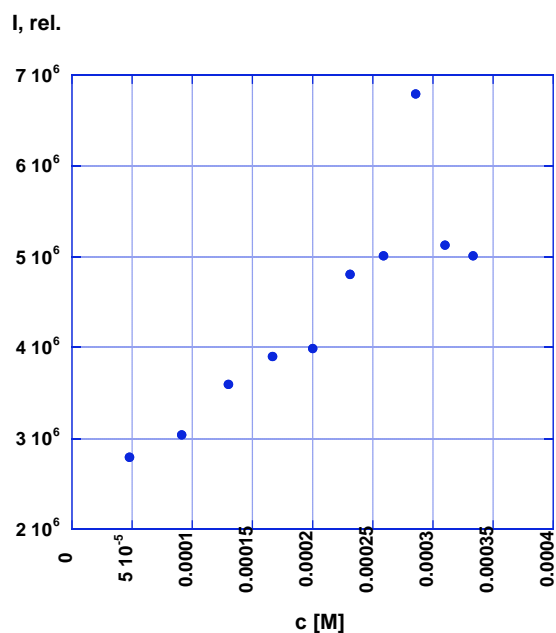
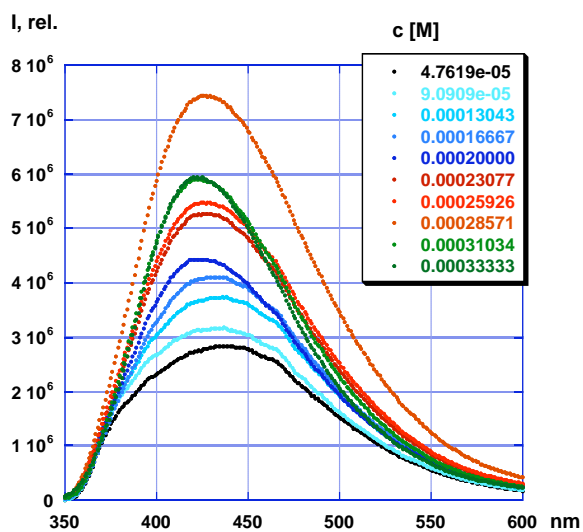


Figure 5.13: Phosphorescence increase of 26 in the presence of DNA ($c = 6.25 \times 10^{-8}$ M in base pairs) in MeOH/buffer, $\lambda_{exc} = 310$ nm.

Figure 5.14: Intensity in the phosphorescence maxima, the data are taken from Figure 5.13: (left)

In this case a Scatchard-plot was prepared as well. The result is shown in Figure 5.15.

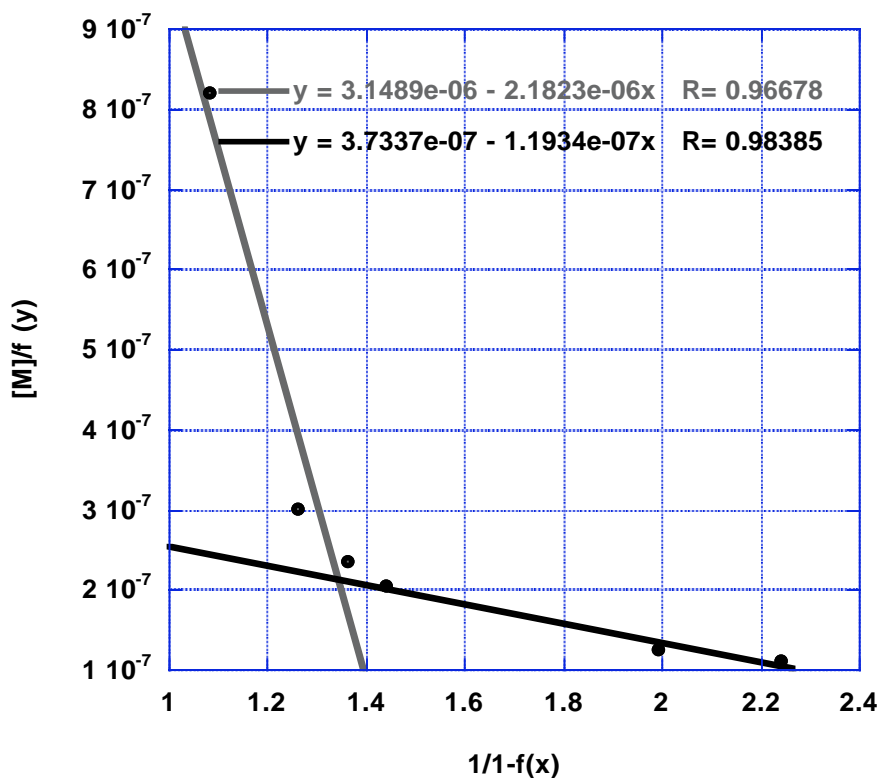


Figure 5.15: Scatchard-plot generated from data shown in Figure 5.13.

Calculations

A) Interval from 0 to 1.3×10^{-4} M of **26**; 6.25×10^{-8} M in base pairs of CT-DNA

$$[L]_{total}/N = 3.2 \times 10^{-5} \text{ M}$$

$$N = 41.28$$

$$k_f = 1.1 \times 10^4 \text{ M}^{-1}$$

B) Interval from 1.3×10^{-4} M to 4.0×10^{-4} M of **26**; 6.25×10^{-8} M in base pairs of CT-DNA

$$[L]_{\text{total}}/N = 3.2 \times 10^{-5} \text{ M}$$

$$N = 1185.75$$

$$k_f = 386.5$$

Two binding constants were found in this system as well. Again, without without further measurements, it is impossible to determine the real mode of binding. Surprisingly, the binding constants for the quinoxaline-bridged resorcin[4]arene were smaller than for the pyrene-bridged resorcin[4]arene. This could be indicative of two different modes of surface binding.

Experimental Session:

General methods:

Solvents (ACS-grade) and inorganic chemicals were purchased from Aldrich and Acros Organics. All chemicals and chromatography materials were either purchased from Aldrich or Acros Organics and used without further purification. H₂O was of bidistilled quality.

All distillations in vacuum were performed using a Büchi-rotavap equipped with a solvent recovery system and pressure control.

Further instrumentation: 200 and 400 MHz NMR (Varian), FT-IR (Nicolet 870), MS: Bruker Esquire 3000, Melting point apparatus ((Fisher) All melting points are uncorrected), Carlo Erba Strumentatione (CHN).

Tris bridged 2-Methyl Cavitand **23** 2,18-Methano-20H,22H,24H-dibenzo[d,d']-[1,3]dioxocino[5,4-i:7,8-i']bis[1,3]benzodioxocin-3,17-diol, 1,21,23,25-tetrapropanol, 7,11,15,28-tetramethyl-

Anhydrous potassium carbonate (3.75g, 24.97mmol) was added under nitrogen atmosphere to a solution of 2-Methyl-dodecol **1**

(Pentacyclo[19.3.1.13,7.19,13.115,19]octacos-1(25),3,5,7(28),9,11,13(27),15,17,19(26),21,23-dodecaene-4,6,10,12,16,18,22,24-octol, 2,8,14,20-tetrakis(3-hydroxypropyl)-5,11,17,23-tetramethyl-) (2.0g, 2.58mmol) in 80ml DMSO. Bromochloromethane (0.375ml, 5.65mmol) was added to the mixture while stirring under nitrogen. The reaction mixture was stirred overnight at RT, then heated to 50°C for 4 hours.

Another 0.139ml (2.09mmol) of bromochloromethane was added after the mixture had cooled to room temperature. The reaction mixture was heated to 50°C again and stirred for another 4h. After cooling to RT again, the mixture was poured into 180ml of saturated ammonium chloride solution in water and the precipitation was collected by filtration. The solid obtained was washed with 15ml water for 3 times and dried under air at normal pressure. Column chromatography using silica as stationary phase and CHCl₃/MeOH (12:1 v/v, then 10:1 v/v) as eluent yielded a white powder. Yield: 1.46g, (70%) mp 224°C

FT-IR (KBr) (cm⁻¹): 3406, 2940, 1470, 1306, 1245, 973

¹H NMR (200 MHz, CDCl₃): 7.08 (2H, s), 6.95 (2H, s), 5.88 (3H, m), 4.77 (4H, m), 4.40 (2H, d, J=7.4Hz), 4.28 (5H, m), 3.77 (12H, m), 1.96 (6H, s), 1.94 (6H, s), 1.62 (12H, m)

2,3-dichloroquinoxaline **24**

1,2-diaminobenzene (2.75g, 25.4mmol) and oxalic acid (3.25g, 36.1mmol) were mixed with 15ml of 4N HCl. The mixture was refluxed for 15 min., then needle like crystals formed. After cooling down to RT, the crystals were filtered and washed 3 times with 5ml of water and dried under air at normal pressure. The dried solid was then suspended in 25ml of POCl₃ and the suspension was refluxed for 6h until all solid was dissolved and the solution became light brown in color. The mixture was then poured onto 60ml of ice water and was allowed to react until the POCl₃ was completely consumed. After filtration and vigorously washing with water, a white solid was obtained. Yield: 2.63 g (52%) mp 120°C

FT-IR (KBr) (cm⁻¹): 3045, 2920, 2860, 1560, 1535, 1460, 1380, 1280, 1190, 1120, 995, 965, 770, 600

¹H NMR (200 MHz, CDCl₃): 7.06 (2H, m), 7.04 (2H, m)

¹³C NMR (400 MHz, CDCl₃): 131.45, 128.43

2,25:3,24-Dimetheno-1H,26H,28H,30H-

[1,3]benzodioxocino[9'',8'':4',5'] [1,3]benzodioxocino[9',8':5,6] [1,3]dioxocino[5',4':9,10] [1,4]benzodioxonino[2,3-b]pyrazine, 1,26,28,30-1,21,23,25-tetrapropanol, 7,11,15,28-tetramethyl- **25**

2,18-Methano-20H,22H,24H-dibenzo[d,d'] [1,3]dioxocino[5,4-i:7,8-i'] bis[1,3]benzodioxocin-3,17-diol, 1,21,23,25-tetrapropanol, 7,11,15,28-tetramethyl- **23**) (0.20 g, 0.246mmol) and 2,3 dichloropyrazine (40mg, 0.268mmol) were dissolved in 5ml of anhydrous DMSO under an argon atmosphere. After both starting materials were completely dissolved,

anhydrous potassium carbonate (0.10g, 0.724mmol) was added to the solution. The mixture was heated to 80°C under argon for 2 d while stirring. After cooling to RT, the reaction mixture was poured into 15ml saturated ammonium chloride solution in water. Slowly, a white solid precipitated, which was filtered after 1h. The solid obtained from filtration was three times washed with water, dried under air at normal pressure, and then recrystallized from toluene. A white powder was obtained. Yield: 0.21g (96%) mp>300°C

FT-IR (KBr) (cm⁻¹): 3401, 2940, 2873, 1475, 1414, 1071, 979

¹H NMR (400 MHz, CDCl₃): 8.00 (4H, m), 7.05 (4H, m), 5.90 (2H, m), 5.84 (1H, d, J=6Hz), 4.84 (4H, m), 4.60-4.20 (7H, m), 3.77 (8H, m), 2.39 (8H, m), 1.95-2.06 (12H, m), 1.30 (8H, m)

¹³C NMR (400 MHz, CDCl₃): 153.60, 138.19, 124.15, 120.22, 117.64, 62.92, 37.49, 31.35, 26.81, 11.73, 11.34, 10.40

2,25:3,24-Dimetheno-1H,26H,28H,30H-

[1,3]benzodioxocino[9'',8'':4',5'] [1,3]benzodioxocino[9',8':5,6] [1,3]dioxocino[5',4':9,10] [1,4]benzodioxonino[2,3-b]quinoxaline, 1,26,28,30-1,21,23,25-tetrapropanol, 7,11,15,28-tetramethyl **26**

2,18-Methano-20H,22H,24H-dibenzo[d,d'] [1,3]dioxocino[5,4-i:7,8-i'] bis[1,3]benzodioxocin-3,17-diol, 1,21,23,25-tetrapropanol, 7,11,15,28-tetramethyl-

, **23**) (0.30 g, 0.369mmol) and 2,3-dichloroquinoxaline (80mg, 0.40 mmol) were dissolved in 7ml of anhydrous DMSO under an argon atmosphere. After both starting materials were completely dissolved, anhydrous potassium carbonate (0.15g, 1.086mmol) was added to the solution. The mixture was heated to 80°C under argon for 3 d while stirring. After cooling to RT, the reaction mixture was poured into 20ml saturated ammonium chloride solution in water. Slowly, a white solid precipitated, which was filtered after 1h. The solid obtained from filtration was three times washed with water, dried under air at normal pressure, and then dissolved in CH₂Cl₂. The product was further purified by column chromatography using silica as stationary phase and CH₂Cl₂/MeOH 20:1 v/v as mobile phase. A white powder was obtained. Yield: 0.25g (72.2%) mp 175°C

FT-IR (KBr) (cm⁻¹): 3324, 2940, 2873, 1726, 1480, 1414, 1373, 1332, 1240, 1076, 973

¹H NMR (200 MHz, CDCl₃): 7.83 (4H, m), 7.60 (4H, m), 7.30 (2H, m), 7.22 (2H, m), 5.91 (3H, m), 4.80 (4H, m), 4.42 (1H, d, J=5.7Hz), 4.31 (2H, d, J=5.7Hz), 3.70 (16H, m), 2.44 (12H, m), 2.03(4H, m), 1.60 (8H, m)

^{13}C NMR (200 MHz, CDCl_3): 154.14, 153.62, 153.29, 151.66, 149.93, 139.21, 131.07, 129.72, 128.98, 127.66, 124.13, 122.99, 120.13, 118.13, 98.61, 68.33, 62.86, 38.90, 37.56, 31.36, 30.53, 29.88, 29.10, 26.96, 23.91, 11.52, 11.14, 10.40

Appendix A - References

-
- (i) Linda M. Tunstad, John A. Tucker, Enrico Dalcanale, Jurgen Weiser, Judi A. Bryant, John C. Sherman, Roger C. Helgeson, Carolyn B. Knobler, and Donald J. Cram *J. Org. Chem.* **1989**, 54, 1305-1312
- (ii) Adam R. Mezo and John C. Sherman *J. Org. Chem.* **1998**, 63, 6824-6829
- (iii) Xuan Gui and John C. Sherman *Chem. Commun.*, **2001**, 2680-2681
- (iv) Del Pilar Taboada, Maria; Tannka, Auro Atsushi; Kubota, Lauro Tatsuo *J. Electroanal. Chem.* **2002**, 536 (1-2), 71-81
- (v) Thomas Heinz, Dmitry M. Rudkevich and Julius Rebek Jr. *Nature* **1998**, 394, 764-766
- (vi) Chen, J; Rebek, J., Jr. *Org. Lett.* **2002**, 4, 327-329
- (vii) Steed, J. W; Atwood, J, L *Supramol. Chem.*, 2000, wiley New York
- (viii) Huaping Xi, Corinne L. D. Gibb, and Bruce C. Gibb *J. Org. Chem.* **1999**, 64, 9286-9288
- (ix) Shorichi Saito, Dmitry M. Rudkevich, and Julius Rebek, Jr. *Org. Lett.*, Vol.1, No. 8, **1999**, 1241-1244
- (x) Patrick Amrhein, Alexander Shivanyuk, Darren W. Johnson, and Julius Rebek, Jr. *J. Am. Chem. Soc.*, 2002, 124, 10349-10358
- (xi) Alexander Shivanyuk and Kari Rissaman *Helvetica Chimica Acta*, **2000**, 83, 1778-1790
- (xii) Shannon M. Biros and Julius Rebek, Jr. *Chem. Soc. Rev.*, **2007**, 36, 93-104
- (xiii) Donald J. Cram, Stefan Karbach, Young Hwan Kim, Lubomir Baczynskyj, and Gregory W. Kallemeyn *J. Am. Chem. Soc.*, **1985**, 107, No. 8, 2575-2576
- (xiv) John C. Sherman and Donald J. Cram *J. Am. Chem. Soc.* **1989**, 111, 4528-4529
- (xv) J. Kevin Judice and Donald J. Cram *J. Am. Chem. Soc.*, **1991**, 113, 2791-2793
- (xvi) Ralf Warmuth and Juyoung Yoon *Acc. Chem. Res.* **2001**, 34, 95-105
- (xvii) a) Paul Roach and Ralf Warmuth *Angew. Chem. Int. Ed.* **2003**, 42 (26) 3039-3042 b) Donald J. Cram, Martin E. Tanner, and Robert Thomas *Angew. Chem. Int. Ed. Engl.* **1991**, 30 (8), 1024-1027 c) Ralf Warmuth *Angew. Chem. Int. Ed. Engl.* **1997**, 36 (12), 1347-1351
- (xviii) a) Ralf Warmuth, Jean-Luc Kerdelhue, Sigifredo Sanchez Carrera, Kevin J. Langenwalter, and Neil Brown *Angew. Chem. Int. Ed.* **2002**, 41(1), 96-99 b) Ralf Warmuth *Chem. Commun.* **1998**, 59-60
- (xix) Xuejun Liuc Gaosheng Chu, Robert A. Moss, Ronald R. Sauers, and Ralf Warmuth *Angew. Chem. Int. Ed.* **2005**, 44, 1994-1997
- (xx) Ralf Warmuth and Slawomir Makowiec *J. Am. Chem. Soc.*, **2005**, 127, 1084-1085
- (xxi) Juyoung Yoon and Donald J. Cram *Chem. Commun.*, **1997**, 497-498
- (xxii) Leonard R. MacGillivray and Jerry L. Atwood *Nature* **1997**, 389, 469-472
- (xxiii) Alexander Shivanyuk and Julius Rebek, Jr. *PNAS*, **2001**, 98 (14), 7662-7665
- (xxiv) Elizabeth S. Barrett, Trevor J. Dale, and Julius Rebek, Jr. *J. Am. Chem. Soc.*, **2007**, 129, 3818-3819
- (xxv) www.who.int
- (xxvi) Mitchison, D. A. *Front. Biosci.* **2004**, 9, 1059-1072.
- (xxvii) Barry, C. E., 3rd; Lee, R. E.; Mdluli, K.; Sampson, A. E.; Schroeder, B. G.; Slayden, R. A.; Yuan, Y. *Prog. Lipid. Res.* **1998**, 37, 143-179.

-
- (^{xxviii}) Minnikin, D. E. in *Lipids: Complex lipids, their chemistry, biosynthesis and roles.*; Ratledge, C. Stanford, J.; Academic Press, London, 1982.
- (^{xxix}) Brennan, P. J.; Nikaido, H. *Annu. Rev. Biochem.* **1995**, *64*, 29-63.
- (^{xxx}) a) Chambers, H. F.; Moreau, D.; Yajko, D.; Miick, C.; Wagner, C.; Hackbarth, C.; Kocagoz, S.; Rosenberg, E.; Hadley, W. K.; Nikaido, H. *Antimicrob. Agents Chemother.* **1995**, *39*, 2620-2624.
- (^{xxxi}) Molloy, M. P.; Herbert, B. R.; Slade, M. B.; Rabilloud, T.; Nouwens, A. S.; Williams, K. L.; Gooley, A. A. *Eur. J. Biochem.* **2000**, *267*, 2871-2881.
- (^{xxxii}) Niederweis, M.; Ehrh, S.; Heinz, C.; Klöcker, U.; Karosi, S.; Swiderek, K. M.; Riley, L. W.; Benz, R. *Mol. Microbiol.* **1999**, *33*, 933-945.
- (^{xxxiii}) (a) Heinz, C.; Engelhardt, H.; Niederweis, M. *J. Biol. Chem.* **2003**, *278*, 8678-8685, (b) Faller, M.; Niederweis, M.; Schulz, G. E. *Science* **2004**, *303*, 1189-1192. (c) Maysa, M.; Suja, S.; Peter, H.; Katrin, G.; Michael, N. *J. Biol. Chem.* **2006**, *281*, 5908-15.
- (^{xxxiv}) Brennan, P. J. *Tuberculosis* **2003**, *83*, 91-97.
- (^{xxxv}) Bossmann, S. H.; Janik, K.; Pokhrel, M. R.; Heinz, C.; Niederweis, M. *Surf. Interface Anal.* **2004**, *36*, 127-134.
- (^{xxxvi}) Mailaender, C.; Reiling, N.; Engelhardt, H.; Bossmann, S.; Ehlers, S.; Niederweis, M. *Microbiology* **2004**, *150*, 853-864.
- (^{xxxvii}) (a) Hansma, P. K.; Cleveland, J. P.; Radmacher, M.; Walters, D. A.; Hillner, P. E.; Bezanilla, M.; Fritz, M.; Vie, D.; Hansma, H. G.; et. al., *Appl. Phys. Lett.* **1994**, *64*, 1738-1740. (b) Han, W.; Lindsay, S. M.; Jing, T. *Appl. Phys. Lett.* **1996**, *69*, 4111-4113.
- (^{xxxviii}) P. Samori, V. Francke, T. Mangel, K. Mullen, J. P. Rabe, *Optical Mat.* **1998**, *9*, 390-393.
- (^{xxxix}) Adronov, Alex; Robello, Douglas R.; Frechet, Jean M. J. *J. Polym. Sci., Part A: Polym. Chem.* **2001**, *39*(9), 1366-1373.
- (^{xl}) Lee, Min Hee; Quang, Duong Tuan; Jung, Hyo Sung; Yoon, Juyoung; Lee, Chang-Hee; Kim, Jong Seung. *J. Org. Chem.* **2007**, *72*(11), 4242-4245.
- (^{xli}) Turro, Nicholas J. *Modern Molecular Photochemistry* **1978**, 628 pp.
- (^{xlii}) Kessler, H.; Haupt, A.; Schudok, M.; Ziegler, K.; Frimmer, M. *International Journal of Peptide & Protein Research* **1988**, *32*(3), 183-93.
- (^{xliii}) Ottaviani, M. F.; Winnik, F. M.; Bossmann, S. H.; Turro, N. J. *Helv. Chim. Acta* **2001**, *84*, 2476-2492.
- (^{xliv}) Niederweis, M.; Bossmann, S. *Ger. Offen.* **2001**, *DE 99-19941416 19990831*, pp.18.
- (^{xlv}) Heinz, C.; Niederweis, M. *Anal. Biochem.* **2000**, *285*, 113-120.
- (^{xlvi}) Heinz, C.; Karosi, S.; Niederweis, M. *J. Chromatogr. B.* **2003**, *790*, 337-348.
- (^{xlvii}) Pashley, C. A.; Parish, T. *FEMS Microbiol. Lett.* **2003**, *229*, 211-215.
- (^{xlviii}) Hoffmann, C.; Lowery, S., Sukumaran, S., Bossmann, S. H. and Niederweis, M., *unpublished*.
- (^{xlix}) Mahfoud, M.; Sukumaran, S.; Hülsmann, P.; Grieger, K.; Niederweis, M. *J. Biol. Chem.* **2006**, *281*, 5908-15.
- (^l) Heinz, C.; Roth, E.; Niederweis, M. *Methods. Mol. Biol.* **2003**, *228*, 139-150.
- (^{li}) Due to the space limitations, the Fresnel equations won't be discussed here, because their physical consequences, but not the equations themselves are of great importance for this work.
- (^{lii}) Englebienne, P. *Analyst* **1998**, *123*, 1599-1603.

-
- (liii) Jain, P. K.; Lee, K. S.; El-Sayed, I. H.; El-Sayed, M. A. *J. Phys. Chem. B.* **2006**, *110*, 7238-7248.
- (liv) Cahill, D. J. *J. Immunol. Methods* **2001**, *250*, 81-91.
- (lv) Schessler, H. M.; Karpovich, D. S.; Blanchard, G. J. *J. Am. Chem. Soc.* **1996**, *118*, 9645-9651.
- (lvi) H. Du, R. A. Fuh, J. Li, A. Corkan, J. S. Lindsey, *Photochem. Photobiol.*, **1998**, *68*, 141-142
- (lvii) Biros, Shannon M.; Rebek, Julius, Jr. *Chem. Soc. Rev.* **2007**, *36*(1), 93-104.
- (lviii) Purse, Byron W.; Rebek, Julius, Jr. *PNAS* **2005**, *102*(31), 10777-10782.
- (lix) Bosch, Eric. *Cryst. Eng. Comm.* **2007**, *9*(3), 191-198.
- (lx) Kobayashi, Kenji; Ishii, Kei; Sakamoto, Shigeru; Shirasaka, Toshiaki; Yamaguchi, Kentaro. *J. Am. Chem. Soc.* **2003**, *125*(35), 10615-10624.
- (lxi) Aakeroy, Christer; Schultheiss, Nate; Desper, John. *Cryst. Eng. Comm.* **2007**, *9*(3), 211-214.
- (lxii) Aakeroy, Christer B.; Desper, John; Valdes-Martinez, Jesus *Cryst. Eng. Comm.* **2004**, *6* 413-418.
- (lxiii) Beard, John. *Sci. Total Environ.* **2006**, *355*(1-3), 78-89.
- (lxiv) Reed, Lamar; Buchner, Virginia; Tchounwou, Paul B *Reviews on Environmental Health* **2007**, *22*(3), 213-243.
- (lxv) Li, Qing Qing; Loganath, Annamalai; Chong, Yap Seng; Tan, Jing; Obbard, Jeffrey Philip. *J. Toxicol. Environ. Health, Part A* **2006**, *69*(21), 1987-2005.
- (lxvi) Pohl, H. R.; McClure, P. R.; Fay, M.; Holler, J.; De Rosa, C. T. *Chemosphere* **2001**, *43*(4-7), 903-908.
- (lxvii) Stone, Richard. *Science* (Washington, DC, United States) **2007**, *315*(5809), 176-179.
- (lxviii) Process for the dehalogenation of organic compounds by alkali metals on solid supports European Patent EP0467053
<http://www.freepatentsonline.com/EP0467053B1.html>
- (lxix) Paramo-Garcio, U.; Avila-Rodriguez, M.; Garcia-Jimenez, M. G.; Gutierrez-Granados, S.; Ibanez-Cornejo, J. G *Electroanalysis* **2006**, *18*(9), 904-910.
- (lxx) Xiaoxuan Leaym, Stefan Kraft and Stefan H. Bossmann. *Unpublished*
- (lxxi) Mandler, D.; Willner, I. *J. Am. Chem. Soc.* **1987**, *109*, 7884-5.
- (lxxii) Willner, I.; Adar, E.; Goren, Z.; Steinberger, B. *New J. Chem.* **1987**, *11*, 769-73.
- (lxxiii) Gurzadyan, G. G.; Steenken, S. *Phys. Chem. Chem. Phys.* **2002**, *4*, 2983-2988.
- (lxxiv) Willner, I.; Maida, R.; Mandler, D.; Duerr, H.; Doerr, G.; Zengerle, K. *J. Am. Chem. Soc.* **1987**, *109*, 6080-6.
- (lxxv) Wang, T. C.; Tan, C. K. *Environ. Sci. Technol.* **1988**, *22*, 916-19.
- (lxxvi) Brett, Christopher M. A.; Oliveira Brett, Ana Maria. *Encyclopedia of Electrochemistry* **2003**, *3* 105-124.
- (lxxvii) Repasky, M. P.; Chandrasekhar, J.; Jorgensen, W. L. *J. Comput. Chem.* **2002**, *23*, 1601-1622
- (lxxviii) Bryant, Judi A.; Blanda, Michael T.; Vincenti, Marco; Cram, Donald J. *J. Am. Chem. Soc.* **1991**, *113*(6), 2167-72.
- (lxxix) Turner, David R.; Pastor, Aurelia; Alajarin, Mateo; Steed, Jonathan W. *Structure and Bonding* (Berlin, Germany) **2004**, *108* (Supramolecular Assembly via Hydrogen Bonds I), 97-168.

-
- (^{lxxx}) Yu, Siwang; Kong, Ah-Ng. *Current Cancer Drug Targets* **2007**, 7(5), 416-424.
- (^{lxxxii}) Gottesman, Michael M.; Ambudkar, Suresh V. *J Bioenerg Biomembr* **2001**, 33(6), 453-458.
- (^{lxxxiii}) Reddy, B. S. P.; Sondhi, S. M.; Lown, J. W. *Pharmacology & Therapeutics* **1999**, 84(1), 1-111.
- (^{lxxxiiii}) Kyrpides, Nikos C.; Ouzounis, Christos A. *Journal of Molecular Evolution* **1995**, 40(6), 564-9
- (^{lxxxv}) Denny, William A.; Baguley, Bruce C. *Curr. Top. Med. Chem.* (Hilversum, Netherlands) **2003**, 3(3), 339-353.
- (^{lxxxvi}) Waterhouse, Dawn N.; Tardi, Paul G.; Mayer, Lawrence D.; Bally, Marcel B. *Drug Safety* **2001**, 24(12), 903-920.
- (^{lxxxvii}) Cutts, Suzanne; Nudelman, Abraham; Rephaeli, Ada; Phillips, Don. *IUBMB Life* **2005**, 57(2), 73-81.
- (^{lxxxviii}) Shaun, N.; Thomas, B. Cell cycle regulation. Textbook of Malignant Hematology (2nd Edition) (2005), 33-63, 1 plate.
- (^{lxxxix}) Kumar, S. *Cell Death and Differentiation* **2007**, 14(1), 32-43.
- (^{xc}) Waring, M. J. *Australian Journal of Pharmaceutical Sciences* **1979**, 8(3), 65-71.
- (^{xc}) Waring, M. J. *Drug Action Mol. Level*, [Rep. Symp.] **1977**, Meeting Date 1976, 167-89.
- (^{xc}) Williams, Loren Dean; Rich, Alexander. *Mol. Struct. Life* **1992**, 3-27.
- (^{xcii}) Dickerson, R. E.; Drew, Horace R.; Conner, B. N.; Kopka, M. L.; Pjura, P. E. *Cold Spring Harbor Symposia on Quantitative Biology* (**1983**), Volume Date 1982, 47(1), 13-24.
- (^{xciii}) Haber-Pohlmeier, S.; Eimer, W. *J. Phys. Chem.* **1993**, 97(13), 3095-7.
- (^{xciv}) Daniel ben-Avraham, L. S. Schulman, Stefan H. Bossmann, Claudia Turro, Nicholas J. Turro, *J. Phys. Chem. B* **1998**, 102, 5088-5093.
- (^{xcv}) Lerman, L. S. *J. Mol. Biol.* **1961**, 3 18-30.
- (^{xcvi}) Luzzati, V.; Masson, F.; Lerman, L. S.. *J. Mol. Biol.* **1961**, 3 634-9.
- (^{xcvii}) Bryant, Judi A.; Knobler, Carolyn B.; Cram, Donald J. *J. Am. Chem. Soc.* **1990**, 112 (3), 1254-5.
- (^{xcviii}) Bryant, Judi A.; Ericson, John L.; Cram, Donald J. *J. Am. Chem. Soc.* **1990**, 112(3), 1255-6.
- (^{xcix}) Pirondini, Laura; Stendardo, Anna G.; Geremia, Silvano; Campagnolo, Mara; Samori, Paolo; Rabe, Jurgen P.; Fokkens, Roel; Dalcanale, Enrico. *Angew. Chem. Int. Ed.* **2003**, 42 (12), 1384-1387.
- (^c) Francis A. Carey. *Organic Chemistry, 4e* Chapter 24 : Phenols
- (^{ci}) Bent, D. V.; Hayon, E.; Moorthy, P. N. *J. Am. Chem. Soc.* **1975**, 97 (18), 5065-71.
- (^{cii}) Steven L. Murov, Ian Carmichael, Gordon L. Hug, *Handbook of Photochemistry, Second Edition*, Marcel Dekker, Inc., New York, 1993, page 123
- (^{ciii}) Schweitzer, Claude; Mehrdad, Zahra; Noll, Astrid; Grabner, Erich-Walter; Schmidt, Reinhard. *J. Phys. Chem. A* **2003**, 107(13), 2192-2198.
- (^{civ}) Naumann, Wolfgang. *Recent Research Developments in Chemical Physics* **2003**, 4(Pt. 1), 191-208 and references provided therein
- (^{cv}) Matsuoka, Keisuke; Moroi, Yoshikiyo. *Curr. Opin. Colloid Interface Sci.* **2003**, 8(3),

(^{cvi}) 227-235
Olmstead E J; Panter J W; Boykin D W Jr; Wilson W D *Biochemistry* **1975**, 14 (3),
521-6.

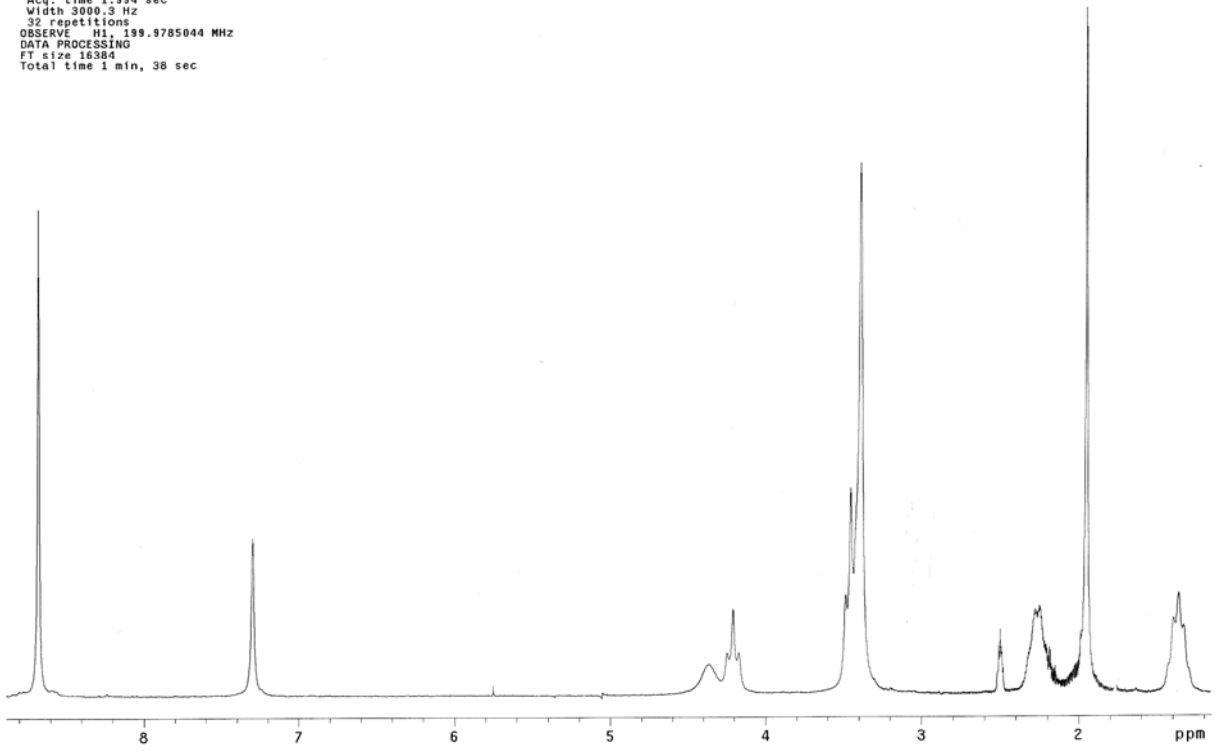
**Appendix B – ^1H -NMR Spectra, ^{13}C -NMR Spectra and
Elemental Analysis Data**

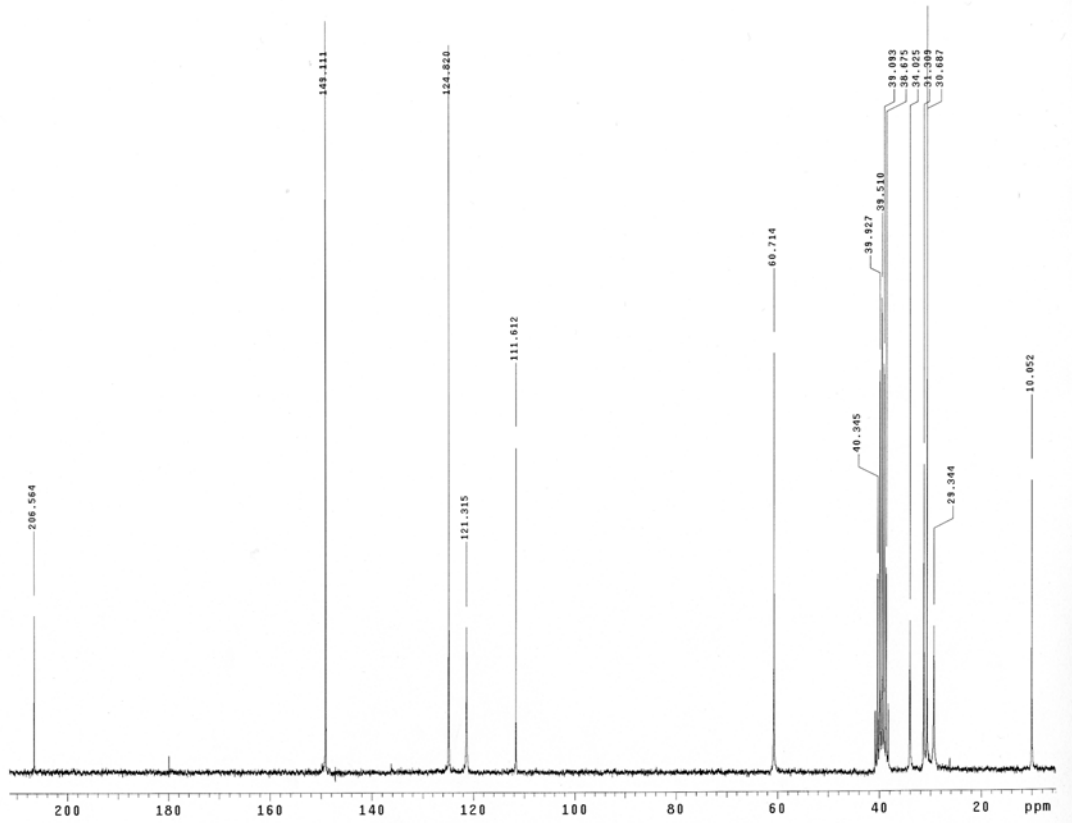
1

Filename: _

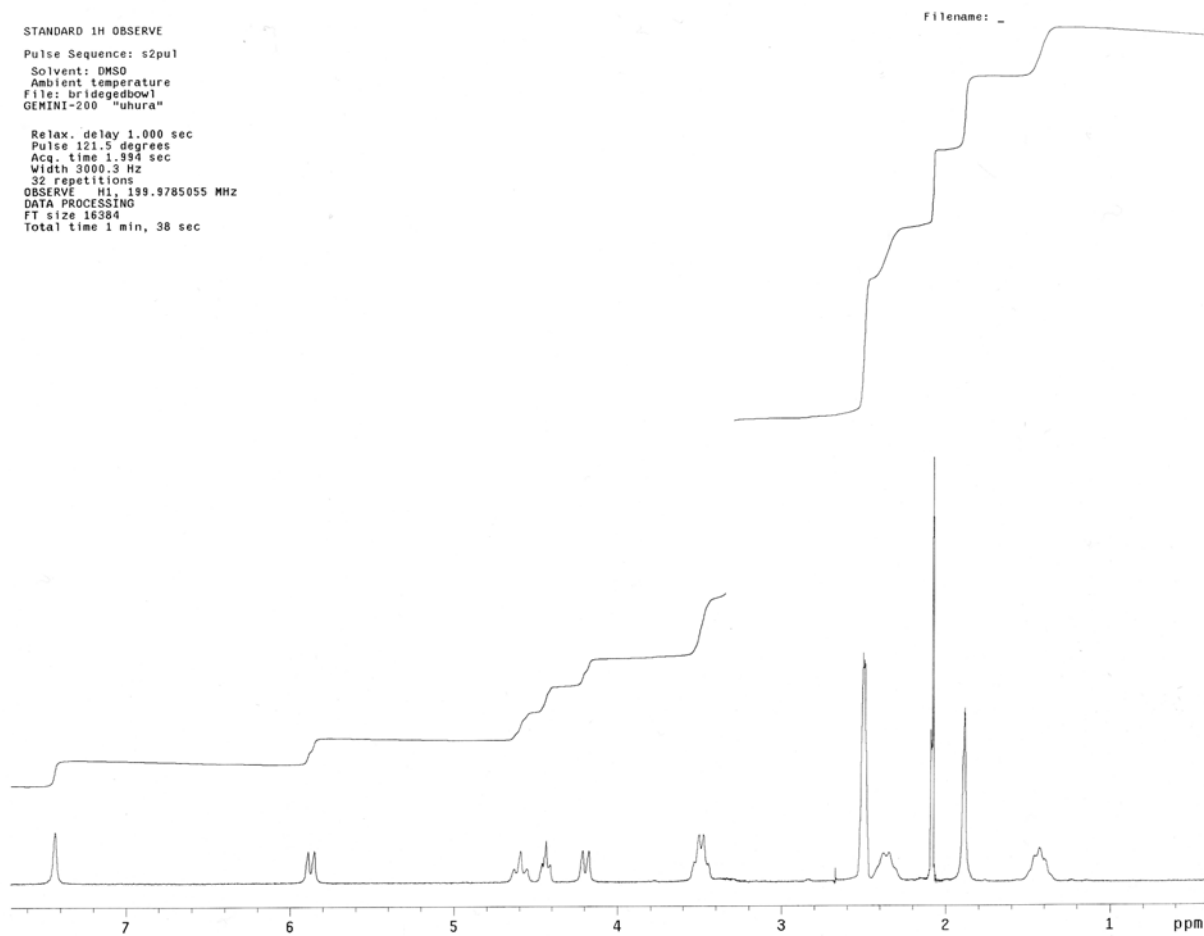
STANDARD 1H OBSERVE
Pulse Sequence: s2pul
Solvent: DMSO
Ambient temperature
File: condensedowl
GEMINI-200 "uhura"

Relax. delay 1.000 sec
Pulse 121.5 degrees
Acq. time 1.994 sec
Width 3000.3 Hz
32 repetitions
OBSERVE H1, 199.9785044 MHz
DATA PROCESSING
FT size 16384
Total time 1 min, 38 sec

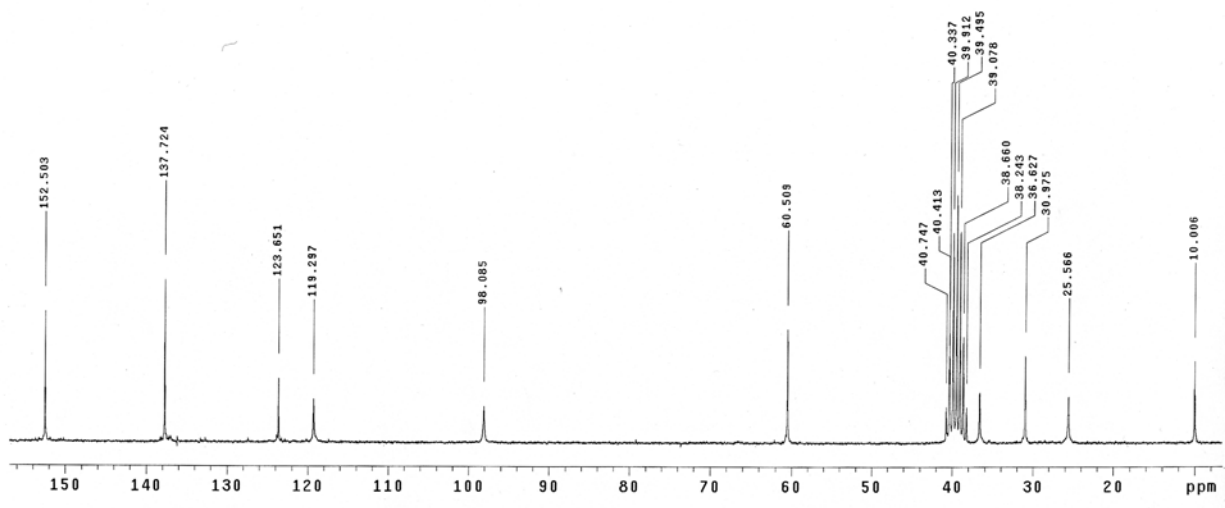


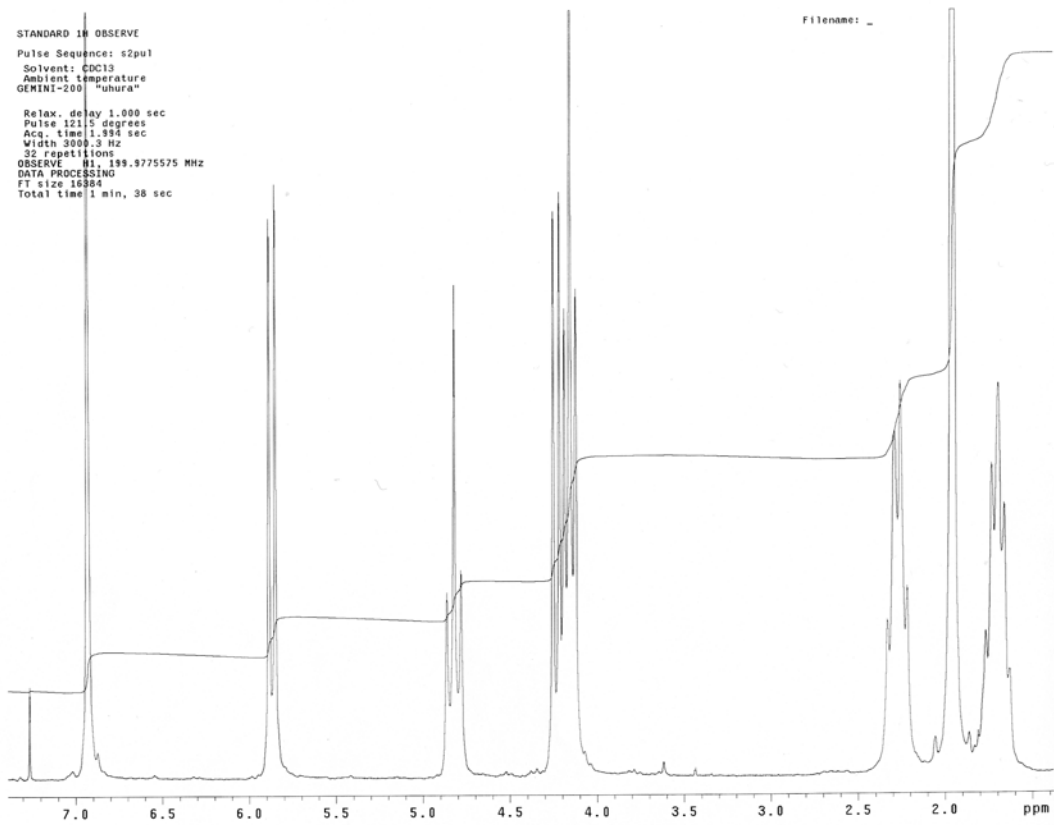


2

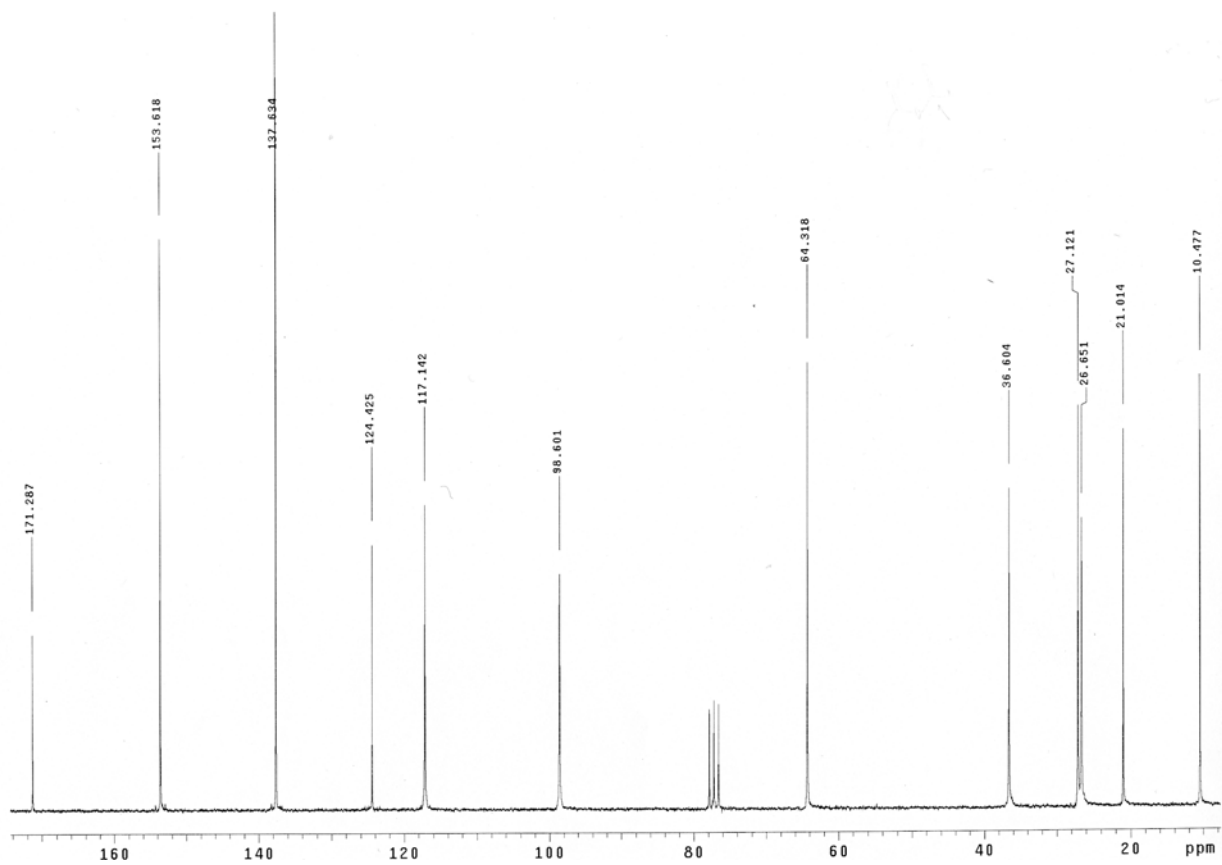


2





3

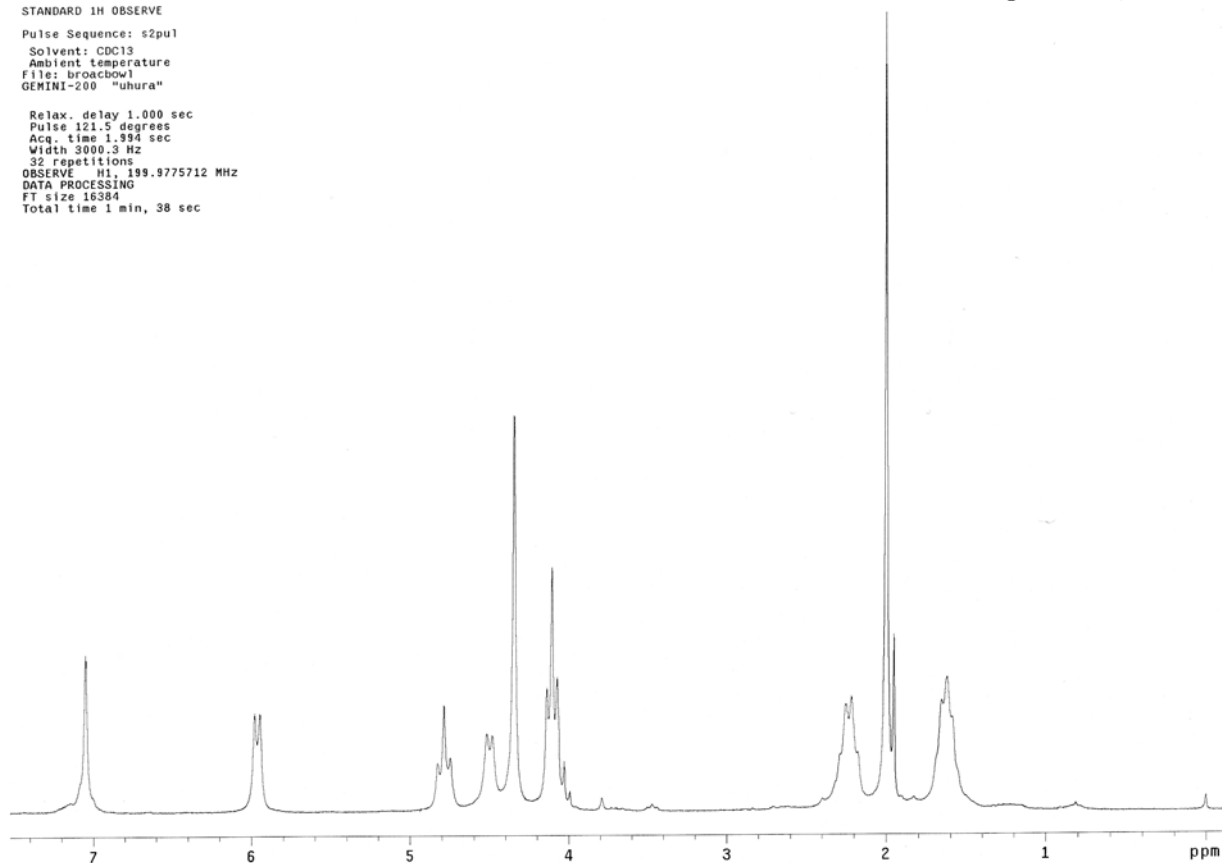


4

STANDARD 1H OBSERVE
Pulse Sequence: s2pu1
Solvent: CDC13
Ambient temperature
File: broacbow1
GEMINI-200 "uhura"

Relax. delay 1.000 sec
Pulse 121.5 degrees
Acq. time 1.934 sec
Width 3000.3 Hz
32 repetitions
OBSERVE H1, 199.9775712 MHz
DATA PROCESSING
FT size 16384
Total time 1 min, 38 sec

Filename: _

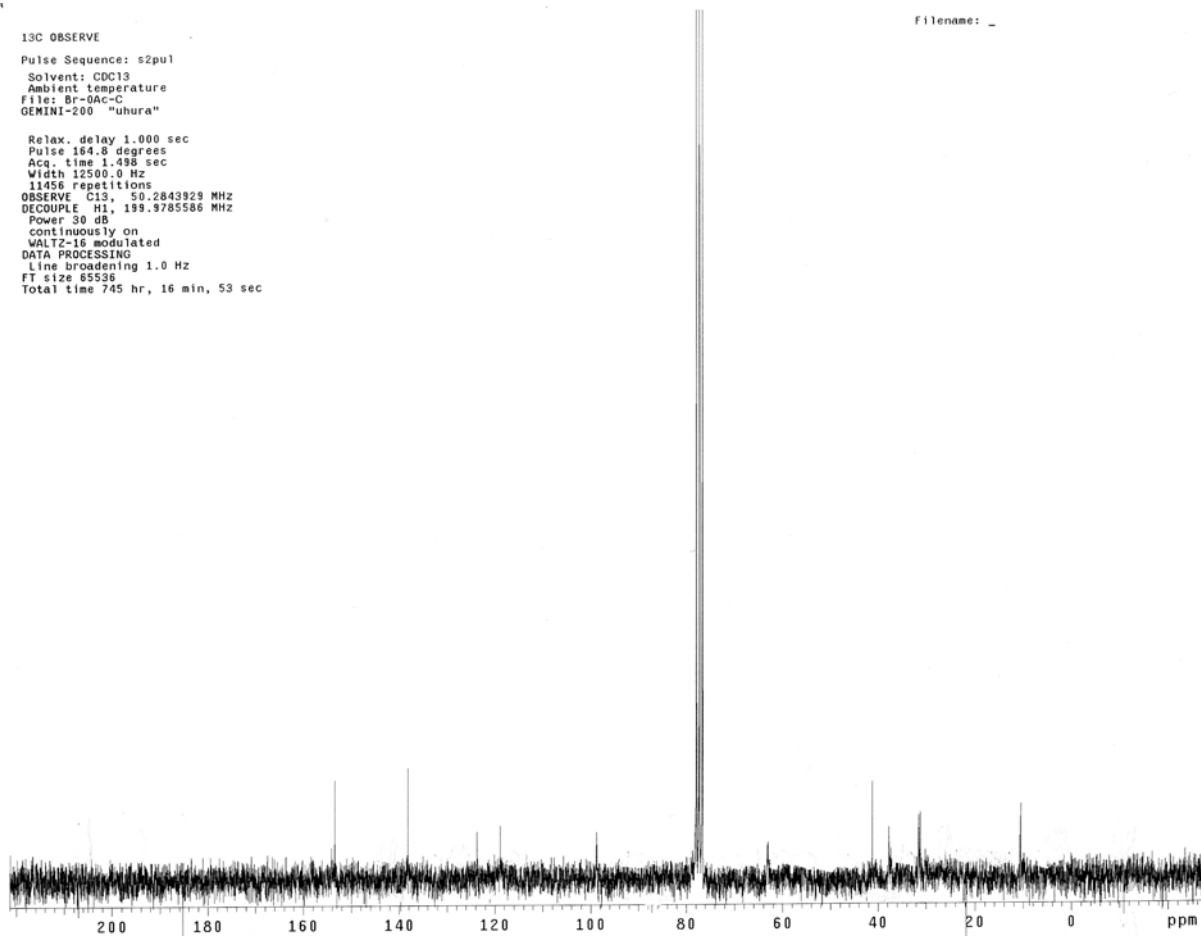


4

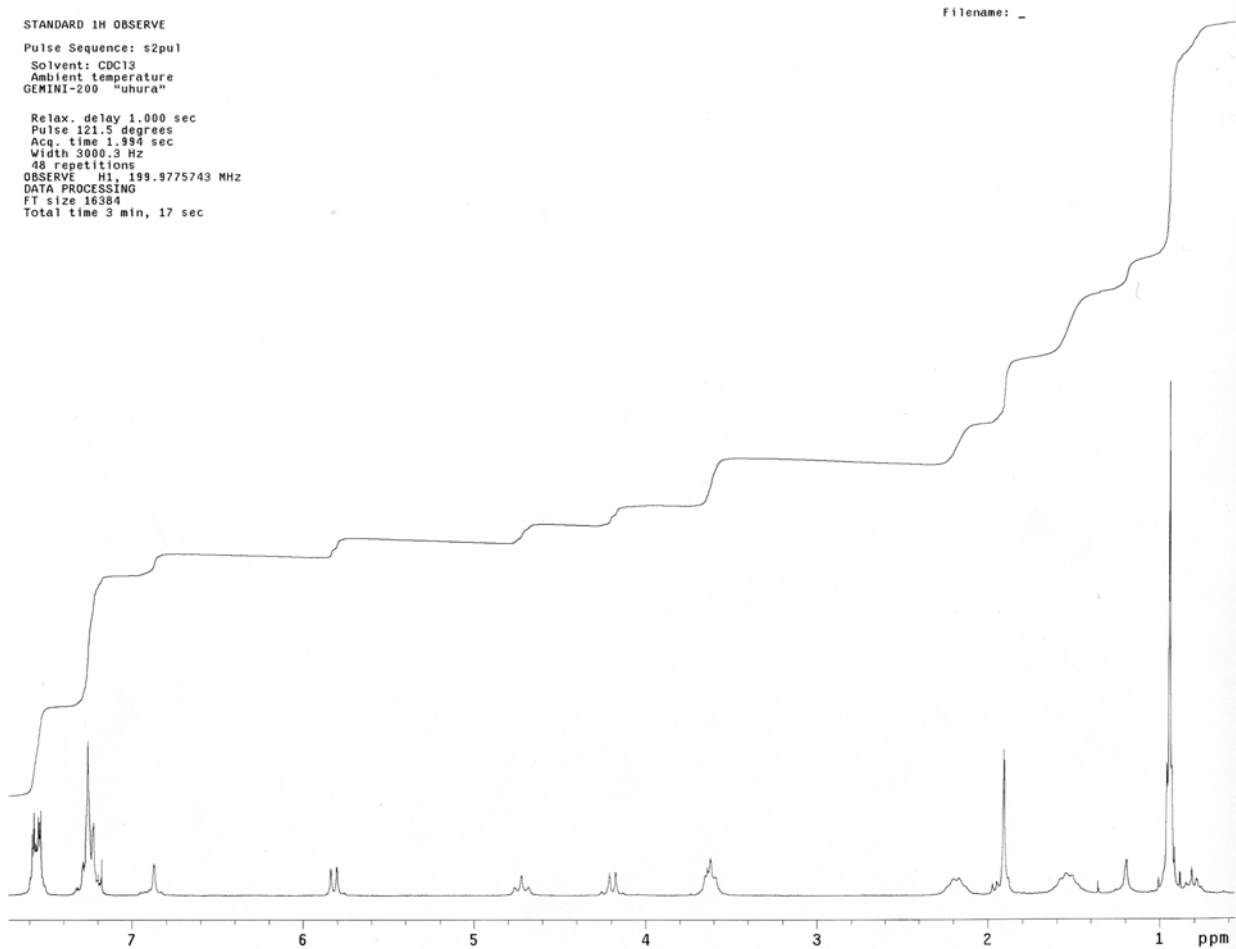
13C OBSERVE
Pulse Sequence: s2pul
Solvent: CDCl3
Ambient temperature
File: Br-OAc-C
GEMINI-200 "uhura"

Relax. delay 1.000 sec
Pulse 164.8 degrees
Acq. time 1.498 sec
Width 12500.0 Hz
11456 repetitions
OBSERVE C13, 50.2843929 MHz
DECOUPLE H1, 199.9785586 MHz
Power 30 dB
continuously on
WALTZ-16 modulated
DATA PROCESSING
Line broadening 1.0 Hz
FT size 65536
Total time 745 hr, 16 min, 53 sec

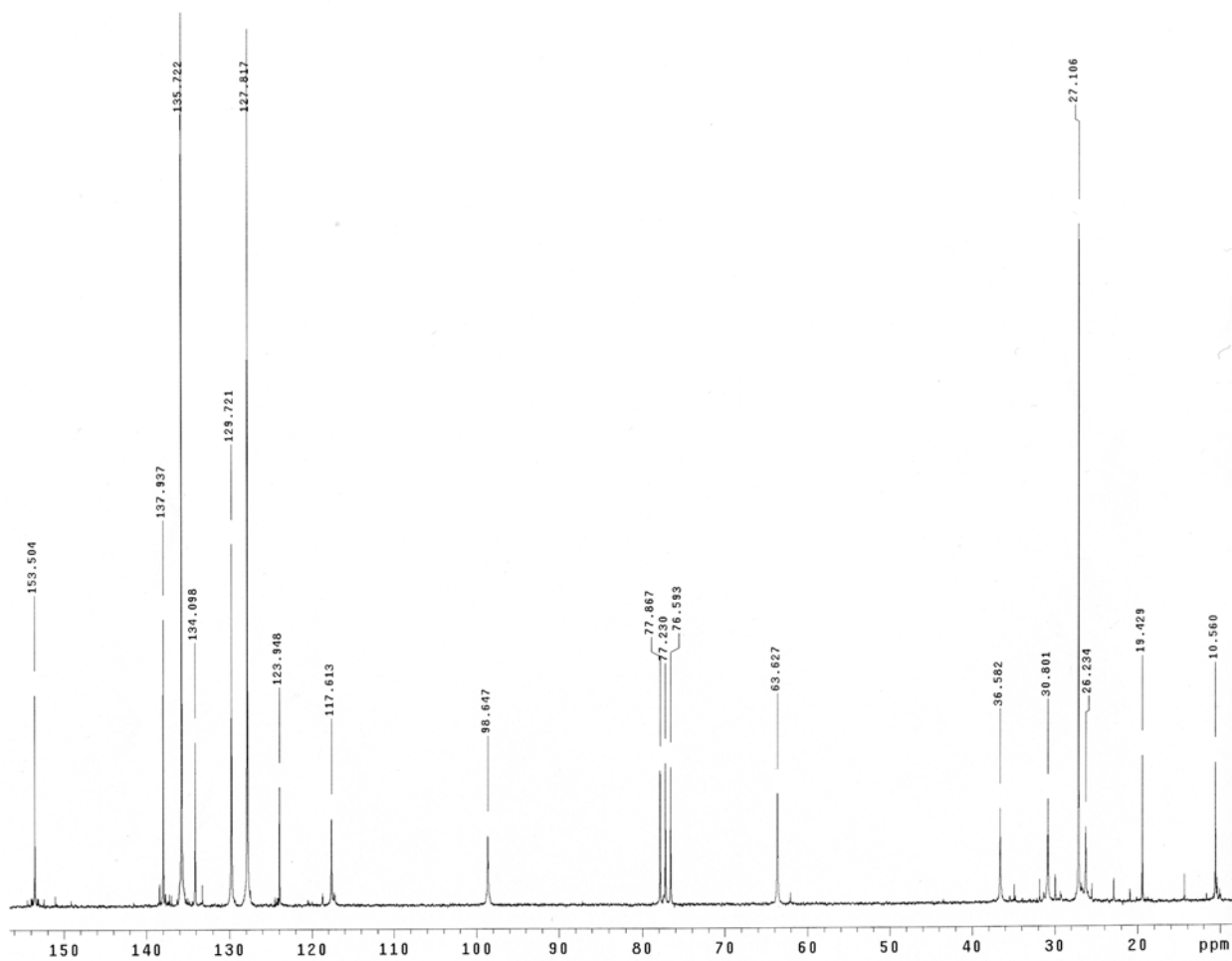
Filename: _



5



5



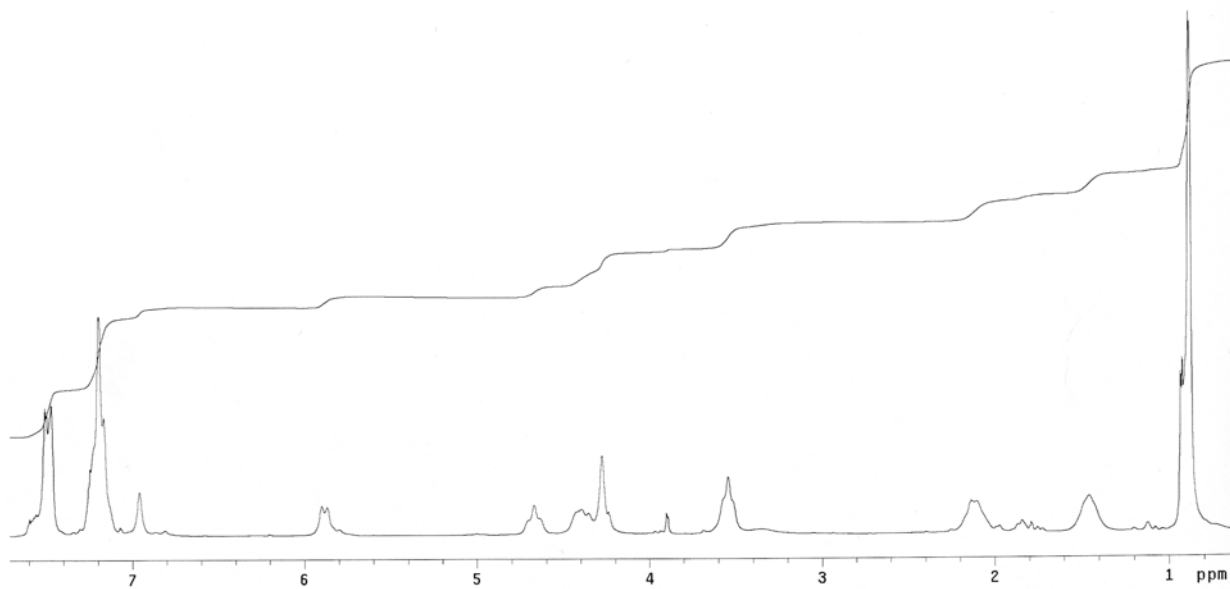
6

Filename: _

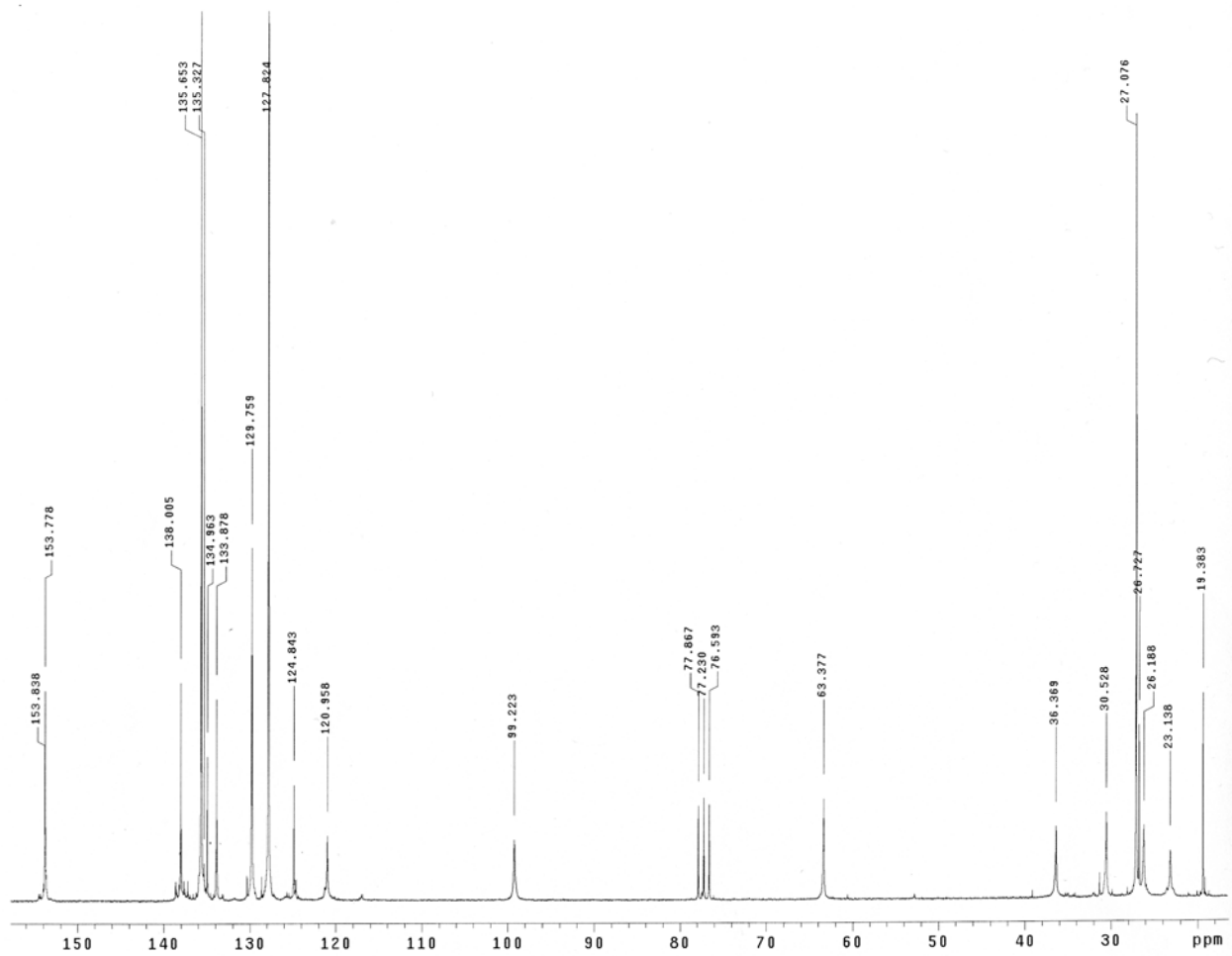
STANDARD 1H OBSERVE

Pulse Sequence: s2pu1
Solvent: CDCl3
Ambient temperature
GEMINI-200 "uhura"

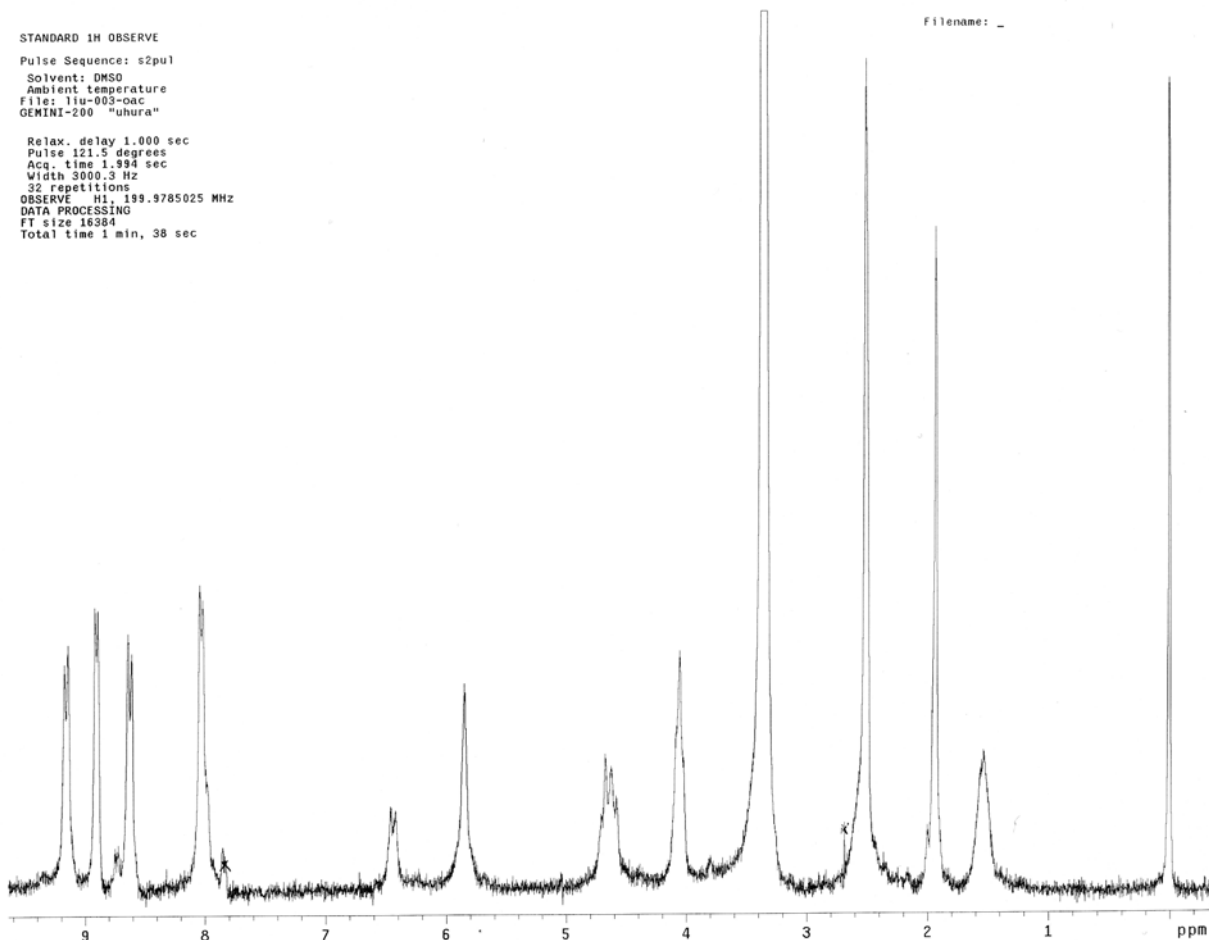
Relax. delay 1.000 sec
Pulse 121.5 degrees
Acq. time 1.394 sec
Width 3000.3 Hz
32 repetitions
OBSERVE H1, 199.9775965 MHz
DATA PROCESSING
FT size 16384
Total time 1 min, 38 sec

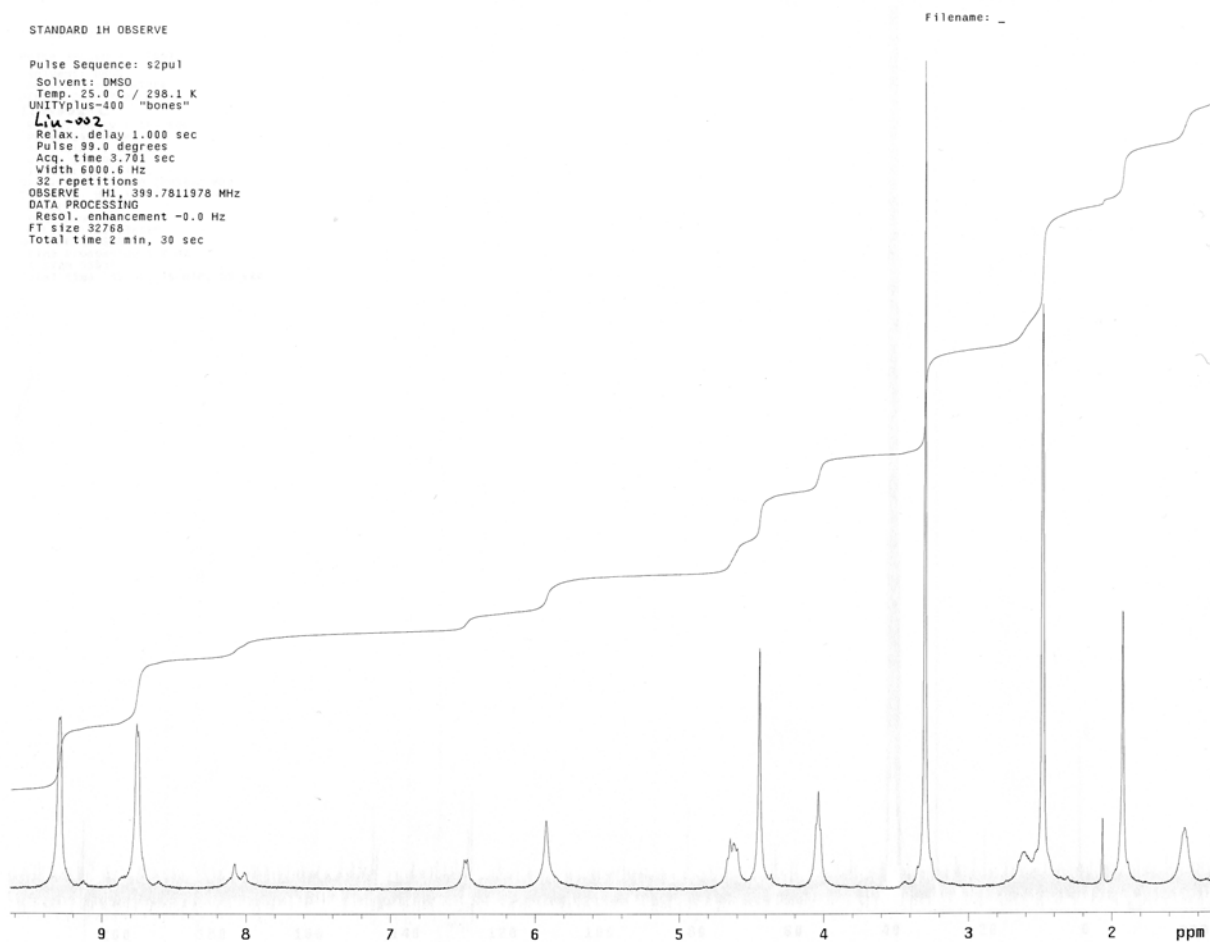


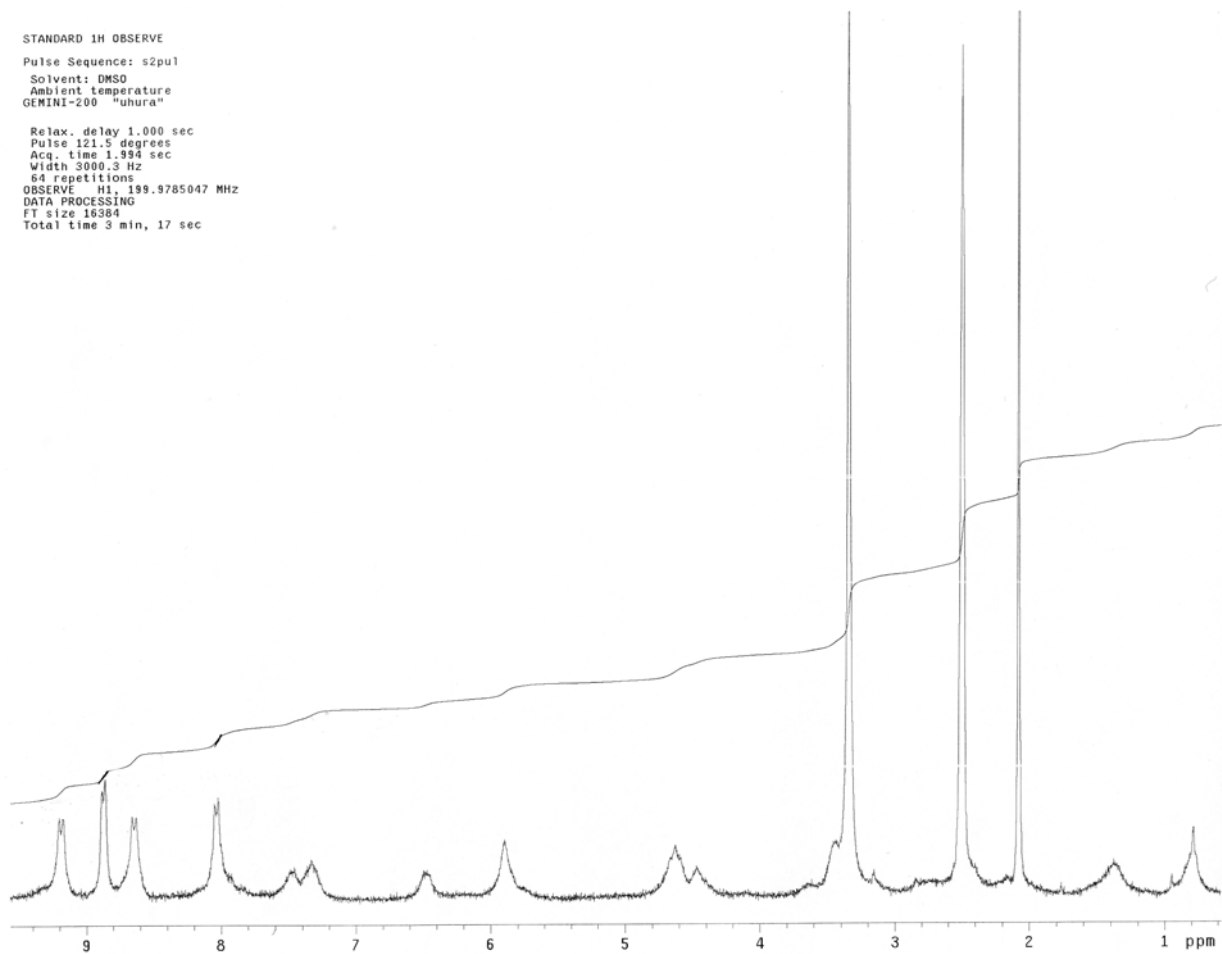
6



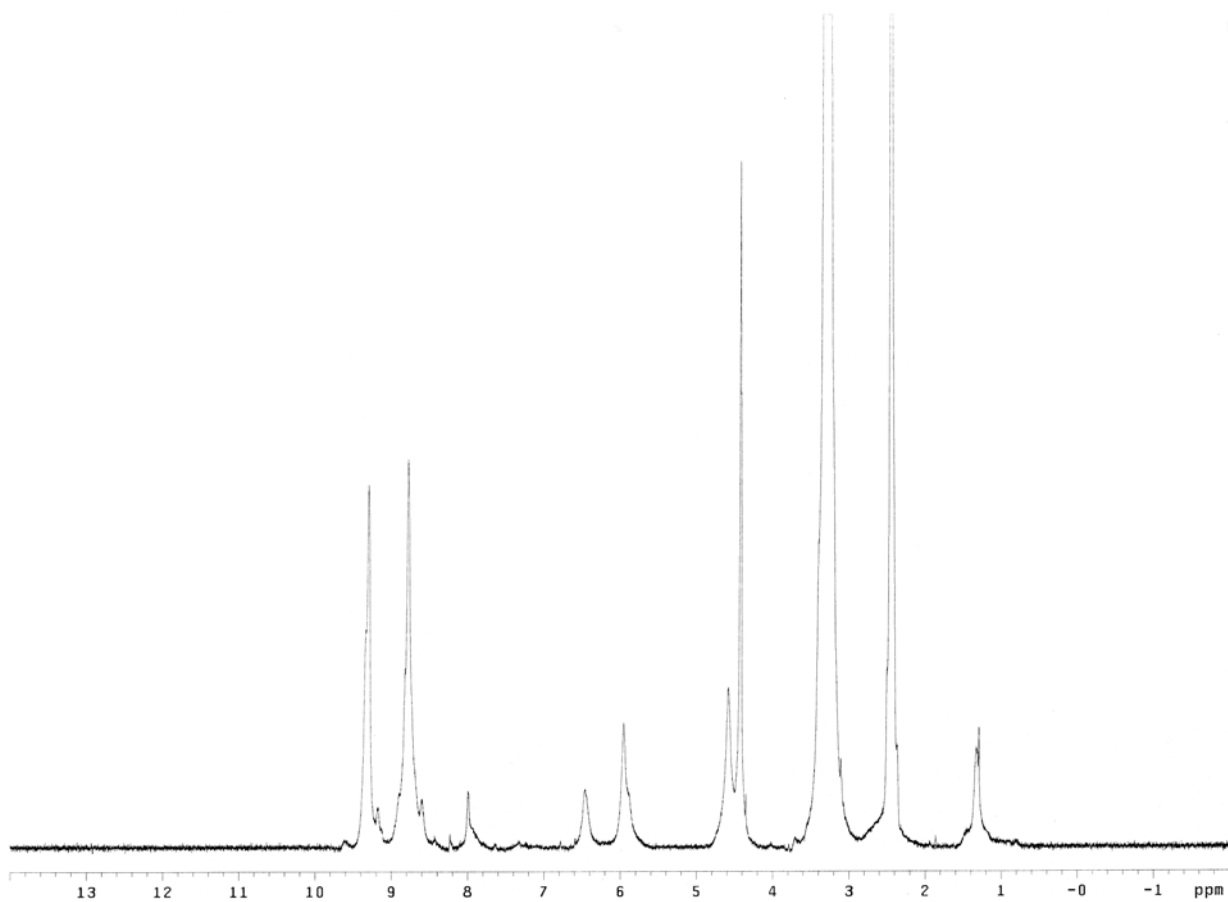
7

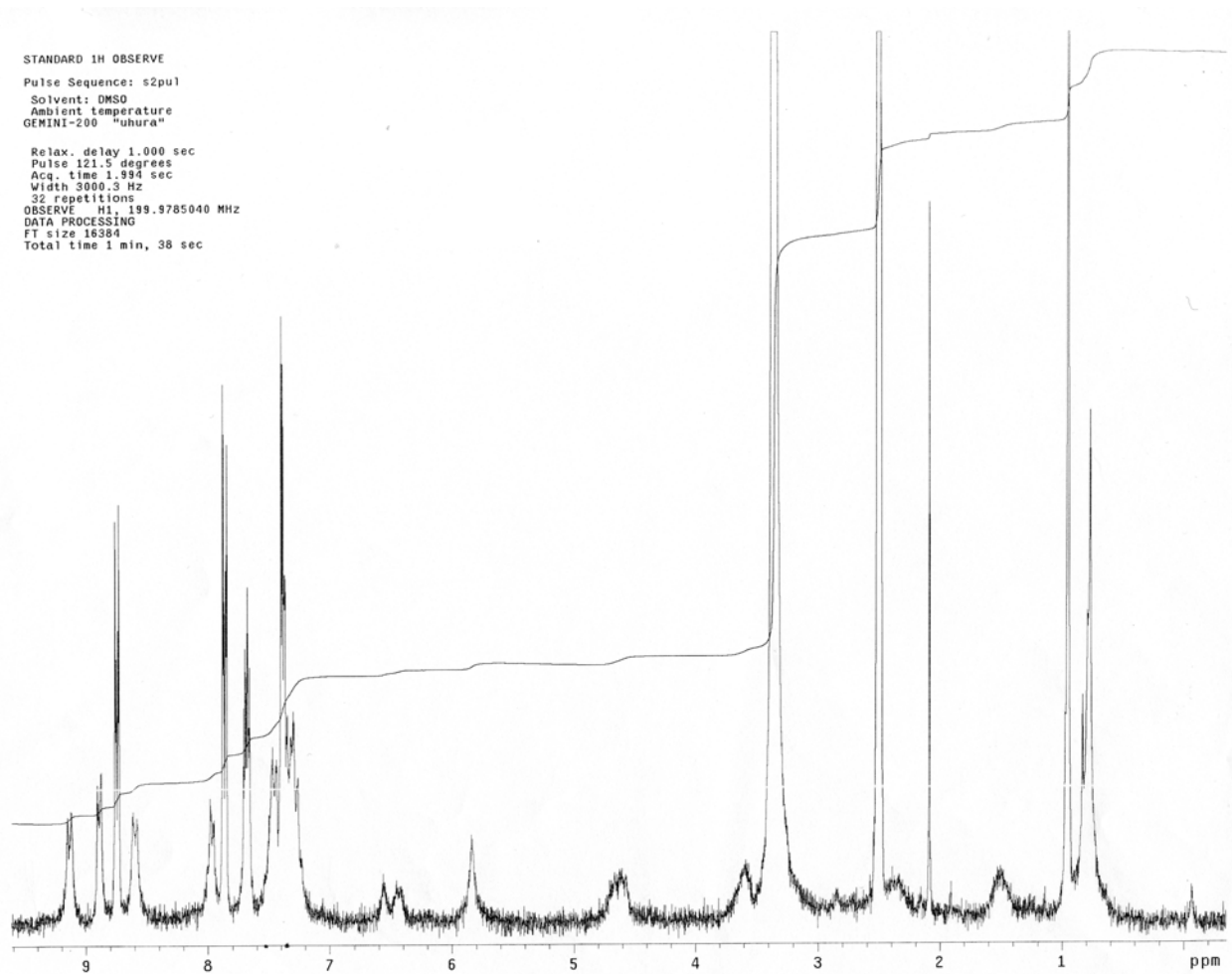


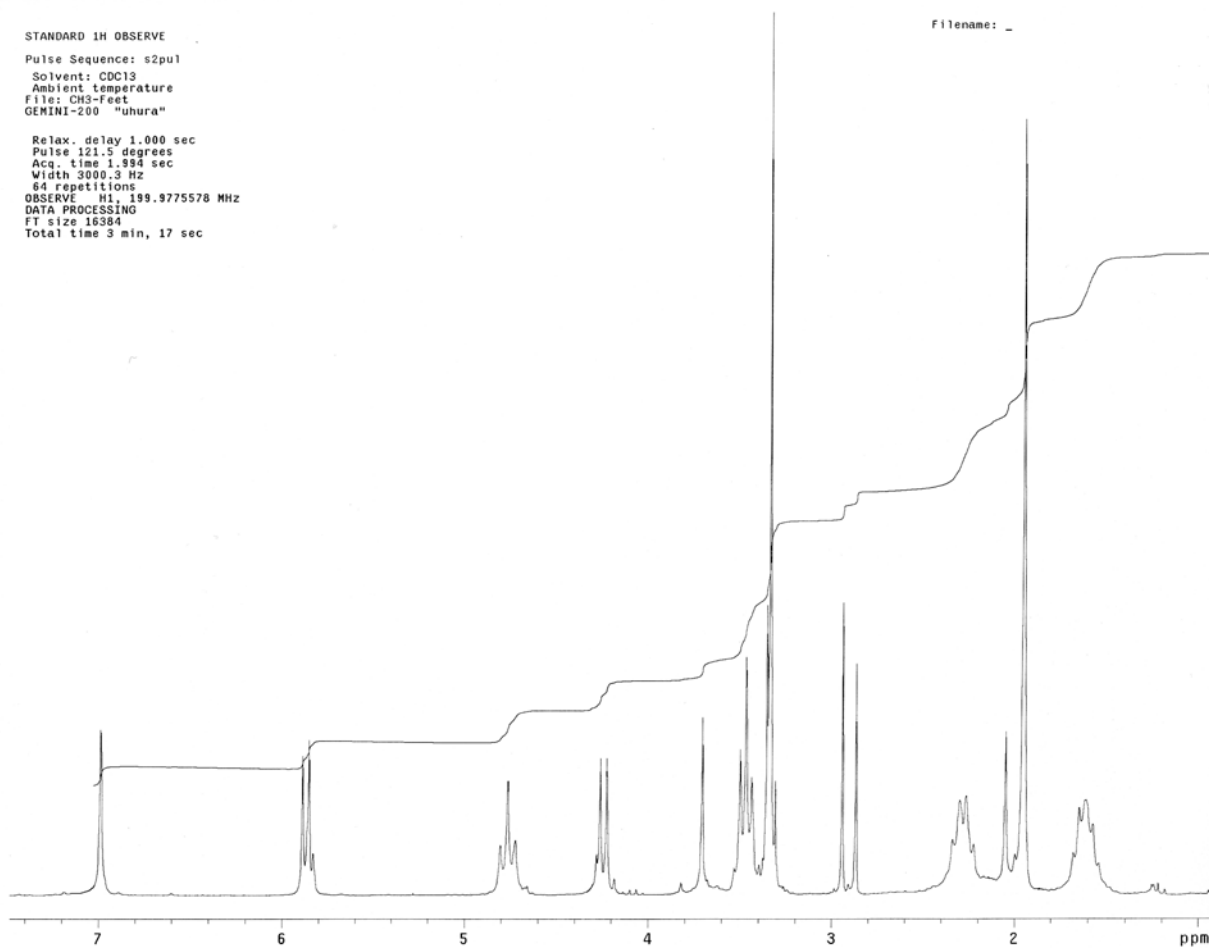




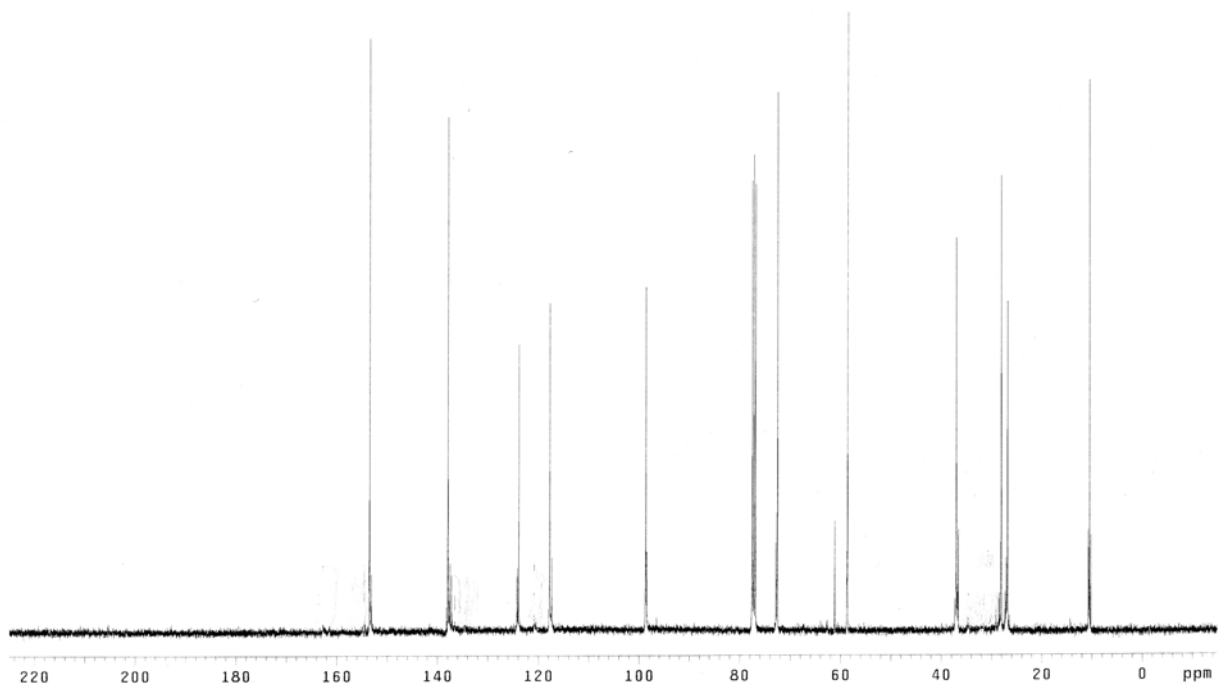
10

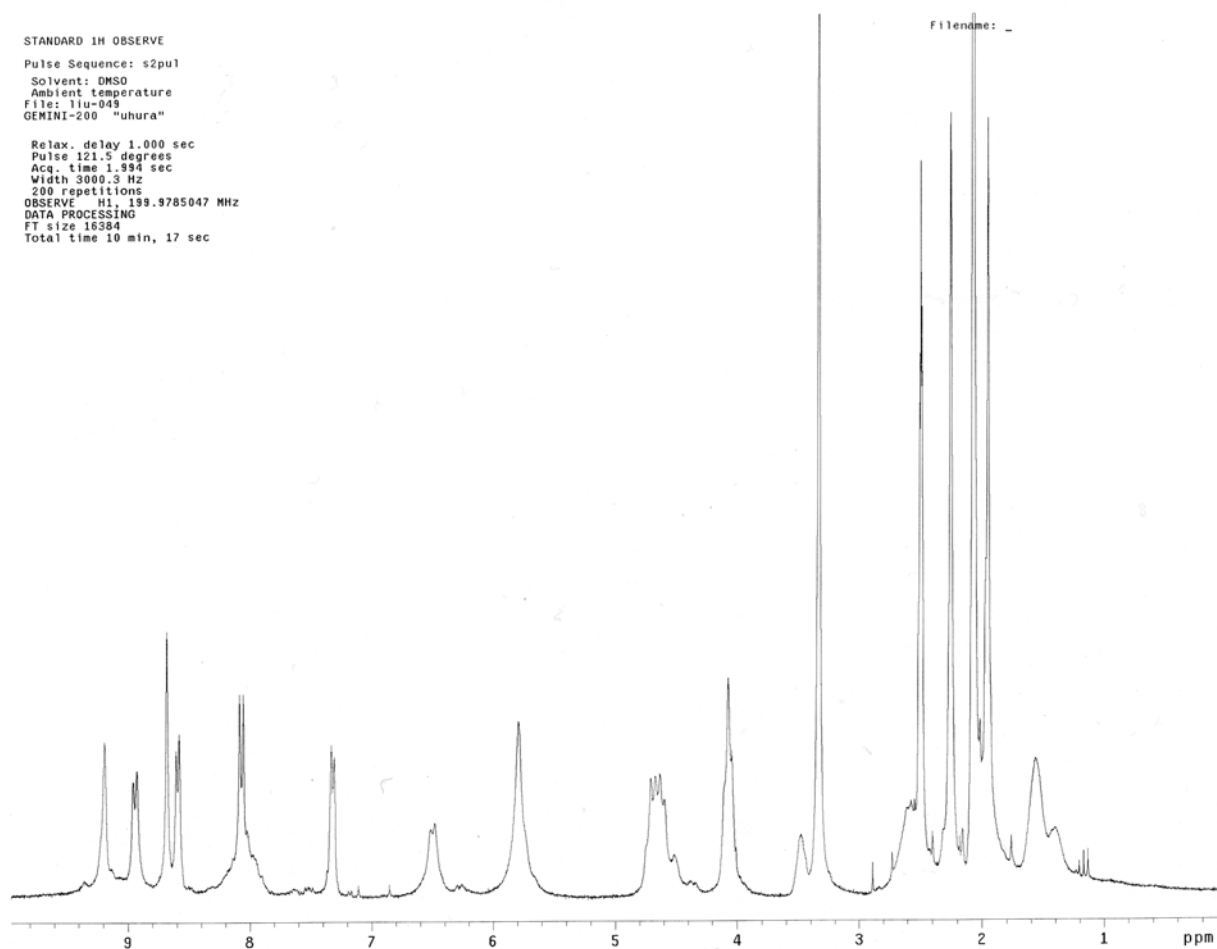


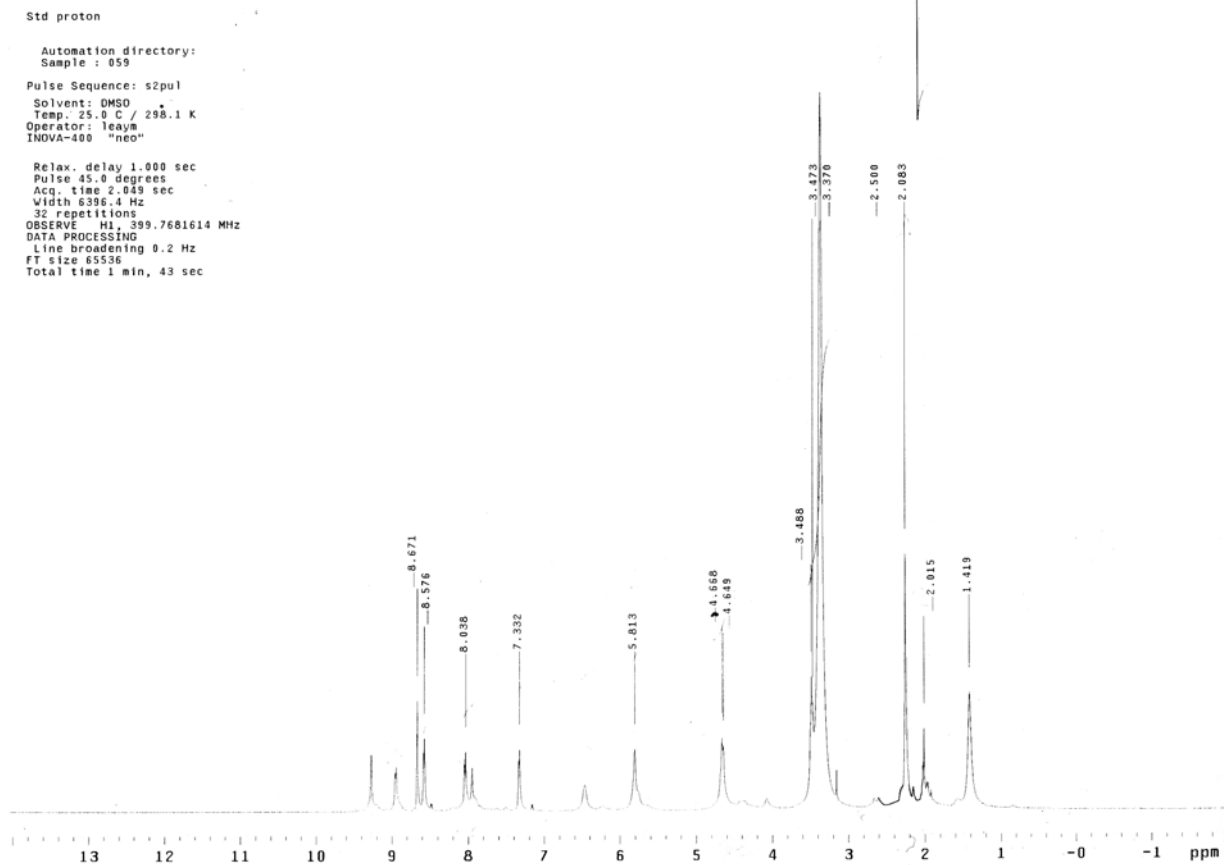


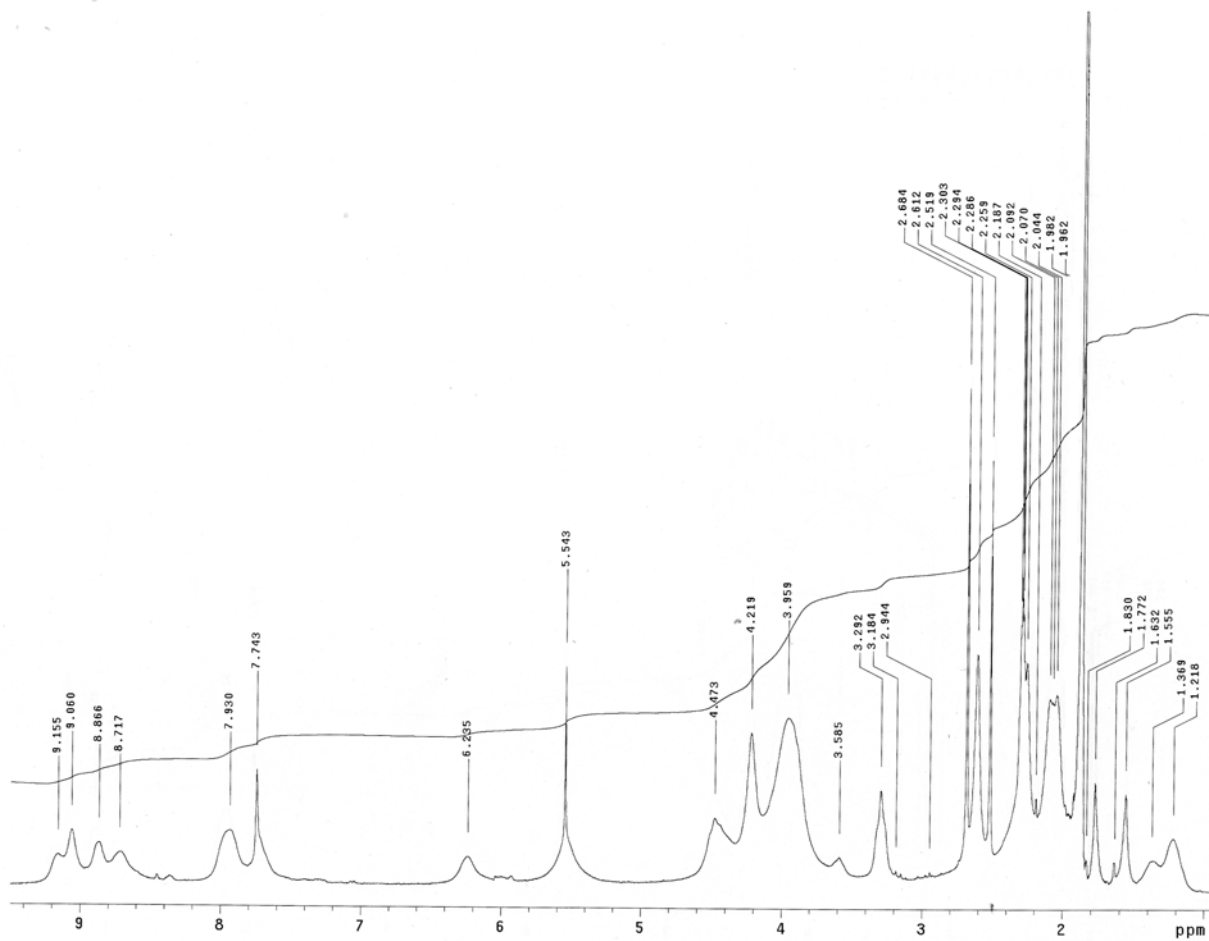


12



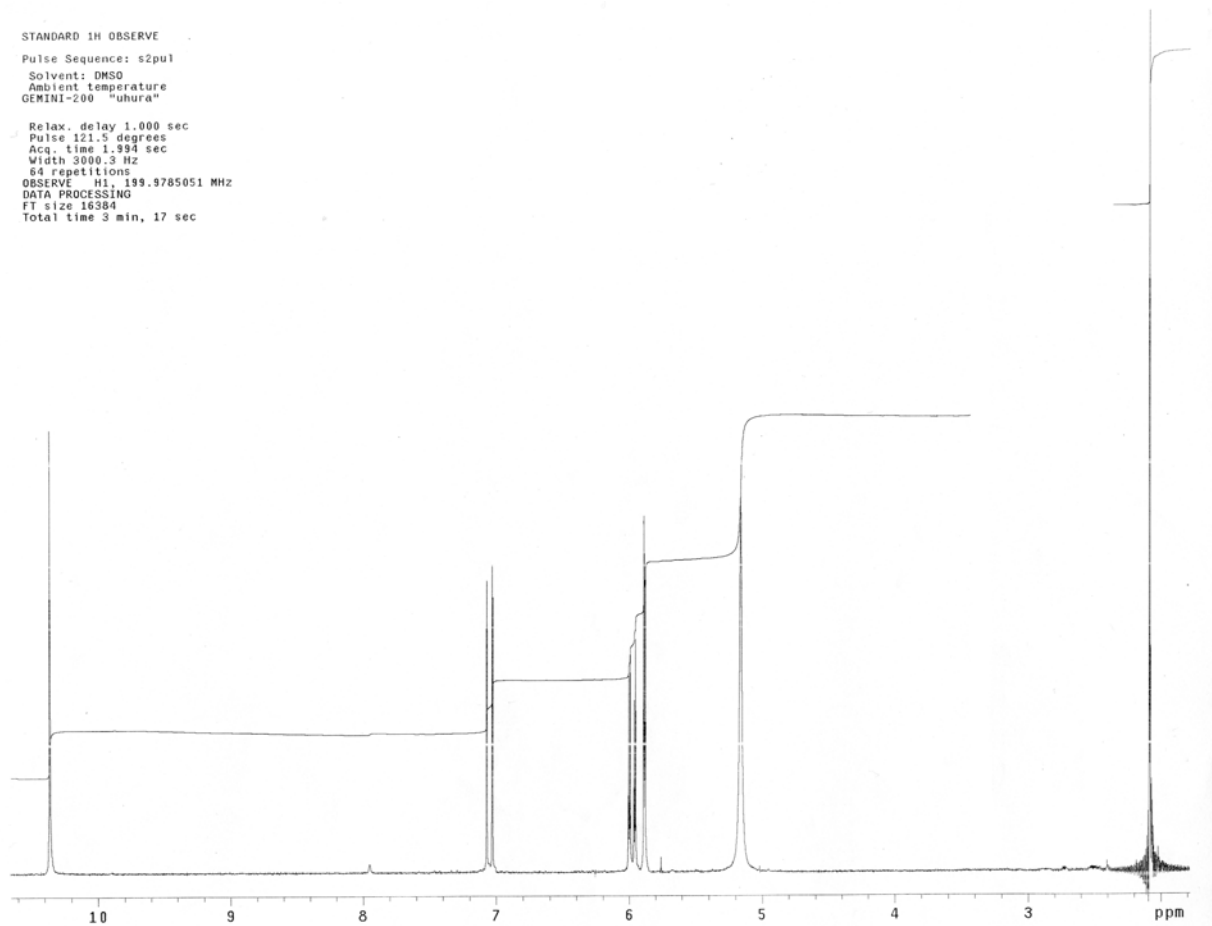






16

STANDARD 1H OBSERVE
Pulse Sequence: s2pu1
Solvent: DMSO
Ambient temperature
GEMINI-200 "uhura"
Relax. delay 1.000 sec
Pulse 121.5 degrees
Acq. time 1.994 sec
Width 3000.3 Hz
64 repetitions
OBSERVE R1: 199.9785051 MHz
DATA PROCESSING
FT size 16384
Total time 3 min, 17 sec

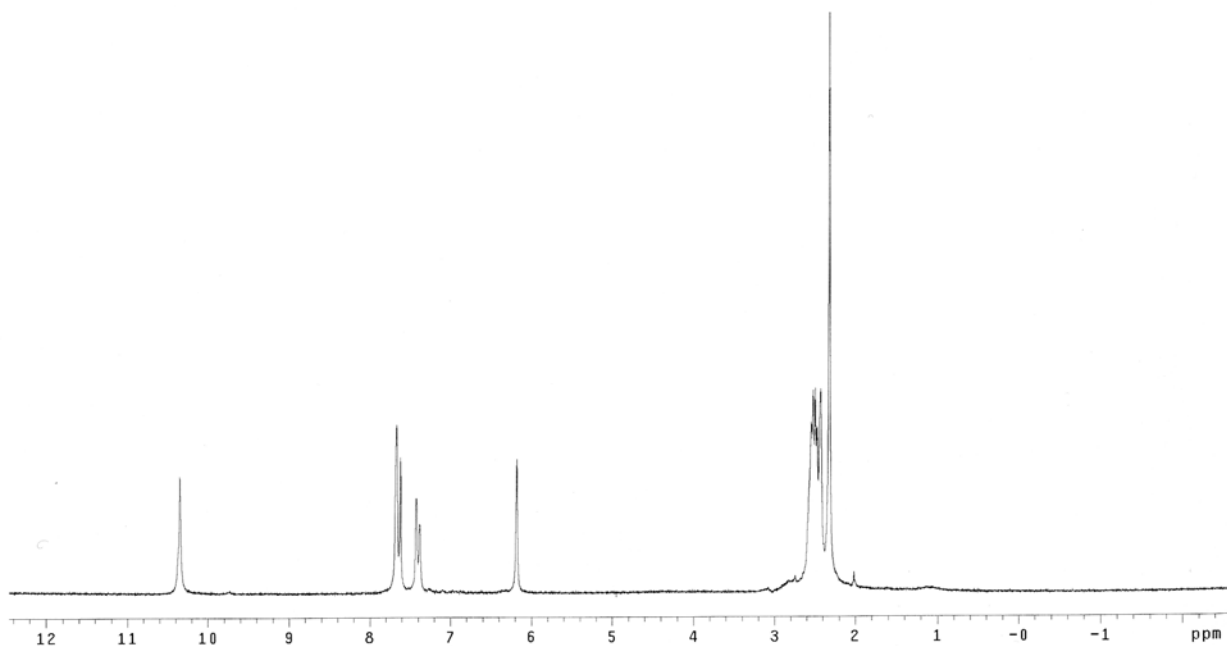


17

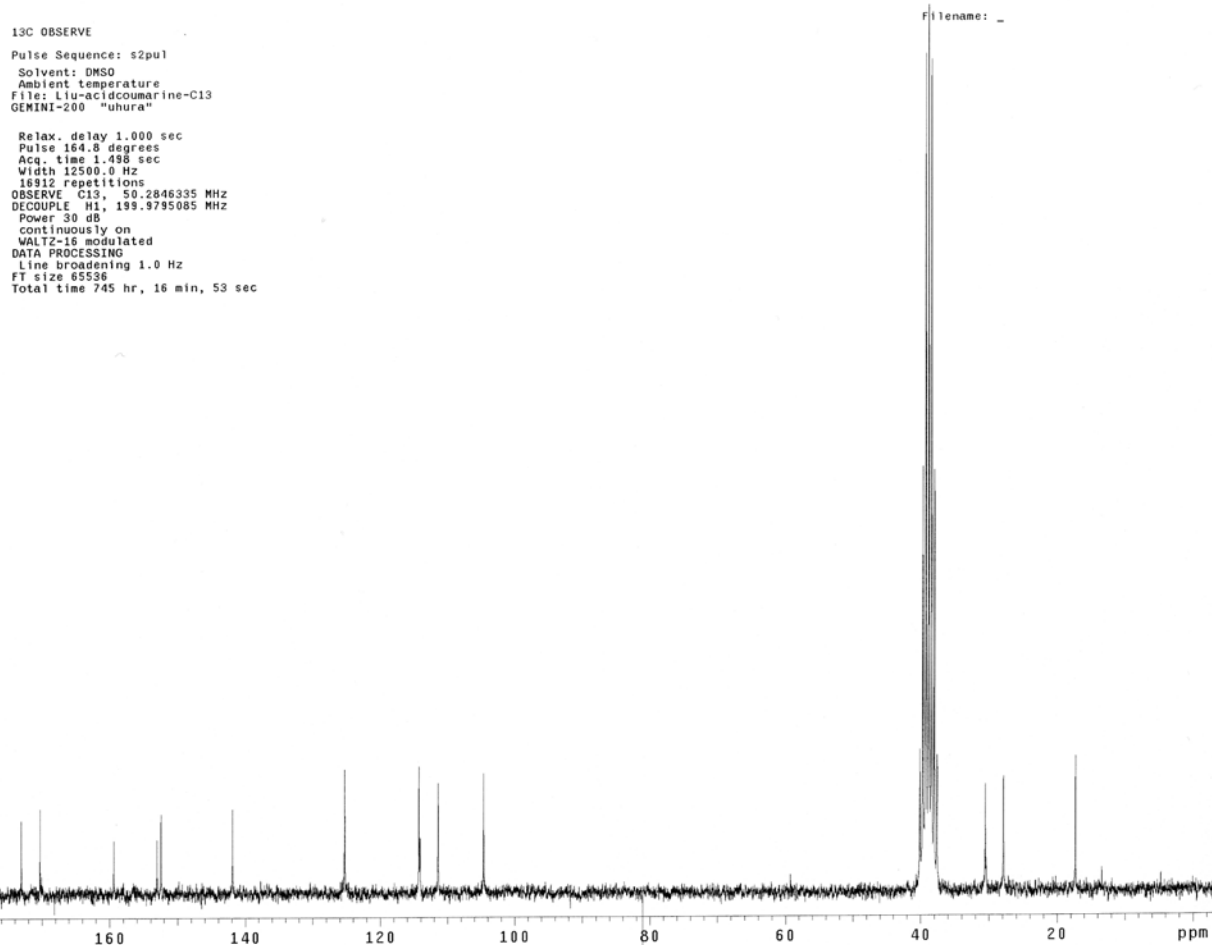
Filename: _

STANDARD 1H OBSERVE
Pulse Sequence: s2pu1
Solvent: DMSO
Ambient temperature
File: 11u-acidcoumarine
GEMINI-200 "uhura"

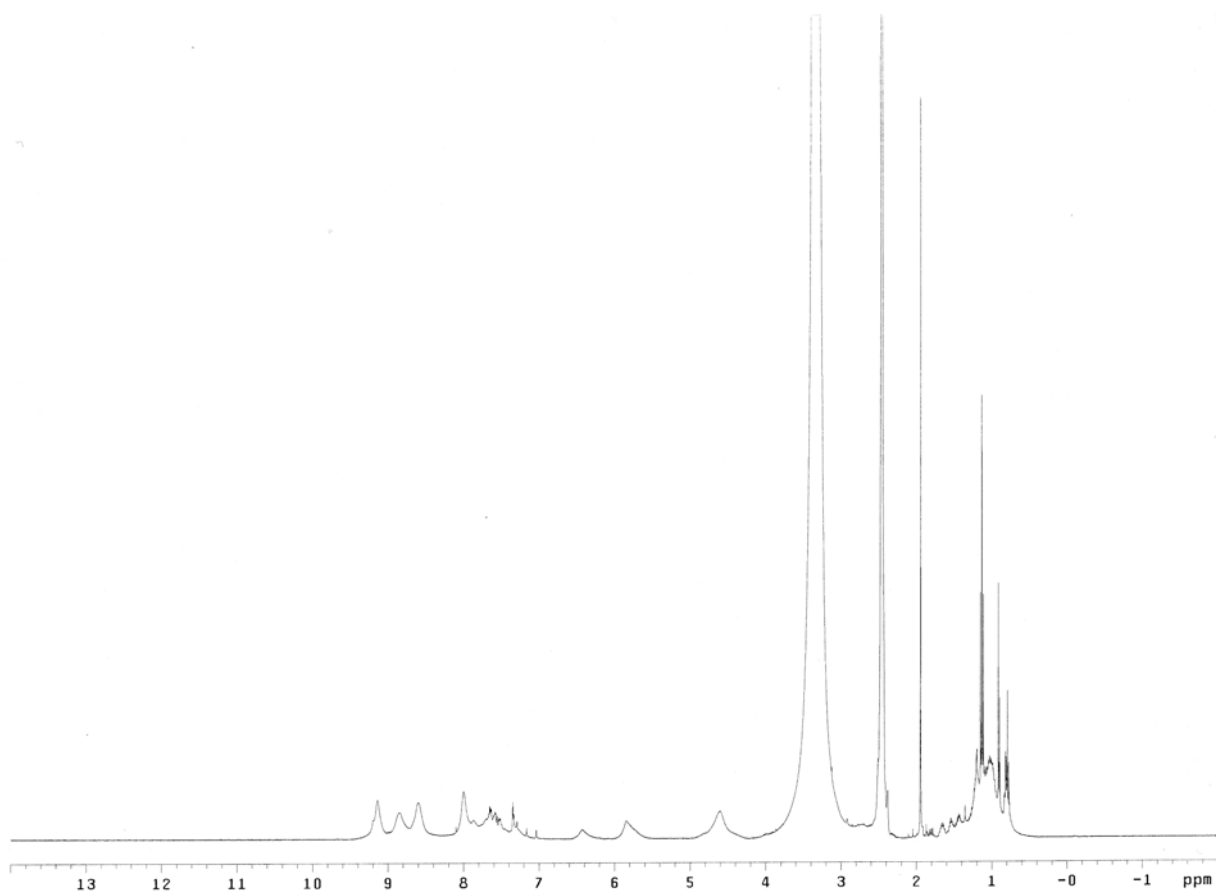
Relax. delay 1.000 sec
Pulse 121.5 degrees
Acq. time 1.994 sec
Width 3000.3 Hz
64 repetitions
OBSERVE H1, 199.9785190 MHz
DATA PROCESSING
FT size 16384
Total time 3 min, 17 sec

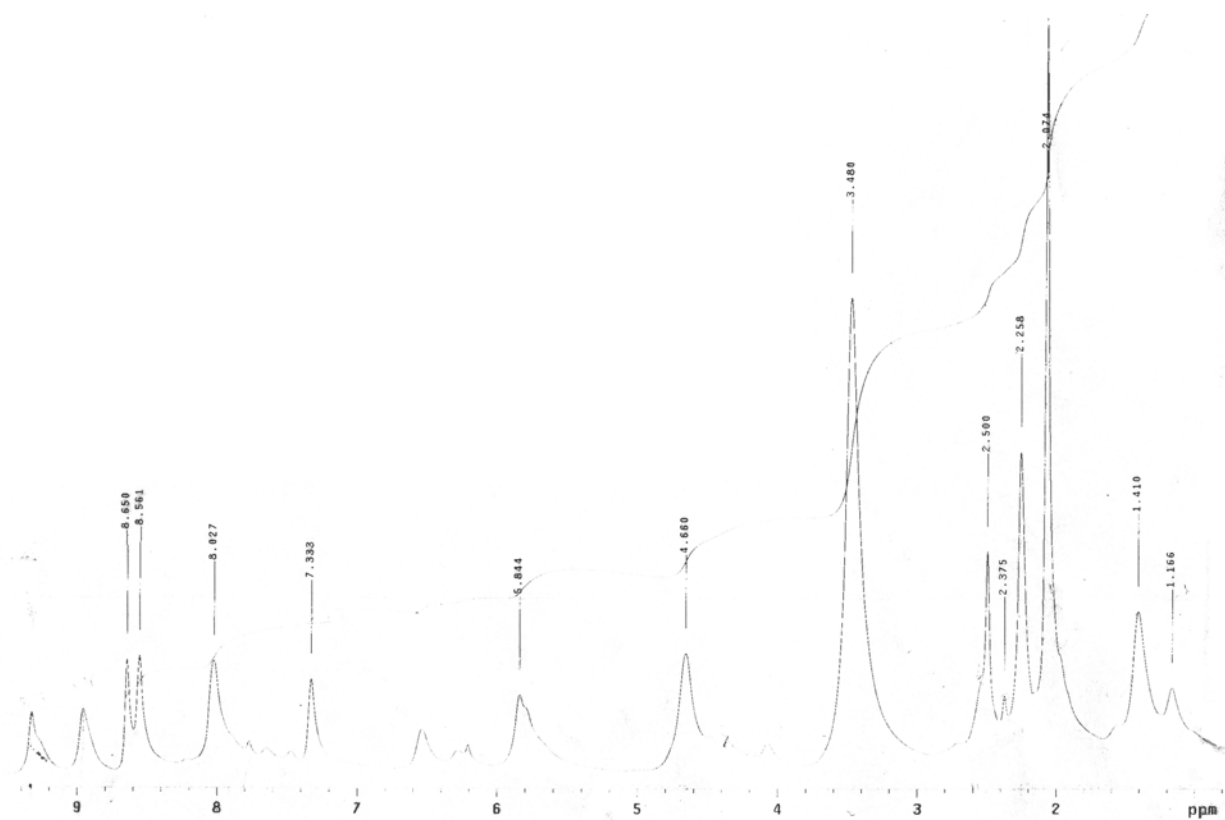


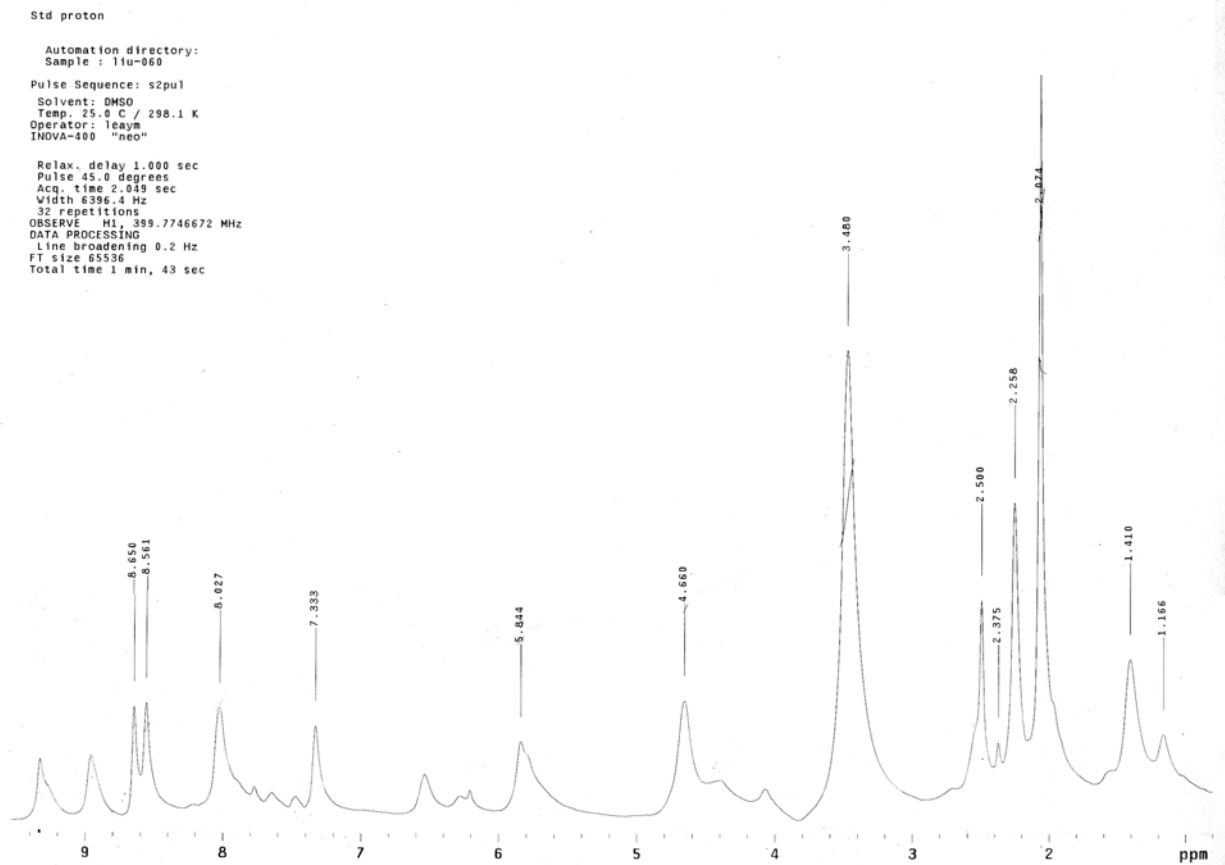
17



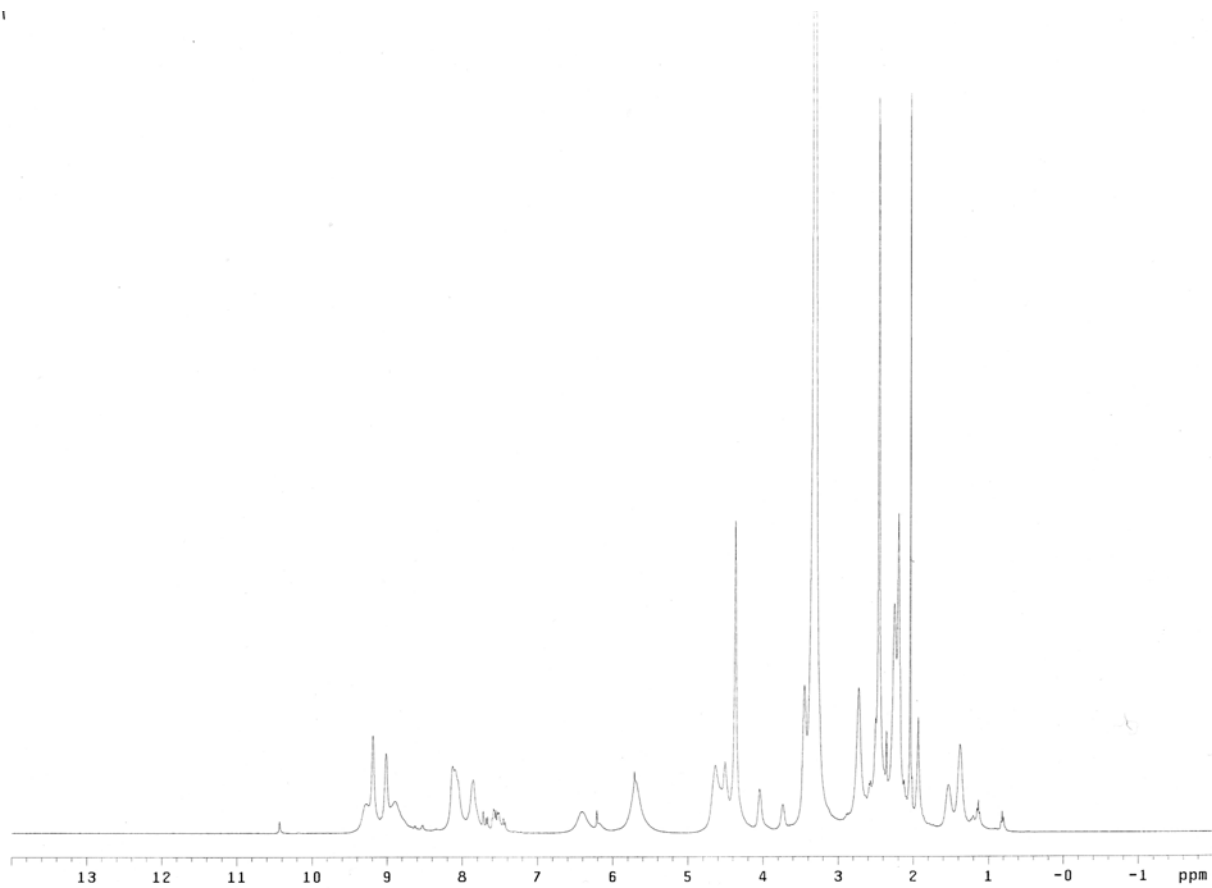
18



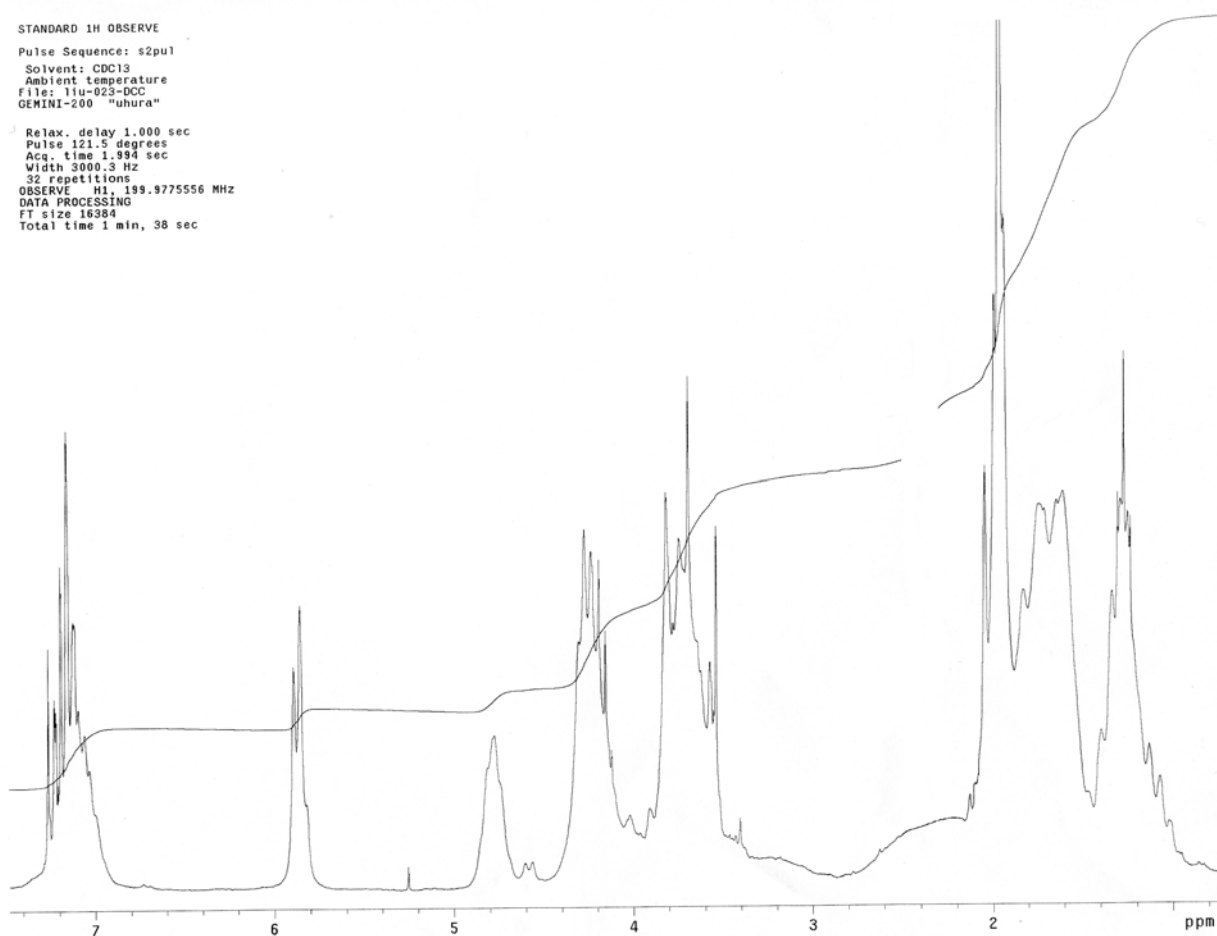




21



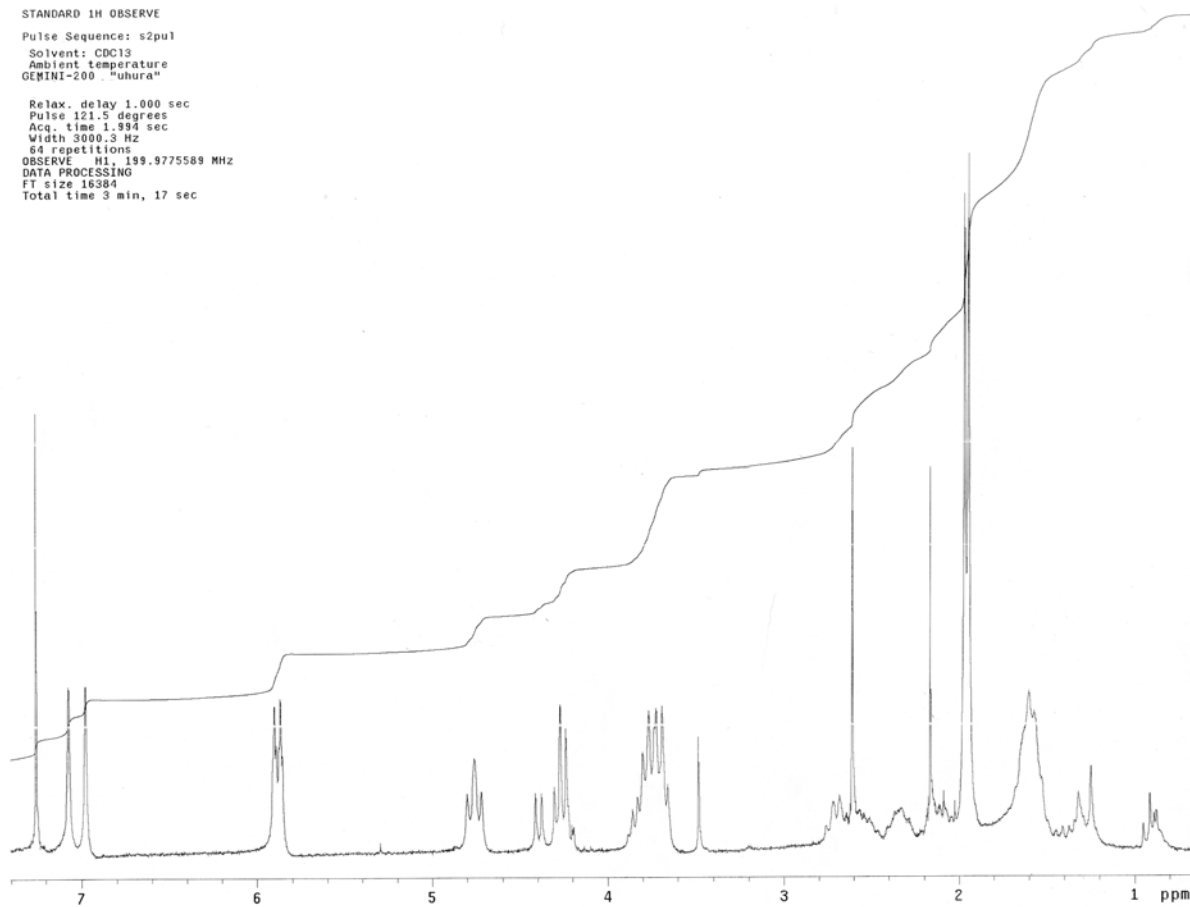
STANDARD 1H OBSERVE
Pulse Sequence: s2pu1
Solvent: CDCl3
Ambient temperature
File: 11u-023-DCC
GEMINI-200 "uhura"
Relax. delay 1.000 sec
Pulse 121.5 degrees
Acq. time 1.994 sec
Width 3000.3 Hz
32 repetitions
OBSERVE H1, 199.977556 MHz
DATA PROCESSING
FT size 16384
Total time 1 min, 38 sec



23

STANDARD 1H OBSERVE
Pulse Sequence: s2pul
Solvent: CDCl3
Ambient temperature
GEMINI-200 "uhura"

Relax. delay 1.000 sec
Pulse 121.5 degrees
Acq. time 1.994 sec
Width 3000.3 Hz
64 repetitions
OBSERVE H1, 199.9775589 MHz
DATA PROCESSING
FT size 16384
Total time 3 min, 17 sec

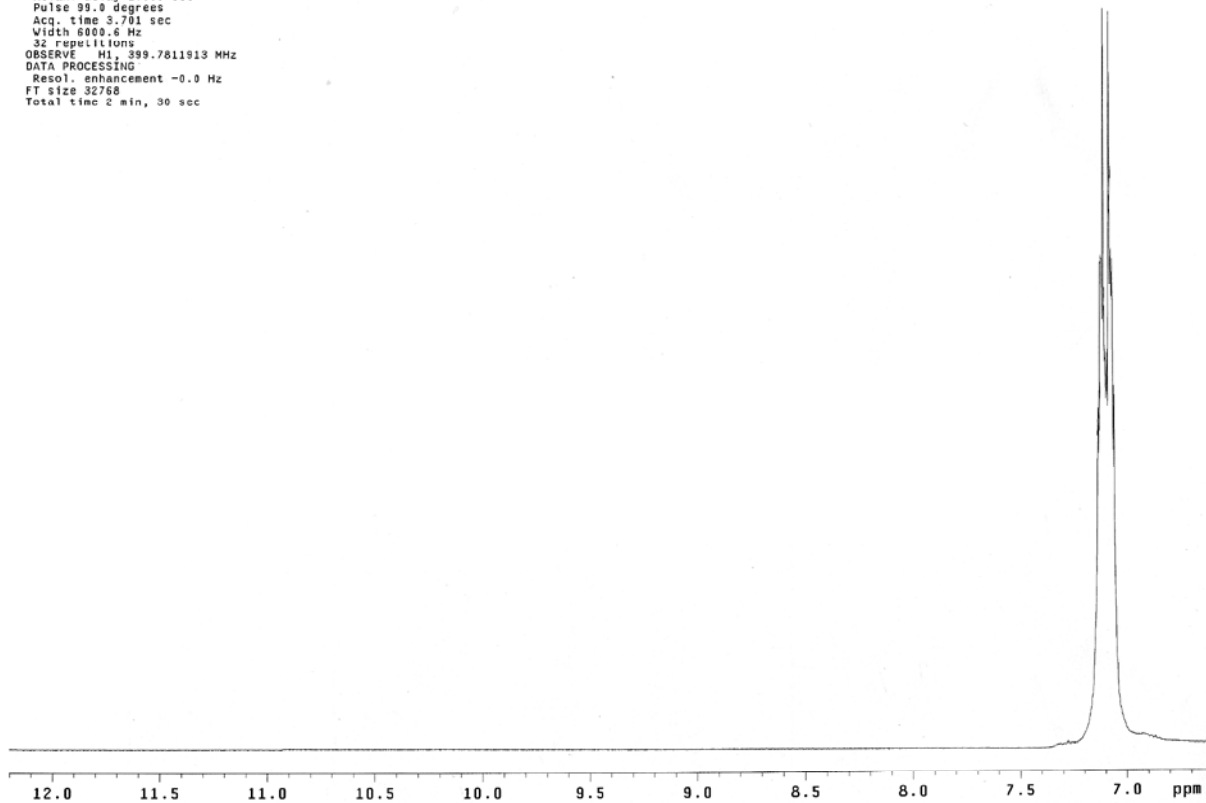


24

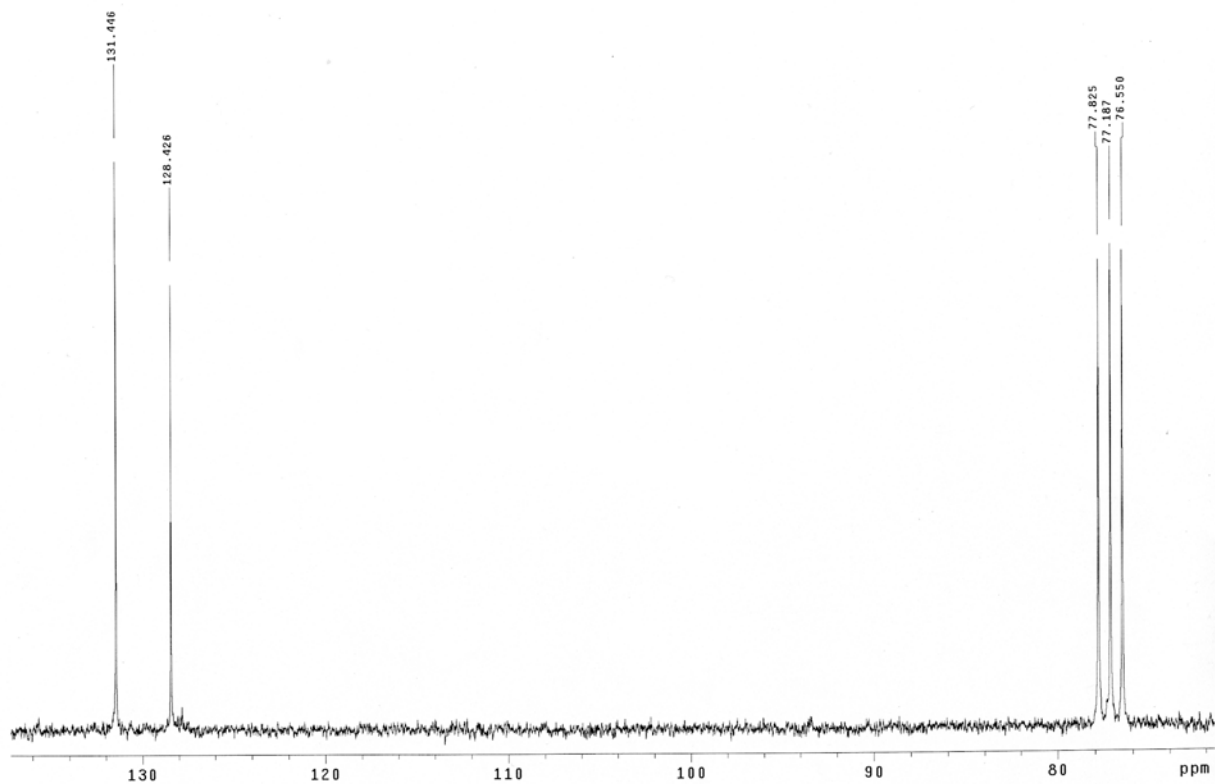
STANDARD 1H OBSERVE

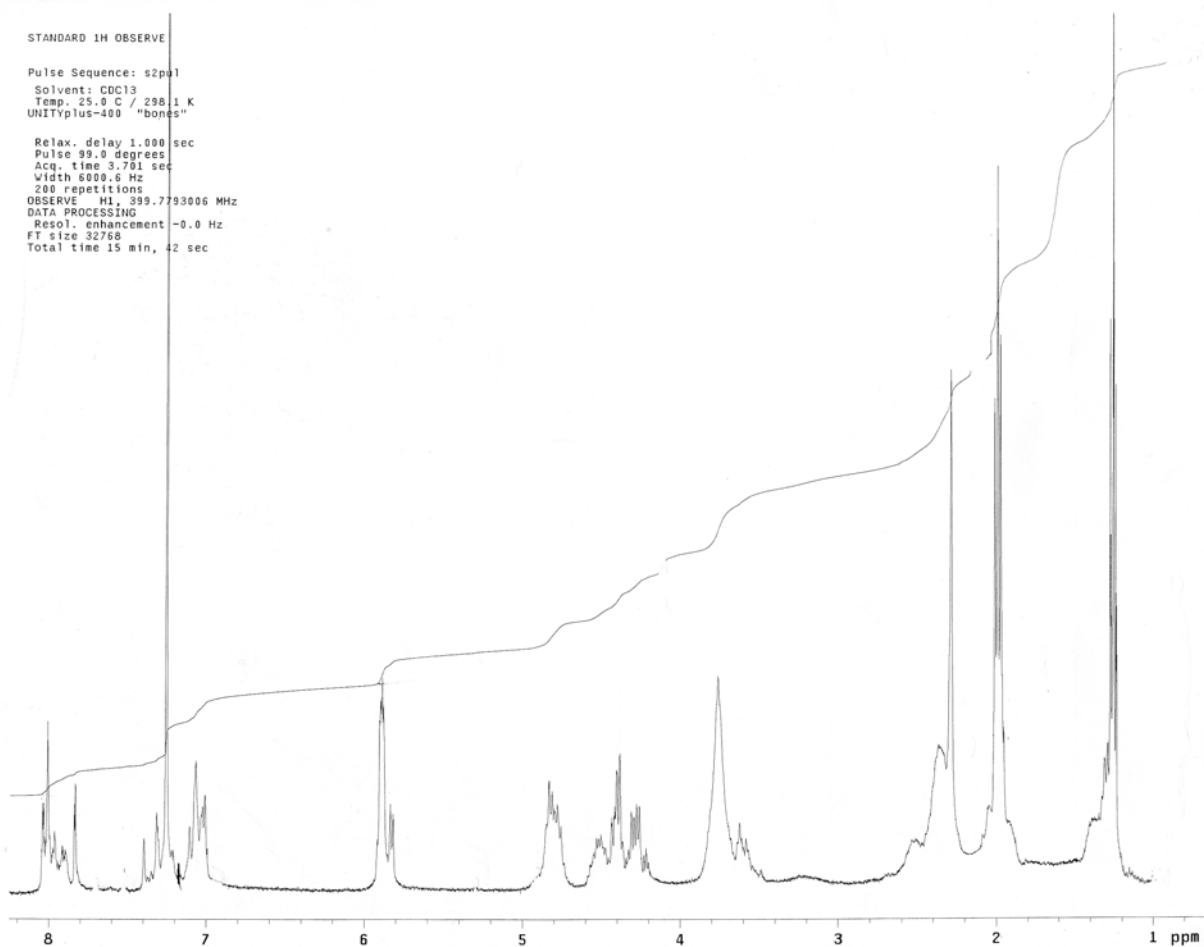
Pulse Sequence: s2pu1
Solvent: DMSO
Temp. 25.0 C / 298.1 K
UNITYplus-400 "bones"

Relax. delay 1.000 sec
Pulse 90.0 degrees
Acq. time 3.701 sec
Width 6000.6 Hz
32 repetitions
OBSERVE H1, 399.7811913 MHz
DATA PROCESSING
Resol. enhancement -0.0 Hz
FT size 32768
Total time 2 min, 30 sec



24

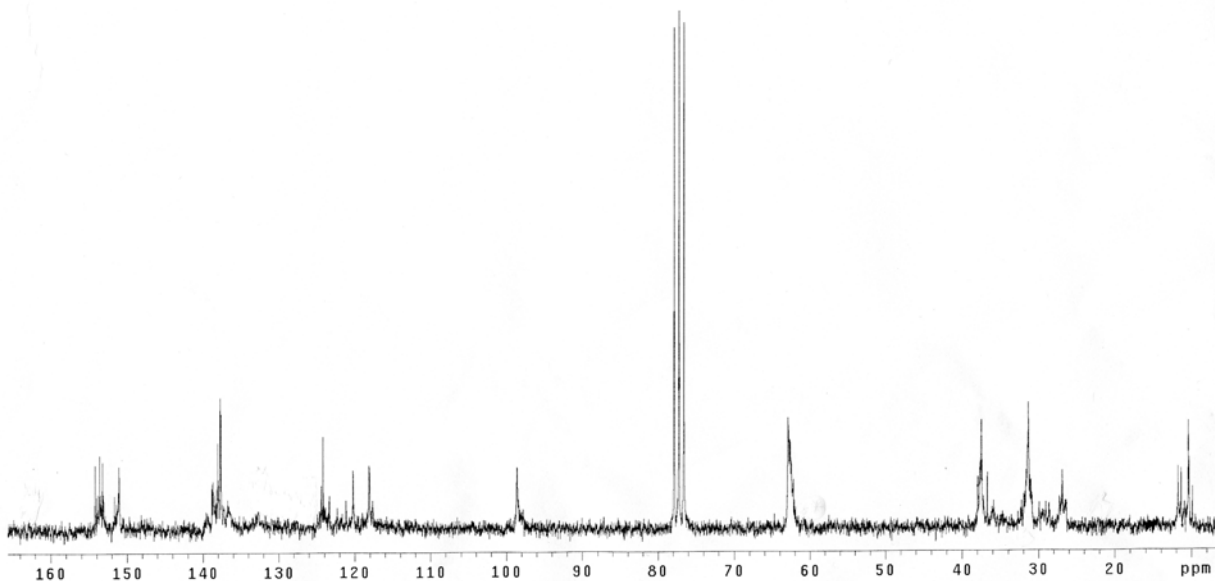


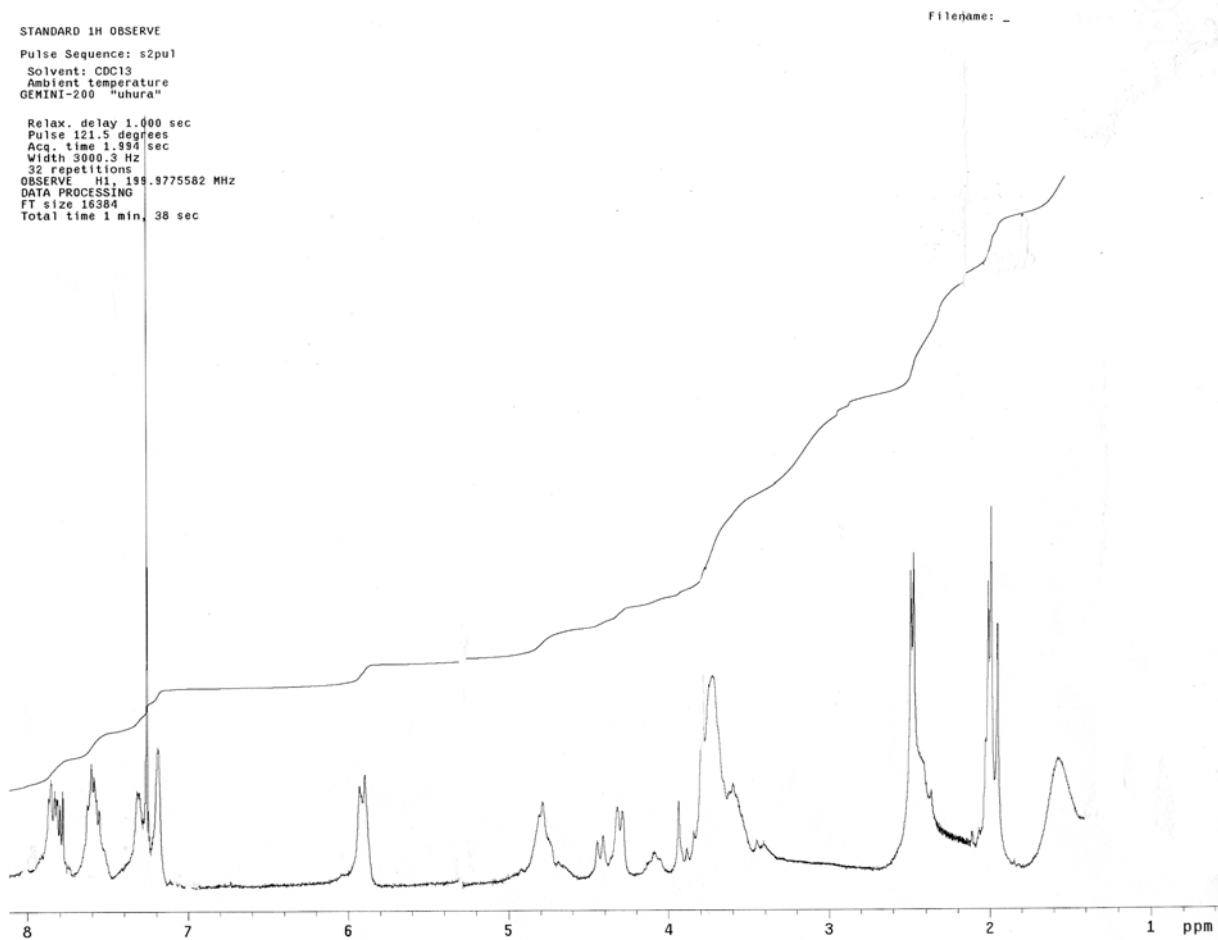


13C OBSERVE
Pulse Sequence: s2pu1
Solvent: CDCl3
Ambient temperature
File: 11u-044-C
GEMINI-200 "uhura"

Relax. delay 1.000 sec
Pulse 164.8 degrees
Acq. time 1.498 sec
Width 12500.0 Hz
11406 repetitions
OBSERVE C13, 50.2843940 MHz
DECOUPLE H1, 199.9785586 MHz
Power 30 dB
continuously on
WALTZ-16 modulated
DATA PROCESSING
Line broadening 1.0 Hz
FT size 65536
Total time 745 hr, 16 min, 53 sec

Filename: _

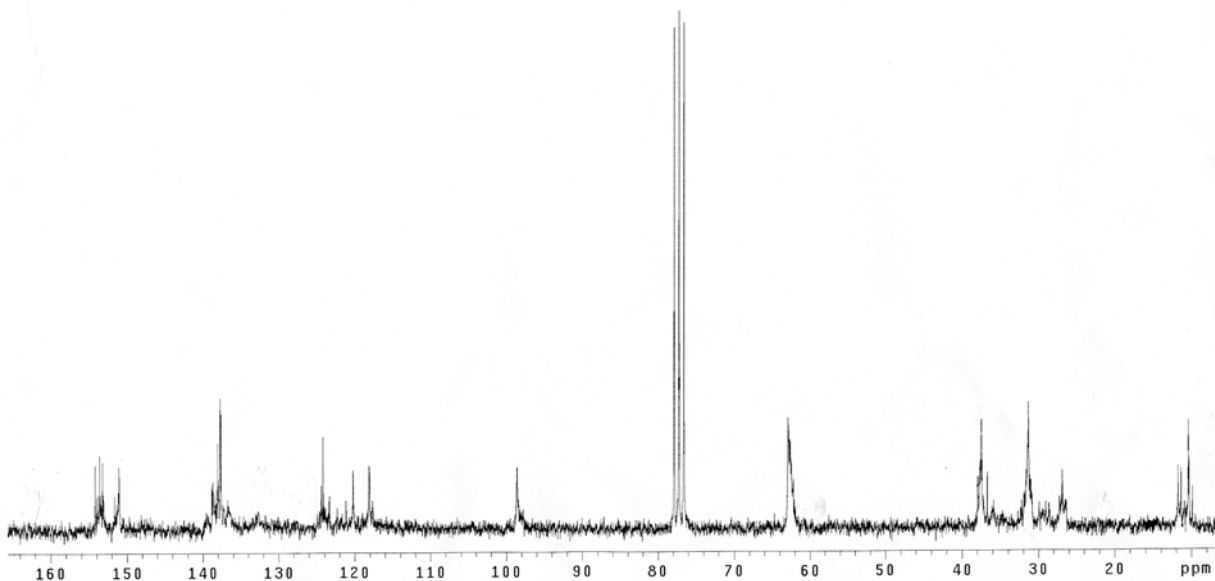




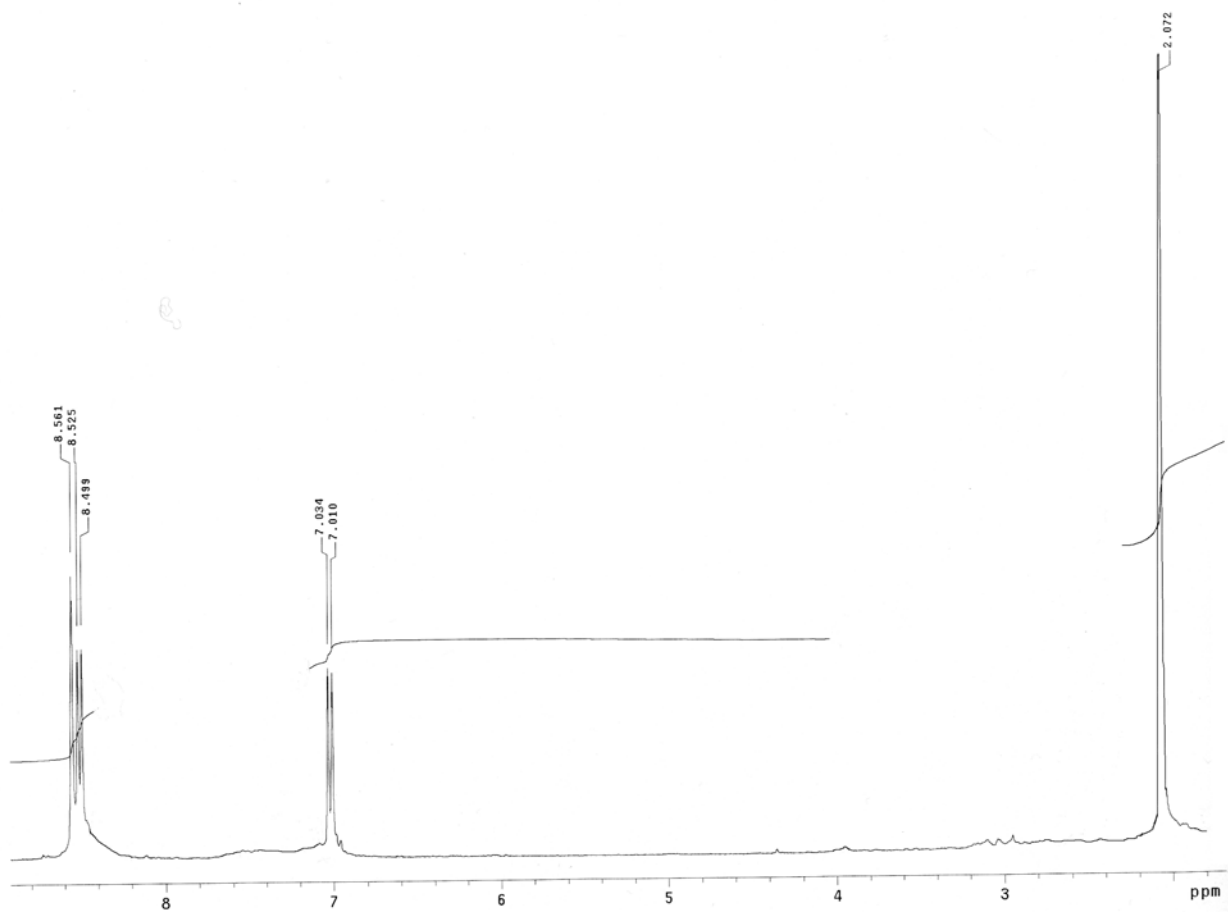
13C OBSERVE
Pulse Sequence: s2pu1
Solvent: CDCl3
Ambient temperature
File: 11u-044-C
GEMINI-200 "uhura"

Relax. delay 1.000 sec
Pulse 164.8 degrees
Acq. time 1.498 sec
Width 12500.0 Hz
11406 repetitions
OBSERVE C13, 50.2843940 MHz
DECOUPLE H1, 199.9785586 MHz
Power 30 dB
continuously on
WALTZ-16 modulated
DATA PROCESSING
Line broadening 1.0 Hz
FT size 65536
Total time 745 hr, 16 min, 53 sec

Filename: _



3,3'-dimethyl 4,4'-bipyridine



Elemental Analysis Table

Compound	C _{calc}	C _{found}	H _{calc}	H _{found}	N _{calc}	N _{found}
3	67.73	67.71	6.50	6.54		
4	51.10	51.21	4.62	4.58		
7	59.64	59.57	4.80	4.87	5.80	5.83
8	48.02	47.98	4.19	4.22	4.48	4.46
10	58.46	58.53	5.12	5.10	5.93	6.01
15	59.99	60.10	5.64	5.71	5.60	5.60
21	60.60	60.48	5.49	5.53	5.58	5.54
25	68.90	68.82	6.35	6.31	3.15	3.05
26	70.35	70.17	6.23	6.22	2.98	3.01